

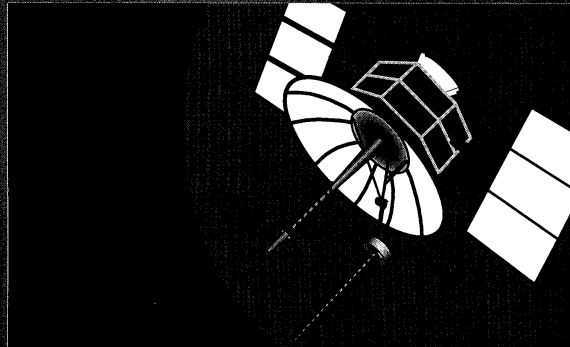
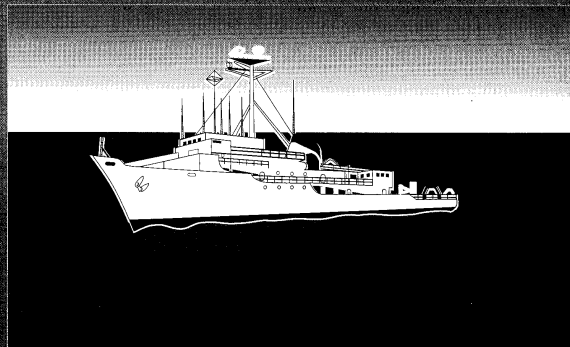
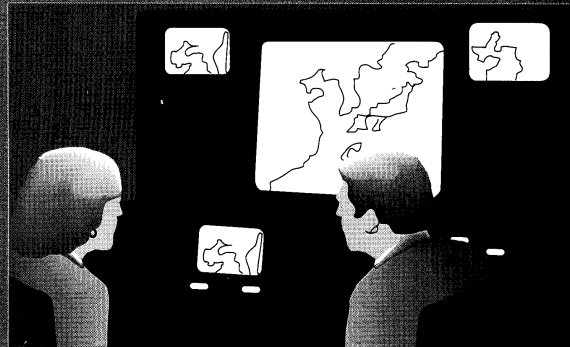
Naval Command,  
Control and Ocean  
Surveillance Center  
RDT&E Division

San Diego, CA  
92152-5001

NRaD TD 2723  
October 1994



# IR '94 ANNUAL REPORT



Approved for public release; distribution is unlimited.

# CONTENTS

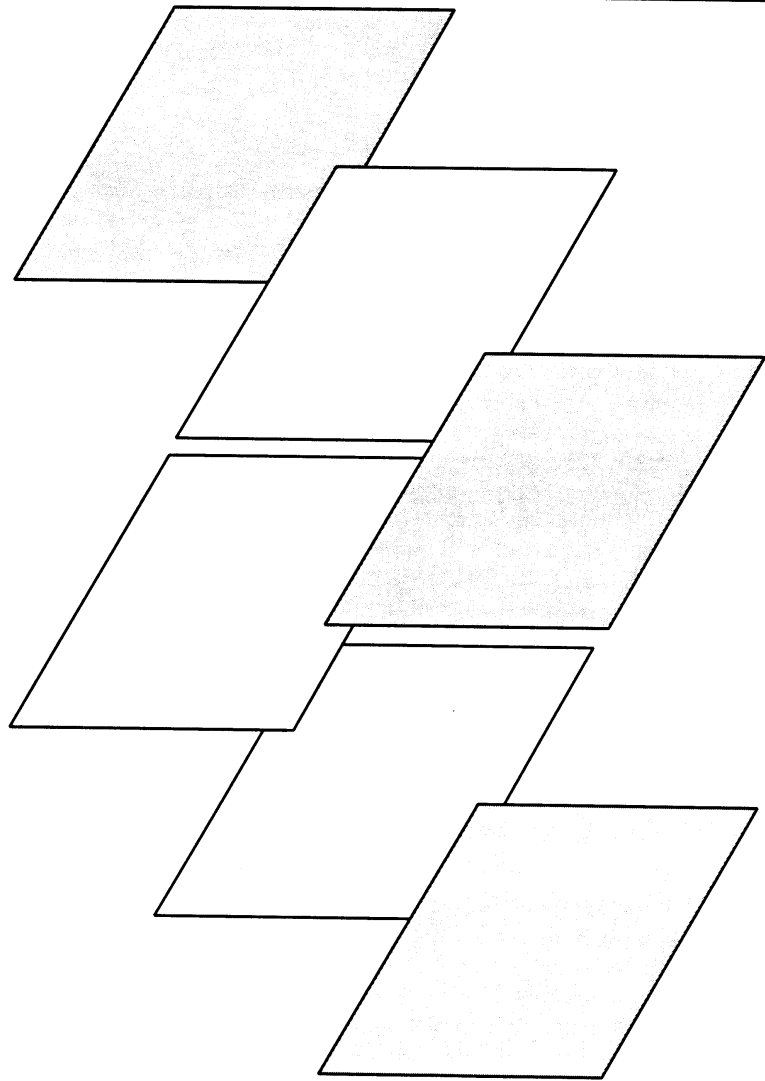
INTRODUCTION .....	1
SELECTED INDEPENDENT RESEARCH PROJECTS .....	5
Preparation of Superconducting $K_3C_{60}$ and $Rb_3C_{60}$ by Precipitation from Liquid Ammonia .....	7
A New Ordering Algorithm for Exposing Parallelism in Sparse Symmetric Matrices .....	19
Evolving Artificial Neural Networks .....	33
Photonic Silicon Device Physics .....	57
APPLICATIONS FROM PAST IR/IED PROJECTS .....	81
Quantum-Well Electroabsorption Optical Modulators .....	83
Optical Properties of Single-Mode, Fiber-Fused, Electronically Tapered Couplers .....	84
Robotic Sensor-Motor Transformations .....	86
PROJECT SUMMARIES: INDEPENDENT RESEARCH .....	87
Command and Control .....	89
Deductive Inference in a Nonmonotonic Logic .....	91
Further Investigations Into the Effects of Using Lasers in Display Devices: Colorimetry and Laser Speckle .....	92
Combining Combinatorial Search with Learning for Command Control .....	94
Communications .....	95
Ultra-Wideband Impulse Radio Propagation .....	97
Blue-Green Iso-Index Filter Material Development .....	98
Adaptive Equalization for High-Data-Rate Communications .....	100
Observation of Ionospheric Dynamics .....	102
Quantitative Performance Evaluation of an ATM-Based Statistical Multiplexer .....	104
Multiwavelength Ultraviolet (UV) Source Development .....	106
Ocean Surveillance .....	107
Three-Dimensional Electric Field Measurements in Shallow Water .....	109
Matched-Field Tracking .....	110
Shallow-Water Three-Dimensional Parabolic Equation Model .....	113
Signal Detection Based on Limited Clues .....	114
Acoustic Bottom Interaction Using the Parabolic Equation .....	116
Wavelets for Ultrabroadband Radar .....	119

Hydrodynamic Characterization of Bioluminescent Stimulus	
Part II—Prediction .....	120
Real Solutions to Maximum Clique and Graph Coloring Patterns .....	125
Coupling Adaptive Beamforming and Adaptive Locally Optimal Detection Algorithms in Nonstationary Noise .....	128
Multimission Research .....	131
Studies of Optical Ringing in Seawater .....	133
Tidal Dispersion Mechanisms in a Coastal Embayment .....	134
n-type Doping of Diamond Using Li and Na .....	137
Implementation of Fuzzy Logic to Choose and Apply Soil Characteristics—Dependent Calibration Curves for Environmental Measurements in the Field .....	138
ZnSe Blue Light-Emitting Devices and Lasers .....	140
Quantum Well Mirror .....	141
PUBLICATIONS AND PRESENTATIONS .....	143
External Publications (Accepted/In Press), Independent Research .....	145
External Publications (Submitted), Independent Research .....	146
In-House Publications, Independent Research .....	147
In-House Publications, Independent Exploratory Development .....	148
Presentations to Professional Meetings, Independent Research .....	149
HONORS AND AWARDS .....	153
PATENT ACTIVITY .....	157
IR PROJECT TABLES .....	169

---

# INTRODUCTION

---



## INTRODUCTION

New and innovative ideas proposed by the scientists and engineers of the Naval Command, Control and Ocean Surveillance Center (NCCOSC), RDT&E Division (NRaD), are supported and encouraged by the Executive Director through the Independent Research (IR) program. This program supports initial research in several areas of interest to the Navy, including command and control, communications, ocean surveillance, and navigation.

The FY 94 IR program was administered by Dr. Alan Gordon. The program began with the Executive Director's March 1993 call for proposals that emphasized Information Understanding, Ocean Surveillance, Anti-Jam/Low Probability of Intercept Communications, Supercomputer Research/Scientific Visualization, Human Factors, Navigation, and Solid-State Materials and Devices. Scientists and engineers responded with 91 written proposals. Of those, 30 were withdrawn or disqualified, and the remaining 61 were each heard in hour-long proposal meetings held throughout the summer of 1993. Each proposal was presented orally before a different *ad hoc* committee chosen for its specific expertise. Members of these committees included Dr. Gordon, Dr. George Dillard, line management, NRaD technical experts, faculty members from local universities, and visiting professors on the ONR-ASEE Summer Faculty Research Program. Based on administrative and peer review, 28 projects were selected for funding that constituted the \$2,312K FY 94 Independent Research Program.

This report contains tables that provide information on active projects, terminated projects, and lists of publications and patents. Although the Independent Exploratory Development (IED) program was terminated at the end of FY 93, this report includes information on patents and publications that resulted from the IED program after the FY 93 IR/IED report. The bulk of this report contains short descriptions of FY 94 IR projects that highlight their objectives and accomplishments. In addition, four IR projects have been selected for more in-depth treatment.

The featured projects are

“Preparation of Superconducting  $K_3C_{60}$  and  $Rb_3C_{60}$  by Precipitation from Liquid Ammonia,” by Dr. R. D. Boss, E. W. Jacobs, J. S. Briggs, Dr. T. E. Jones, and Dr. P. A. Mosier-Boss. The authors describe results of synthesis of stoichiometric, superconducting  $K_3C_{60}$  and  $Rb_3C_{60}$  by precipitation from liquid ammonia. The material was studied by means of X-ray diffraction and magnetic susceptibility measurements, and the observed magnetic properties were interpreted in terms of grain size and the links between the grains.

“A New Ordering Algorithm for Exposing Parallelism in Sparse Symmetric Matrices,” by Dr. Aram Kevorkian. He describes an ordering algorithm to compute a permutation matrix  $P$  so that the parallelism inherent in a sparse matrix  $M$  is fully exposed in the structured matrix  $PMP^T$ . This parallelism is used to simplify computations in the solution of linear systems of equations of the form  $Mx = b$ , where  $M$  is a large sparse symmetric matrix.

“Evolving Artificial Neural Networks,” by J. R. McDonnell. He discusses the construction of variable topology, feed-forward networks by training a population of hidden units and then incorporating the best hidden unit from the population into an artificial neural network's structure. Evolutionary search was used in the optimization of both the hidden unit's structure and the network's weights.

“Photonic Silicon Device Physics,” by Dr. S. Russell. He describes the investigation of the fundamental mechanisms involved in light-emitting silicon structures and fabricated silicon-based photonic devices. The approach evolved into a study of three distinct areas of interest: porous silicon layers, silicon microplasmas, and silicon nanostructures.

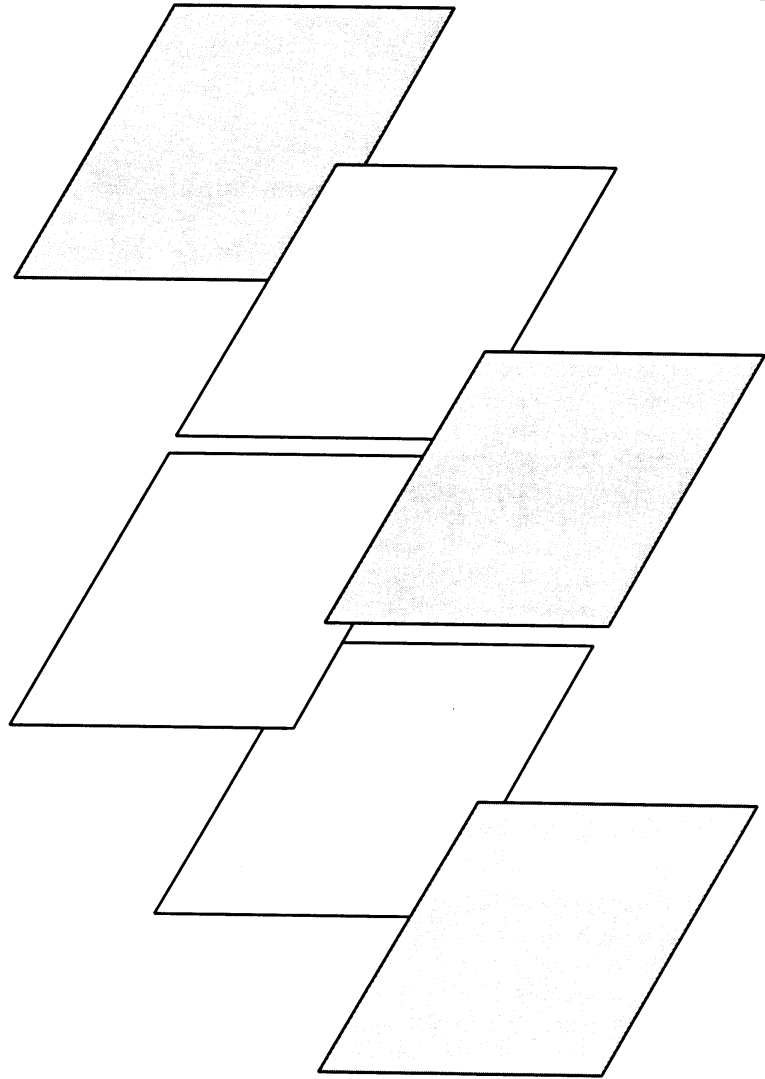
Printed below is a summary of statistics of the IR program for the past 5 years. These data indicate a productive program, but such an enumeration does not allow for a critical evaluation. The project descriptions included in this report offer a more extensive documentation of program results and achievements. Final evaluation, however, is only possible after the full impact of these concepts is tested through applications that increase the capabilities of the Navy.

Fiscal Year	Independent Research					Independent Exploratory Development				
	90	91	92	93	94	90	91	92	93	94
Funding (\$K)	3,151	3,118	1,745	2,278	2,312	1,591	1,820	888	834	—
Number of projects	37	35	21	26	28	18	23	13	12	—
Professional work-years	23	23	13	15	14	13	14	7	7	—
Journal publications and books (accepted/in press)	21	28	21	26	13	10	10	1	2	—
Journal publications and books (submitted)	N/A	N/A	N/A	N/A	10	N/A	N/A	N/A	N/A	—
In-house publications	12	13	11	5	5	9	14	10	3	1
Invited presentations	11	16	23	12	6	6	12	7	—	—
Contributed presentations	23	38	16	54	19	20	7	8	6	—
Patents issued	1	5	5	4	7	4	4	8	6	3
Claims allowed; pending issue	1	1	—	—	2	1	2	3	4	—
Patent applications filed	10	10	11	14	6	7	14	10	7	5
Invention disclosures made or authorized	2	5	6	4	7	11	4	3	2	2
Terminated projects transitioned to sponsored projects (%)	37	39	54	36	25	56	56	56	10	—

---

SELECTED INDEPENDENT  
RESEARCH PROJECTS

---





# Preparation of Superconducting $K_3C_{60}$ and $Rb_3C_{60}$ by Precipitation from Liquid Ammonia

R. D. Boss, E. W. Jacobs, J. S. Briggs, T. E. Jones,  
and P. A. Mosier-Boss

*Results of synthesis of stoichiometric, superconducting  $K_3C_{60}$  and  $Rb_3C_{60}$  by precipitation from liquid ammonia are described. The material was studied by means of X-ray diffraction and magnetic susceptibility measurements. The superconducting phases produced from this synthesis, without recourse to high-temperature anneal, have properties consistent with those of vapor-doped materials. The observed magnetic properties are interpreted in terms of the grain size and the links between the grains.*

## INTRODUCTION

One of the most surprising developments of modern chemistry occurred in 1985 when Kroto, Smalley, and co-workers discovered that carbon could exist in a pure form as something other than diamond or graphite, namely the spherical molecule  $C_{60}$  (see figure 1) and its analogs [1]. The subsequent discovery that  $C_{60}$  could be produced in bulk quantities [2] has produced a flurry of research activities. The subsequent discovery that  $C_{60}$  could be doped by alkali metals to produce conductive, semiconductive, and even superconductive phases [3–5] has led to even more expanded efforts. The superconducting phases hold the record for the highest critical temperature (the temperature below which superconductivity occurs) for organic-based superconductors, for true three-dimensional superconductors, and for nonceramic superconductors [6] (only the copper-oxide materials have higher critical temperatures). Due to the wide range of properties available in the doped  $C_{60}$  materials, there exists much speculation concerning possible applications, including several that are of interest to the Navy. Among these are the possibilities of producing a single material that is superconducting in one region and semiconducting in another (thereby producing highly compact semiconductor/interconnect structures); the use of  $C_{60}$  as an electrode material in featherweight batteries; and the creation of superconducting devices.

Many of the uses envisioned for  $C_{60}$  require that the doped phases be produced in large quantities without compromising on material quality. The first method for producing alkali-doped  $C_{60}$  was to expose a small amount of  $C_{60}$  (usually in the form of a thin film) to vapor-phase alkali metal [3,4]. This is a relatively slow process, in which the final ratio of the  $C_{60}$  to alkali is poorly controlled. Further, past experience with this sort of doping process suggests that the material produced is likely to form domains of varying alkali to  $C_{60}$  ratios. Many of these problems can be overcome by replacing the vapor-doping synthetic method with a synthesis using solution doping.

Despite the large amount of work that has been done with regard to measurement of the electrical and magnetic properties of various doped  $C_{60}$  materials [7], there has been little work on the preparation of the doped phases using methods other than the vapor-doping process. The published works on other methods have involved solid-state reaction [8–10], electrochemical doping [11,12], and solution precipitation [13–15]. Each of these techniques has its strong and weak points. Clearly, to produce the best possible material, it is desirable to guarantee the

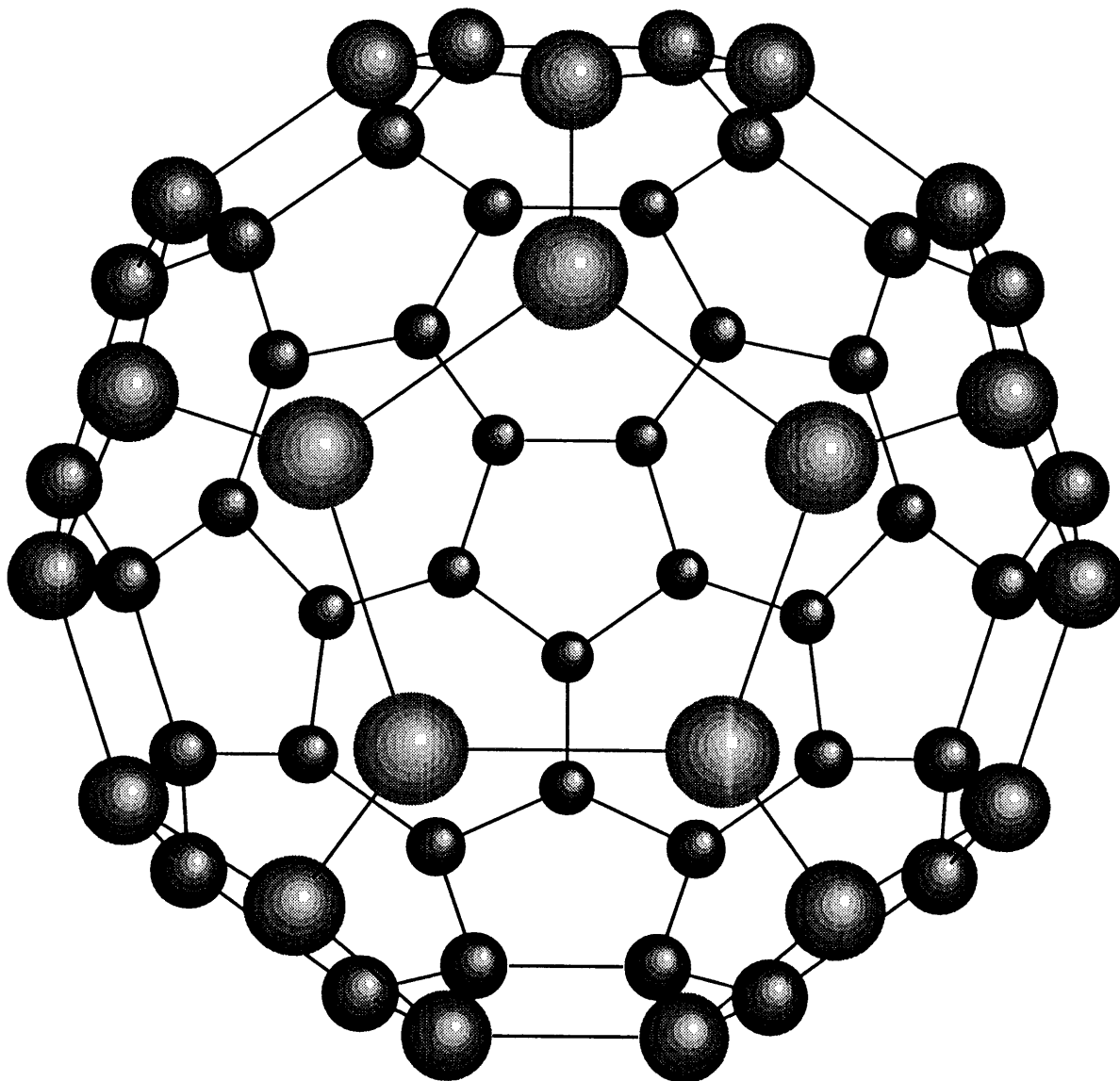


*Figure 1. The structure of C<sub>60</sub>.*

stoichiometry of the end product, such as by precipitation from a stoichiometric solution with complete removal of the solvent. For a solution to precipitate a stoichiometric doped phase, it is necessary to have solubility of both the alkali metal cation and the C<sub>60</sub> anion. It is well known that liquid ammonia solubilizes alkali metals to form the alkali cation and a solvated electron [16], and recently it has been shown that various C<sub>60</sub><sup>-n</sup> anions are soluble in liquid ammonia [17,18].

The first report of an attempt to produce doped C<sub>60</sub> from liquid ammonia [15] claimed that: A<sub>3</sub>C<sub>60</sub> was soluble in liquid ammonia; the solvent could only be removed from the precipitate material above 300°C; the material was noncrystalline; and the material showed only “small amounts” of superconductivity (as was confirmed by Fullagar et al. [18]). More recently, the same group [19] reported that the superconducting transition temperature of Na<sub>2</sub>CsC<sub>60</sub> could be increased by approximately 20K by exposure to NH<sub>3</sub> vapor. This reversible increase is due to the formation of a Na(NH<sub>3</sub>)<sub>4</sub> complex that displaces the Cs cation from the octahedral site into a tetrahedral site. The reaction was observed to be

reversible with a few minutes of gentle heating under dynamic vacuum. It is well known that the strength of interaction between ammonia and alkali cations increases with decreasing cation size. Furthermore, ammonia intercalation in alkali-doped graphite is known to be reversible [20], with the ease of reversibility having the expected dependence on cation size. One would expect, based on these results, that removal of ammonia from  $C_{60}$  doped with potassium or rubidium would be even more facile than that observed for the sodium complexation. Since the experimental result was that it was difficult to remove ammonia from precipitated  $A_3C_{60}$ , one might interpret this as indication that something other than simple complexation occurred, such as perhaps amide formation.

More recently, Buffinger et al. [21] have reported that superconducting alkali-doped phases of  $C_{60}$  can be produced from liquid ammonia. Their results disagree with those described above in that their data indicate little ammonia present after a short heating at  $<100^\circ\text{C}$  under dynamic vacuum, but with significant crystallinity and superconducting fractions appearing only after a 24-hour anneal at  $375^\circ\text{C}$ . This suggests that the presence of residual ammonia (as either amide or complexate) is not the barrier to the superconducting phase, but rather that the precipitate formed is simply not of the proper crystal phase. The proper phase is apparently produced in a subsequent solid-state reaction during the high-temperature anneal.

The work presented here describes the preparation of superconducting alkali-doped  $C_{60}$  by precipitation from liquid ammonia in which the superconducting phase is produced quantitatively without recourse to a high-temperature anneal. The results are interpreted with regard to those of Murphy et al. [15] and Buffinger et al. [21], and the size and nature of the superconducting grains are investigated.

## EXPERIMENTAL PROCEDURE

The materials used to produce alkali-metal-doped  $C_{60}$  (as well as the final doped materials themselves) are sensitive to air and water. Consequently, all materials must be handled under an inert atmosphere and/or vacuum. Further, liquid ammonia has a boiling point of  $-33^\circ\text{C}$  so all steps in the handling of the solutions must be done at cryogenic temperatures. The synthetic process is described below and shown schematically in figure 2.

After placing stoichiometric amounts of the alkali metal and  $C_{60}$  into a reaction vessel, the vessel is connected to a vacuum line such as shown in figure 2a. Sufficient ammonia to produce about 30 ml of liquid was frozen at liquid nitrogen temperature in a storage vessel connected to the vacuum line (figure 2b). The reaction vessel was then immersed into a Chlorobenzene slush ( $-45^\circ\text{C}$ ). Approximately 15 ml of liquid ammonia was distilled from the storage vessel into the reaction vessel by allowing the storage vessel to warm (figure 2c). No drying of the ammonia was performed, other than that which occurs due to the vacuum distillation process. The resultant solution was black in color, thereby indicating dissolution of the  $C_{60}$  [15,17,18] as an anion. This is in contrast to the blue observed for pure alkali metal/liquid ammonia solutions [22] and which was reported to be briefly observed by Buffinger et al. [21] when they condensed ammonia at  $-78^\circ\text{C}$ .

After  $\approx 5$  minutes the liquid ammonia was *slowly* distilled back into the storage container. This was done by immersing the storage container in a  $-45^\circ\text{C}$  chlorobenzene slush, and allowing the reaction vessel chlorobenzene bath to warm (figure 2d). After the liquid appeared to be completely removed (about 1 hour) the storage flask was immersed in liquid nitrogen while the reaction vessel was warmed to room temperature to complete the distillation (figure 2e). The

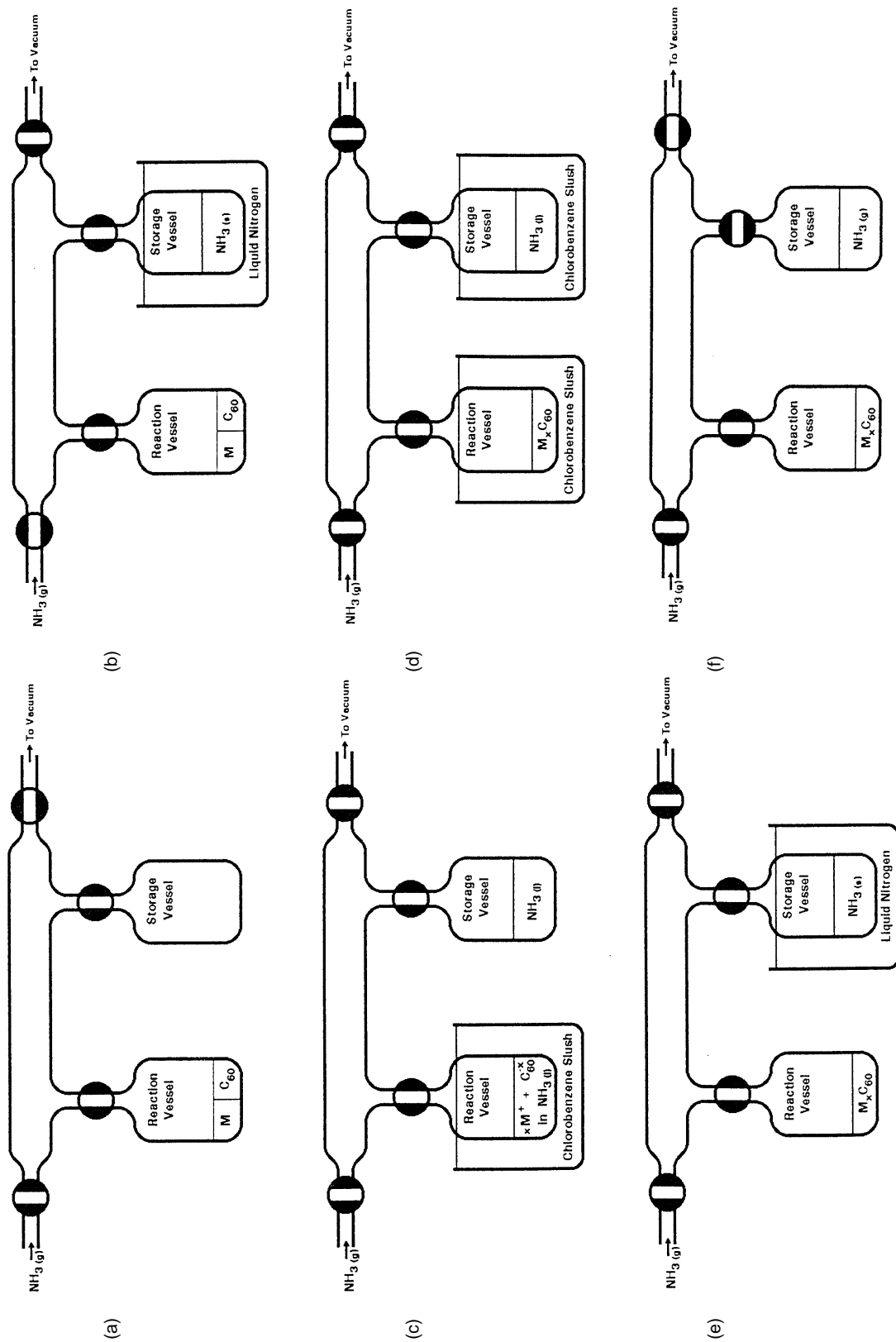
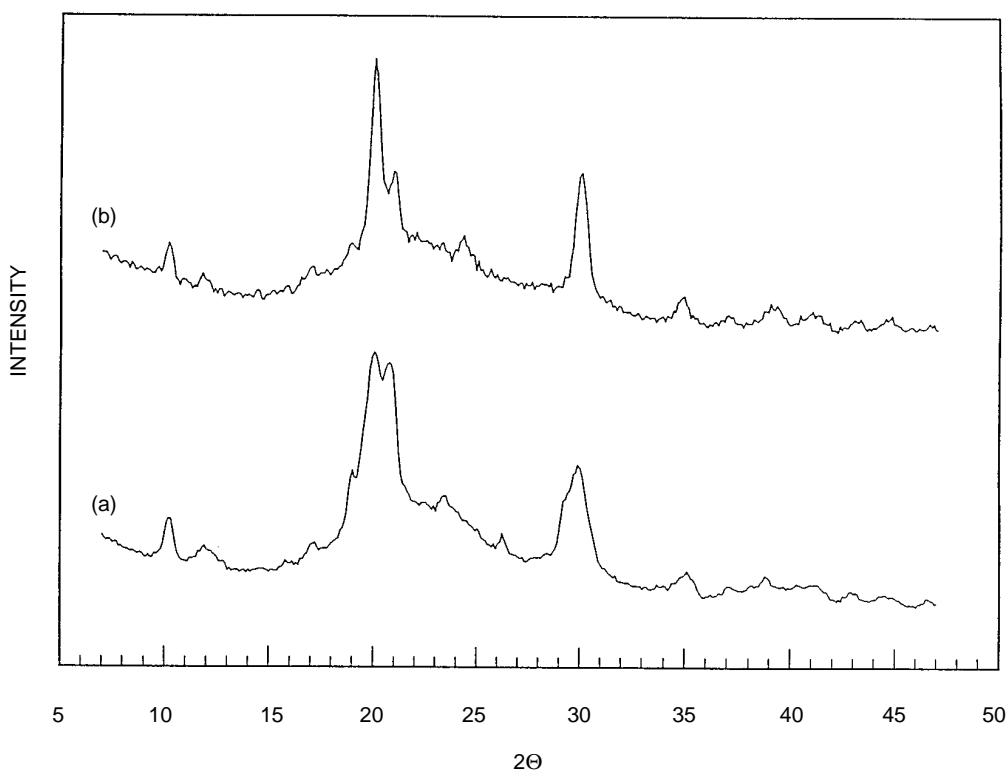


Figure 2. A schematic representation of the synthetic process used to produce alkali doped C<sub>60</sub> from liquid ammonia.

reaction vessel was then reconnected to dynamic vacuum and heated to about 100°C for about 1 hour (figure 2f). During this heating, the pressure (as monitored by a thermocouple pressure gauge) rapidly rose to 100 to 200 mTorr, and then fell slowly to essentially zero. The material thus produced (called “as made”) was then subjected to various heat treatments under dynamic vacuum, and the as-made and processed materials were studied by X-ray diffractometry and both AC and DC magnetic susceptibility.

## RESULTS

In figure 3a, the X-ray diffraction pattern for a sample of as-made  $\text{Rb}_3\text{C}_{60}$  is shown. The results are typical for both rubidium and potassium syntheses. The pattern appears to be a mixture of the desired phase and a phase similar to that reported by Zhou et al. [23] for  $\text{K}_3(\text{NH}_3)\text{C}_{60}$ . Further heat treatment is required to remove the additional  $\text{NH}_3$ . In figure 3b, the X-ray pattern is shown for a sample of  $\text{Rb}_3\text{C}_{60}$  that was heated at 150°C for 3 days. Further heat treatment at 250°C for an additional 2 days resulted in the pattern of figure 4a, which is equivalent to those reported for vapor-doped  $\text{Rb}_3\text{C}_{60}$  [8,24]. Figure 4b shows the diffraction pattern for  $\text{K}_3\text{C}_{60}$  which has been treated by heating at  $\approx 100^\circ\text{C}$  for 6 days. This pattern is also equivalent to those reported for vapor-doped  $\text{K}_3\text{C}_{60}$  [24,25]. Calculation of the lattice parameter,  $a_0$ , has been done from other samples that include  $\text{MoS}_2$  as an internal standard. The values obtained are  $14.45 \pm 0.05 \text{ \AA}$  and  $14.36 \pm 0.09 \text{ \AA}$  for  $\text{Rb}_3\text{C}_{60}$  and  $\text{K}_3\text{C}_{60}$ , respectively.



*Figure 3. X-ray diffraction patterns for (a) the as made  $\text{Rb}_3\text{C}_{60}$  and (b) the  $\text{Rb}_3\text{C}_{60}$  after 3 days at 150°C under dynamic vacuum.*

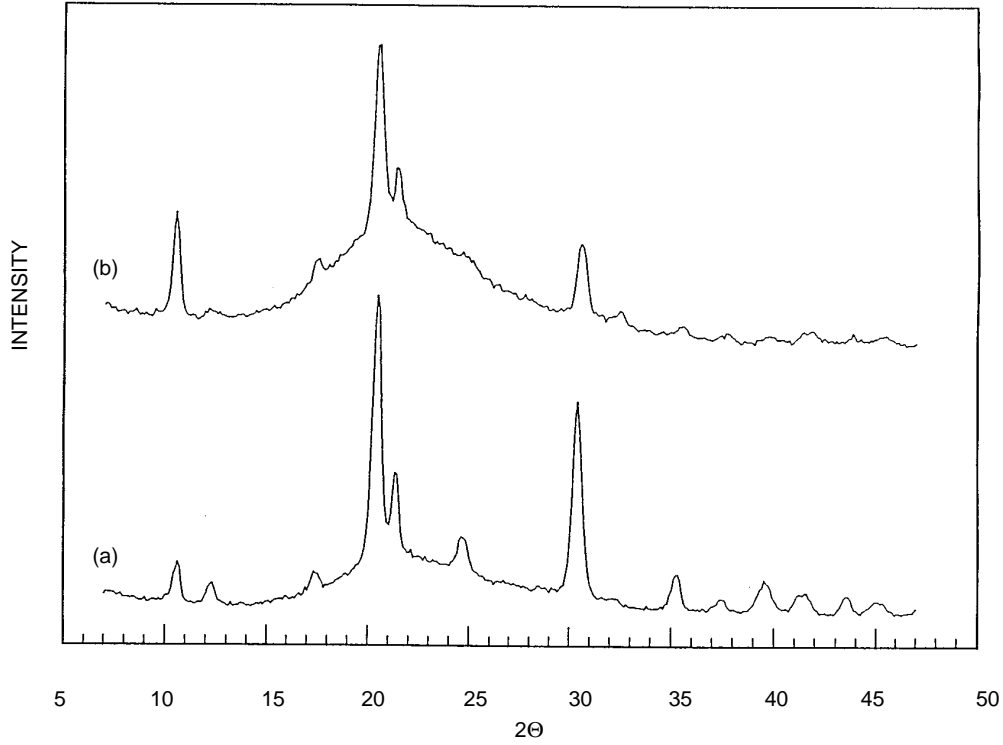


Figure 4. X-ray diffraction patterns for (a) the  $Rb_3C_{60}$  of figure 1b after an additional 2 days at  $250^\circ C$  under dynamic vacuum and (b) the  $K_3C_{60}$  after 6 days at  $100^\circ C$  under dynamic vacuum.

The AC susceptibility data for samples of these materials are shown in figure 5 along with a comparison of the AC susceptibility of a standard sample of niobium metal powder. All three samples shown display strong diamagnetic shielding. The transition temperatures for shielding are  $9.15 \pm 0.15K$ ,  $21.2 \pm 0.2K$ , and  $29.6 \pm 0.3K$ , for the Nb,  $K_3C_{60}$ , and  $Rb_3C_{60}$ , respectively. At low temperatures, each sample gives an apparent shielding volume fraction of about 140 percent of the theoretical value calculated for a perfect superconducting solid ( $X'_{vol} = 1.4$  in SI units). This value is consistent with 100-percent shielding from a powdered sample filling the sample holder with a packing fraction of about 71 percent, which is a reasonable value for packed spheres.

Magnetization versus applied field loops for these samples of  $K_3C_{60}$  and  $Rb_3C_{60}$  are shown in figure 6. The critical current data in table 1 were calculated from the equation  $J_c = (32/3\pi) \times (M/R)$ , where  $M$  is the volume magnetization (loop half-width if a full loop is taken) in SI units,  $R$  is the radius in meters of the grains carrying the current, and  $J_c$  is the critical current density in  $A/m^2$ . The data have been converted to standard laboratory units for ease of comparison.

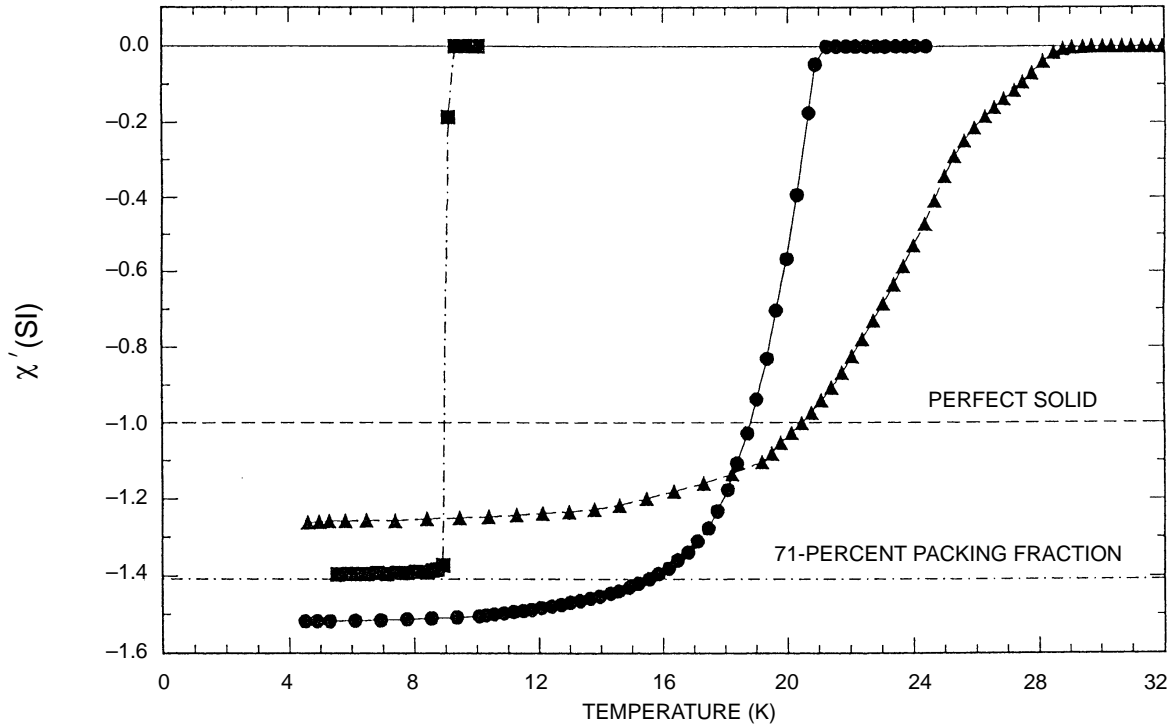
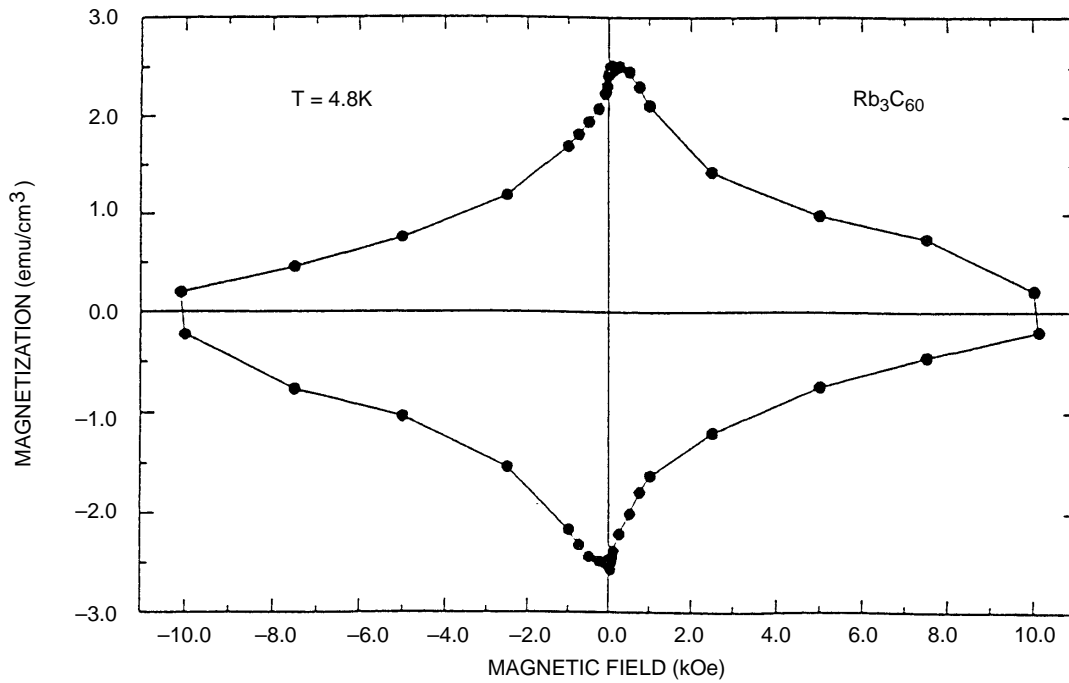


Figure 5. The real part of the AC volume susceptibility versus absolute temperature for a powdered sample of  $Rb_3C_{60}$  annealed as for the sample of figure 2a ( $\blacktriangle$ ), a powdered sample of  $K_3C_{60}$  annealed as for the sample of figure 2b ( $\bullet$ ), and a sample of 60 mesh niobium metal powder ( $\blacksquare$ ).

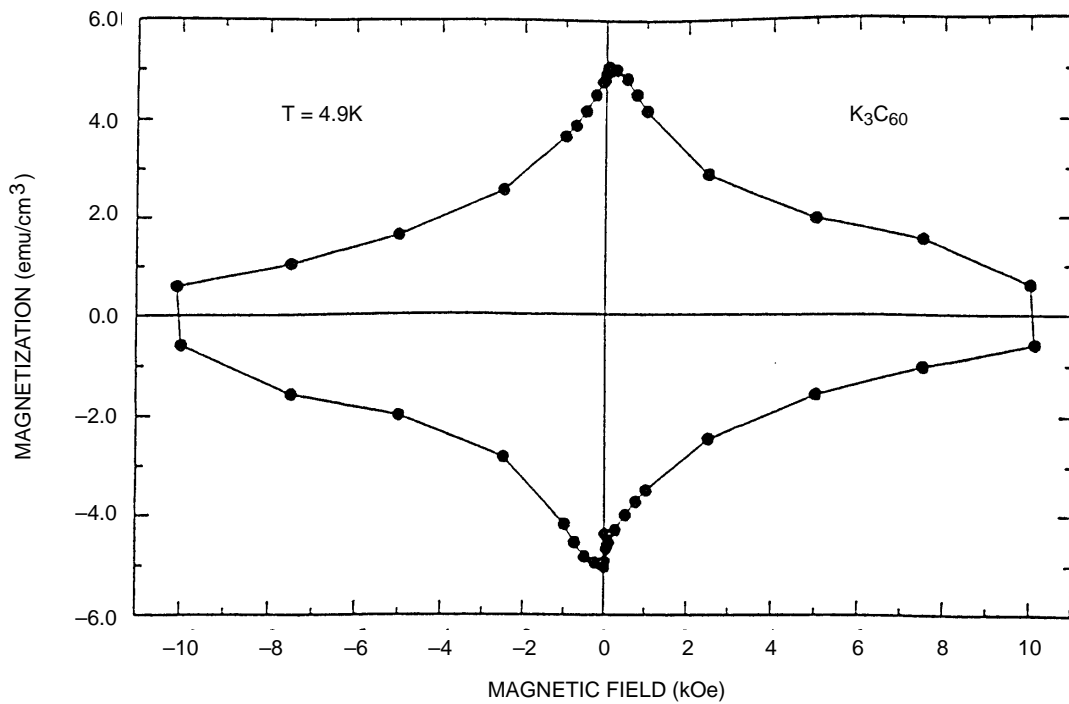
Since the critical current necessary to produce an observed magnetization depends upon the size (and geometry) of the physical piece within which the current flows, it is necessary to try to evaluate the approximate size of the grains. Microscopic examination of similar materials suggests that the largest physical aggregate in these samples is of the order of 0.3-mm diameter; however, these materials are quite fragile and can be broken apart quite easily. Examination of the fragments that these aggregates produce when broken indicated a largest fragment size of  $\approx 0.01$  m. The critical currents reported in table 1 are reported for various possible grain sizes over this range.

Table 1. The calculated critical current density necessary to produce the observed DC magnetization of figure 6 as a function of particle size.

Size of Superconducting Grains (in $\mu\text{m}$ )	Critical Current Density (in $\text{A}/\text{cm}^2$ )	
	$K_3C_{60}$	$Rb_3C_{60}$
1	$4.8 \times 10^6$	$2.4 \times 10^6$
3	$1.6 \times 10^6$	$8.0 \times 10^5$
10	$1.8 \times 10^5$	$2.1 \times 10^5$
30	$1.6 \times 10^5$	$8.0 \times 10^4$
100	$4.8 \times 10^4$	$2.4 \times 10^4$
300	$1.6 \times 10^4$	$8.0 \times 10^3$



(a)



(b)

Figure 6. The DC magnetization versus applied magnetic field (a) at 4.8 K for a powdered sample of Rb<sub>3</sub>C<sub>60</sub> annealed as for the sample of figure 2a and (b) at 4.9 K for a powdered sample of K<sub>3</sub>C<sub>60</sub> annealed as for the sample of figure 2b.

## DISCUSSION

The X-ray diffraction patterns shown in figures 3 and 4a for  $\text{Rb}_3\text{C}_{60}$  and equivalent spectra for  $\text{K}_3\text{C}_{60}$  (not shown) indicate that the primary process observed during post-precipitation anneal is the removal of  $\text{NH}_3$ . This is confirmed by the similarity of the spectra to those observed by Zhou et al. [23] during intercalation of  $\text{NH}_3$  gas into  $\text{K}_3\text{C}_{60}$ . They observe the reversible formation of two compounds  $\text{K}_3(\text{NH}_3)\text{C}_{60}$  and  $\text{K}_3(\text{NH}_3)_8\text{C}_{60}$ . The as-made materials appear to be mixtures of  $\text{A}_3\text{C}_{60}$  and  $\text{A}_3(\text{NH}_3)\text{C}_{60}$ . It is also of interest that samples taken from material from which the ammonia has been fully distilled, but not fully dried (i.e., taken before the initial 1-hr,  $100^\circ\text{C}$  bake) appear to be similar to the reported  $\text{K}_3(\text{NH}_3)_8\text{C}_{60}$  phase.

Additional heat treatment of vacuum-sealed X-ray capillaries of as-made samples tends to cause the capillaries to burst, apparently due to pressurization from the liberated  $\text{NH}_3$ . The only as-made X-ray capillary sample that did not burst during additional heat treatment was observed to be completely converted to the proper superconducting phase by the heat treatment (about 4 days at  $415^\circ\text{C}$ ). This sample's X-ray spectrum then slowly reverted, during a 2-month storage, back towards its pre-heat treatment X-ray pattern. These data, when coupled with the  $100^\circ\text{C}$  anneal of the  $\text{K}_3\text{C}_{60}$  sample, suggest that the precipitate forms in the proper crystal structure (with ammonia complexed alkali cations), and that the primary process that occurs during the subsequent heat treatments is the complete removal of the ammonia, rather than solid-state reaction.

Once the removal of  $\text{NH}_3$  is complete, the samples show only the known superconducting phase. The value determined for the lattice parameter,  $14.45 \pm 0.05 \text{ \AA}$  for  $\text{Rb}_3\text{C}_{60}$ , is in good agreement with those reported ( $14.39$  [8] and  $14.436 \text{ \AA}$  [24]). However, the value determined for  $\text{K}_3\text{C}_{60}$ ,  $14.36 \pm 0.09 \text{ \AA}$  is slightly larger than reported values ( $14.24$  [8,26], and  $14.253 \text{ \AA}$  [24]), which may be due to the presence of a very small amount of residual ammonia.

The AC magnetization data confirm the result that the material is essentially 100-percent superconducting phase. Further, the observed magnetic transition temperatures are consistent with the observed lattice parameters. The observed transition temperature for shielding for  $\text{Rb}_3\text{C}_{60}$  is  $29.6 \pm 0.3\text{K}$ , which is in complete agreement with the known value [8,24]. The shape of the transition for the rubidium-doped material is consistent with a poorly connected granular material, which is to be expected for a sample of noncompacted, nonannealed granular pieces.

The transition temperature for shielding for  $\text{K}_3\text{C}_{60}$  is  $21.2 \pm 0.2\text{K}$ , which is about  $1.5\text{K}$  higher than the accepted value [24,26]. The consistency of the measured transition temperature of both the niobium metal and the  $\text{Rb}_3\text{C}_{60}$  with known values suggests that this difference is not due to an error in thermometry, but rather reflects a true difference in the material. In fact, given that the  $\text{K}_3\text{C}_{60}$  shows a slight increase in the lattice parameter, the slightly raised transition temperature is consistent with the known dependence of the superconducting transition temperature on lattice spacing for doped  $\text{C}_{60}$  [24].

The reported values for the critical current density are of the order  $(1 \text{ to } 5) \times 10^5 \text{ A/cm}^2$  for  $\text{K}_3\text{C}_{60}$  [27,28] and  $10^6 \text{ A/cm}^2$  for  $\text{Rb}_3\text{C}_{60}$  [27,29]. For the data presented here (table 1), this corresponds to apparent superconducting grain sizes of about  $20 \mu\text{m}$  for  $\text{K}_3\text{C}_{60}$  and about  $2 \mu\text{m}$  for  $\text{Rb}_3\text{C}_{60}$ . The superconducting grain size is within the observed range of particle sizes for the  $\text{K}_3\text{C}_{60}$ , but is about an order of magnitude smaller than the observed particle size for the  $\text{Rb}_3\text{C}_{60}$ .

The shielding data presented in figure 5 are consistent with this result. That is, the shielding for the potassium-doped material has a smooth transition with a very sharp onset point, while the rubidium-doped material shows a two-transition shielding curve (note the inflection around  $25\text{K}$ ). These curves can be interpreted as indicating that the potassium-doped material has well-connected grains, while the

rubidium-doped material has poorly connected grains. There is no obvious explanation for why the  $\text{Rb}_3\text{C}_{60}$  grains would be less well connected than the  $\text{K}_3\text{C}_{60}$  grains; however, these data suggest that such is the case.

## SUMMARY

The synthesis of superconducting phases of alkali-doped  $\text{C}_{60}$  can be performed with 100-percent efficiency by precipitation from stoichiometric solutions in liquid ammonia. The complete removal of the trapped (complexed) ammonia can be accomplished by a low-temperature anneal under dynamic vacuum. The materials produced show appropriate X-ray diffraction patterns and AC-shielding transition temperatures. The critical current densities of the materials produced are probably not less than  $5 \times 10^5 \text{ A/cm}^2$ , although the  $\text{Rb}_3\text{C}_{60}$  may have poorly connected superconducting grains. This synthesis should be scalable to produce any amount of material desired with equal ease. Finally, this synthetic route may open up the possibility of intercalation of  $\text{C}_{60}$  by a series of various size cations and complexed cations that have been heretofore unavailable for intercalation.

## REFERENCES

- [1] Kroto, H. W., J. R. Heath, S. C. O'Brien, R. F. Curl, and R. E. Smalley. 1985. *Nature* 318, 162.
- [2] Kratschmer, W., L. D. Lamb, K. Fostiropoulos, and D. R. Huffman. 1990. *Nature* 347, 354.
- [3] Haddon, R. C., A. F. Hebard, M. J. Rosseinsky, D. W. Murphy, S. J. Duclos, K. B. Lyons, B. Miller, J. M. Rosamilia, R. M. Fleming, A. R. Kortan, S. H. Glarum, A. V. Mahkiha, A. J. Muller, R. H. Eick, S. M. Zahurak, R. Tycko, G. Dabbagh, and F. A. Thiel. 1991. *Nature* 350, 320.
- [4] Hebard, A. F., M. J. Rosseinsky, R. C. Haddon, D. W. Murphy, S. H. Glarum, T. T. M. Palstra, A. P. Ramirez, and A. R. Kortan. 1991. *Nature* 350, 600.
- [5] Kochanski, G. P., A. F. Hebard, R. C. Haddon, and A. T. Fiory. 1992. *Science* 255, 184.
- [6] Tanigaki, K., T. W. Ebbeson, S. Saito, J. Mizuki, J. S. Tsai, Y. Kubo, and S. Kuroshima. 1991. *Nature* 352, 222.
- [7] for reviews see (a) R. C. Haddon, *Acc. Chem. Res.* 25 (1992) 127, and (b) A. F. Hebard. *Phys. Today*, November (1992) 26.
- [8] McCauley, J. P., Jr., Q. Zhu, N. Coustel, O. Zhou, G. Vaughan, S. H. J. Idziak, J. E. Fischer, S. W. Tozer, D. M. Groski, N. Bykovetz, C. L. Lin, A. R. McGhie, B. H. Allen, W. J. Romanov, A. M. Denenstien, and A. B. Smith, III. 1991. *J. Am. Chem. Soc.* 113, 8537.
- [9] Bensebaa, F., B. Xiang, and L. Kevan. 1992. *J. Phys. Chem.* 96, 6118.
- [10] Tokumoto, M., Y. Tanaka, N. Kinoshita, T. Kinoshita, Y. Ishibashi, and H. Ihara. 1993. Meeting of the Materials Research Society, Boston, MA.
- [11] Chabre, Y., D. Djurado, M. Armand, W. R. Romonow, N. Coustel, J. P. McCauley, Jr., J. E. Fischer, and A. B. Smith, III. 1992. *J. Am. Chem. Soc.* 114, 764.

- [12] Koh, W., D. Dubois, W. Kutner, M. T. Jones, and K. M. Kadish. 1993. *J. Phys. Chem.* 97, 6871.
- [13] Wang, H. H., A. M. Kini, D. M. Savall, K. D. Carlson, J. M. Williams, M. W. Lathrop, K. R. Lykke, D. H. Parker, M. J. Pellin, D. M. Gruen, U. Welp, W.-K. Kwok, S. Fleshler, and G. W. Crabtree. 1991. *Inorg. Chem.* 30, 2838.
- [14] Wang, H. H., A. M. Kini, B. M. Savall, K. D. Carlson, J. M. Williams, M. W. Lathrop, K. R. Lykke, D. H. Parker, P. Wurz, M. J. Pellin, D. M. Gruen, U. Welp, W.-K. Kwok, S. Fleshler, G. W. Crabtree, J. E. Schirber, and D. L. Overmyer. 1991. *Inorg. Chem.* 30, 2962.
- [15] Murphy, D. W., M. J. Rosseinsky, R. M. Fleming, R. Tycko, A. P. Ramirez, R. C. Haddon, T. Siegrist, G. Dabbagh, J. C. Tully, and R. E. Walstedt. 1992. *J. Phys. Chem. Solids*, vol. 53, p. 1321.
- [16] see for example J. L. Dye, *Science* 247 (1990) 663 or "Metal-Ammonia Solutions," G. Lepoutre, and M. J. Sienko (eds.), W. A. Benjamin, Inc., New York, (1964).
- [17] Heath, G. A., J. E. McGrady, and R. L. Martin. 1992. *J. Chem. Soc., Chem. Commun.* 1272.
- [18] Fullagar, W. K., I. R. Gentle, G. A. Heath, and J. W. White. 1993. *J. Chem. Soc., Chem. Comm.* 525.
- [19] Zhou, O., R. M. Fleming, D. W. Murphy, M. J. Rosseinsky, A. P. Ramirez, R. B. van Dover, and R. C. Haddon. 1993. *Nature* 362, 433.
- [20] Setton, R. 1990. "Graphite Intercalation Compounds," H. Zabel, and S. A. Solis (eds.), Springer-Verlag, Berlin.
- [21] Buffinger, D. R., R. P. Ziebarth, V. A. Stenger, and C. H. Pennington. 1993. *J. Am. Chem. Soc.* 115, 9267.
- [22] Kraus, C. A. 1908. *J. Am. Chem. Soc.* 30, 1323.
- [23] Zhou, O., R. M. Fleming, D. W. Murphy, A. F. Hebard, and R. C. Haddon. 1993. Meeting of the Materials Research Society, Boston, MA.
- [24] Fleming, R. M., A. P. Ramirez, M. J. Rosseinsky, D. W. Murphy, R. C. Haddon, and S. M. Zahurak. 1991. *Nature* 352, 787.
- [25] Fleming, R. M., M. J. Rosseinsky, A. P. Ramirez, D. W. Murphy, J. C. Tully, R. C. Haddon, T. Siegrist, R. Tycko, S. H. Glarum, P. Marsh, G. Dabbagh, S. M. Zahurak, A. V. Makhija, and C. Hampton. 1991. *Nature* 352, 701.
- [26] Stephens, P. W., L. Mihaly, P. L. Lee, R. L. Whetten, S.-M. Huang, R. Kaner, F. Deiderich, and K. Holczer. 1991. *Nature* 351, 362.
- [27] Holczer, K., and R. L. Whetten. 1992. *Carbon* 30, 1261.

[28] Zhao, W. B., X. D. Zhang, Z. Y. Ye, J. L. Zhang, C. Y. Li, D. L. Yin, Z. N. Gu, X. H. Zhou, and Z. X. Jin. 1993. Meeting Abstracts for Fullerenes '93, Santa Barbara, CA, 90.

[29] Buntar, V., and C. Politis. 1993. Meeting of the Materials Research Society, Boston, MA.

Principal Investigator:

R. D. Boss

0601152N

NRaD ZW68

# A New Ordering Algorithm for Exposing Parallelism in Sparse Symmetric Matrices

A. K. Kevorkian

*Given a sparse symmetric matrix  $M$ , we develop an ordering algorithm to find a permutation matrix  $P$  so that parallelism inherent in  $M$  is fully exposed in the matrix  $PMP^T$ . The key steps in the ordering algorithm are as follows. First, compute in the undirected graph  $G = (V, E)$  of  $M$  a set of vertices  $S^*$  such that the induced subgraph  $G(V - S^*)$  contains parallel regions inherent in  $M$ . This step gives rise to a block diagonal matrix  $A$  such that each diagonal block is a full matrix in  $M$ . Second, factor block diagonal matrix  $A$  symbolically and compute the symbolic form of the Schur complement of  $A$  in  $M$ . Third, replace original matrix  $M$  by the symbolic Schur complement, and repeat the process until the symbolic Schur complement is a full matrix. By a property of the set  $S^*$ , the ordering algorithm takes advantage of all principal submatrices of  $M$  that do not produce fill-in in any part of  $M$  when symbolically factored. Applications to a large collection of sparse matrices show that the new ordering algorithm is an effective tool for exposing parallelism in sparse symmetric problems. Also, comparisons show that the new algorithm fares favorably with commonly used ordering methods.*

## INTRODUCTION

A central problem in the solution of large sparse symmetric positive definite systems of equations

$$Mx = b$$

is the finding of a permutation matrix  $P$  such that  $PMP^T$  has sparse Cholesky factor. The pivotal importance of the permutation matrix  $P$  in the total solution of the symmetric system of equations  $Mx = b$  has led to several highly successful and widely used sparse matrix ordering methods. These include the nested dissection method [3], minimum degree ordering [3], [4], [8], and band and envelope reduction methods [3].

With the arrival of parallel architecture machines in the mainstream of advanced scientific computing, the main objective of the permutation matrix has been expanded so that the Cholesky factor of  $PMP^T$  is not only sparse but also suitable for parallel computation. The most popular notion used to date for the parallel ordering problem is that of the elimination tree associated with a Cholesky factor [9], [14]. The key role of the elimination tree model in the parallel ordering problem is to find a sparse Cholesky factor whose elimination tree has small height. Liu [10] has described a two-stage method that accomplishes this objective by combining minimum degree and nested dissection orderings. Pothien, Simon, and Wang [12] have recently reported a spectral nested dissection algorithm that recursively uses spectral separator algorithm to compute parallel orderings.

In this work, we present a new ordering algorithm to compute a permutation matrix  $P$  such that  $PMP^T$  has sparse Cholesky factor and is suitable for parallel computation. Letting  $G = (V, E)$  denote the undirected graph of the sparse symmetric matrix  $M$ , the ordering algorithm comprises three distinct steps that are covered next.

## A VERTEX PARTITION FOR EXPOSING HIDDEN PARALLELISMS

The first step of the ordering algorithm consists of a four-stage parallelization tool for exposing parallelism in general sparse symmetric matrices. These four stages are

1. Compute the set of vertices  $S = \{v \in V \mid \exists (v,w) \in E \text{ with } \deg_G v > \deg_G w\}$ ,
2. Compute connected components of induced subgraph  $G(V - S)$ ,
3. Classify the clique connected components of  $G(V - S)$ , and
4. Compute independent cliques in nonclique connected components of  $G(V - S)$ .

Through these four algorithmic stages, we arrive at a vertex partition

$$\Pi^* = (V_1, V_2, \dots, V_r, S^*),$$

where

$$S \subseteq S^*,$$

satisfying the following three properties:

- a. For any two distinct sets  $V_i$  and  $V_j$ , no vertex in  $V_i$  is adjacent to a vertex in  $V_j$ ;
- b. For any set  $V_i$ ,  $G(V_i)$  is a clique in  $G$ ; and
- c. The interior of any clique in  $G$  is an element of the vertex partition.

By property (a), condensation of  $G$  with respect to  $\Pi^*$  is a graph with root vertex  $S^*$  and leaf vertices  $V_1$  through  $V_r$ . Figure 1 illustrates condensation of  $G$  with respect to vertex partition  $\Pi^*$ . By the star shape of the graph in figure 1 and property (b), the leaf vertices  $V_1$  through  $V_r$  correspond to  $r$  dense computational tasks that are independent of each other and thus can be processed in parallel. Property (c) forms the most novel and critical part. To highlight this property, we need to elaborate on the concept of interior clique [6]. Let  $G$  be the undirected graph of any  $n$  by  $n$  symmetric matrix  $M$ , and let  $A$  be any principal submatrix of  $M$  whose graph is an interior clique in  $G$ . Then by the definition of interior clique, the symbolic factorization of block  $A$  will not create any nonzero in a position that is zero in  $M$  (fill-in). Thus, property (c) states that any principal submatrix of  $M$  that fully preserves sparsity when symbolically factored, is part of an independent task identified by the parallelization tool.

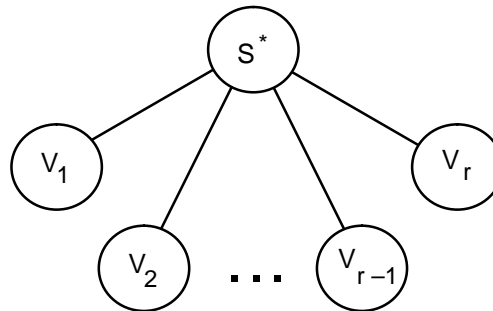
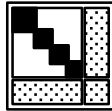


**Figure 1. Condensation of  $G$  with respect to vertex partition  $\Pi^*$ .**

## A PARALLEL ORDERING ALGORITHM DERIVED FROM VERTEX PARTITION $\Pi^*$

Let  $M$  be any symmetric matrix with undirected graph  $G = (V, E)$ . By property (a) of vertex partition  $\Pi^*$ , there exists in  $M$  an  $r$  by  $r$  block diagonal matrix  $A$  with diagonal blocks  $A_1$  through  $A_r$  such that block  $A_i$  corresponds to induced subgraph  $G(V_i)$  for  $1 \leq i \leq r$ . Thus by property (a) of vertex partition  $\Pi^*$ , there exists a permutation matrix  $P$  such that  $PMP^T$  has the block bordered diagonal form

$$PMP^T = \begin{bmatrix} A & B \\ B^T & D \end{bmatrix}. \quad (1)$$



Property (b) of vertex partition  $\Pi^*$  ensures that each diagonal block of the leading block  $A$  is a full matrix (we assume that the original matrix  $M$  has nonzero main diagonal). We will refer to  $A$  as the block pivot in  $PMP^T$ .

Without loss of generality, suppose the block pivot  $A$  is nonsingular, and let  $U$  be the upper Cholesky factor of  $A$ . Then the block matrix  $PMP^T$  can be written in the block product form

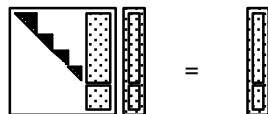
$$PMP^T = \begin{bmatrix} U^T & 0 \\ X^T & I \end{bmatrix} \begin{bmatrix} U & X \\ 0 & D - X^T X \end{bmatrix} \quad (2)$$

in which  $I$  is an identity matrix, the  $0$ 's are zero matrices, and the block  $X$  is the solution of the multiple right-hand-side triangular system  $U^T X = B$ . The matrix  $D - X^T X$  is the familiar Schur complement of  $A$  in  $M$ . Replacing  $M$  by  $PMP^T$  in the original system of equations  $Mx = b$ , we obtain the following equivalent system

$$(PMP^T)(Px) = (Pb). \quad (3)$$

Consider this system where  $PMP^T$  has been factored into the block product form (2) and the vectors  $Px$  and  $Pb$  have been partitioned conformably into the direct sums of  $y$  and  $z$ , and  $f$  and  $h$ , respectively. The system of equations (3) then becomes

$$\begin{bmatrix} U & X \\ 0 & D - X^T X \end{bmatrix} \begin{bmatrix} y \\ z \end{bmatrix} = \begin{bmatrix} w \\ h - X^T w \end{bmatrix} \quad (4)$$



where  $w$  is the solution of the lower triangular system  $U^T w = f$ . The zero-nonzero structure of the Cholesky factor  $U$  in (4) serves to illustrate the point that all  $r$  diagonal blocks of  $A$  can be factored in parallel, and that block  $X$  can be computed from  $U^T X = B$  by solving  $r$  triangular systems with multiple right-hand sides in parallel.

If the Schur complement  $D - X^T X$  in (4) is dense, the solution of  $Mx = b$  is obtained by solving the two systems of equations  $(D - X^T X)z = h - X^T w$  and  $Uy = w - Xz$  in that order and setting  $x = P^T[y \ z]^T$ . However, in many industrial sparse matrix applications the Schur complement  $D - X^T X$  is generally sparse and large. Therefore, to deal with the most general case we need an algorithm that recursively uses the four-stage parallelization tool until the symbolic form of the Schur complement  $D - X^T X$  is either full or dense. In the Algol-like language adopted by Aho, Hopcroft, and Ullman [1], the new sparse matrix ordering algorithm takes the following form.

```

procedure parallel_ordering:
while G is not a clique do
  begin
    search;
    if S is not empty then
      dfs
    else
      cliques(V)
    end;
    comment we now have vertex partition  $\Pi^*$  or block pivot A in  $PMP^T$ ;
    sfp;
    comment procedure sfp computes symbolic form  $\Delta$  of  $D - X^T X$ ;
    replace  $G = (V, E)$  by graph of  $\Delta$ 
  end

```

Procedure search computes the set of vertices S. If S is empty, we call procedure cliques(V) to compute independent cliques in G. If S is not empty, we call procedure dfs (depth-first search) to compute the connected components of induced subgraph  $G(V - S)$ . For each connected component  $G(U)$  of  $G(V - S)$ , dfs invokes a procedure called classify(U) to analyze  $G(U)$ . If  $G(U)$  is a clique, then the set of vertices U is a leaf element of vertex partition  $\Pi^*$ . If  $G(U)$  is not a clique, then procedure classify(U) calls cliques(U) to compute independent cliques in  $G(U)$ . For each independent clique  $G(U')$  in  $G(U)$ , the set of vertices  $U'$  is a leaf element of vertex partition  $\Pi^*$ . At the completion of procedure dfs, the computation of vertex partition  $\Pi^*$  or block pivot A in  $PMP^T$  is complete. Subsequently, we call procedure sfp (symbolic factorization procedure) to compute the symbolic form  $\Delta$  of the Schur complement  $D - X^T X$ . The symbolic form of block X in (2) is computed in procedure classify. Finally, we set G to the graph of the symbolic Schur complement and repeat the above steps until G is a clique. In practice, the recursion in the parallel ordering algorithm may be terminated when the Schur complement becomes very dense. Detailed descriptions of the procedures used in the algorithm parallel\_ordering are given in [7].

## COMPUTATIONAL RESULTS AND COMPARISONS

In this section, we evaluate the new parallel ordering algorithm and compare it with two commonly used ordering methods implemented in MATLAB [11]. These are the minimum degree method and the reverse Cuthill–McKee band-reduction method. The MATLAB implementation of the minimum degree ordering incorporates many of the latest developments of minimum degree as well as ideas for enhancing parallel sparse matrix factorizations [5]. The reverse Cuthill–McKee was included in the evaluation since the benchmark contained banded matrices. The benchmark for the comparisons comprised a set of 21 sparse symmetric matrices drawn from applications of linear and quadratic programming to industrial problems [13] and from the Harwell–Boeing sparse matrix collection [2].

Table 1 summarizes the results for the sparse matrices from linear and quadratic programming applications. The heading **identifier / n / nz** in the first column of table 1 refers to the name of the specific application, the order of the sparse symmetric matrix  $M$ , and the number of nonzeros in  $M$ , respectively. The second-column heading **method** includes the MATLAB minimum degree method (mmd), the MATLAB reverse Cuthill–McKee method (rcm), and the new parallel ordering algorithm (pal). The third-column heading **nz** gives the total number of nonzero entries in  $R^T + R$  where  $R$  is the upper Cholesky factor of  $PMP^T$ . The fourth-column heading **fill-in** gives the number of fill-ins created in the upper Cholesky factor  $R$  by each of the three methods: rcm, mmd, and pal. The fifth and last column gives the elimination tree height for each of the three methods.

For the second through tenth problems in table 1, the new ordering algorithm performs better than the minimum degree and reverse Cuthill–McKee methods in the number of fill-ins. It also performs better than the minimum degree method in computing elimination trees with smaller heights. It is worth noting that for problem *scfxm1*, the height of the elimination tree of the Cholesky factor computed by the new ordering method is about 65 percent of the elimination tree height computed by the minimum degree method. Figures 2 through 4 show the zero-nonzero structures of the matrix  $R^T + R$  for the three problems **scfxm1** (5th example), **seba** (6th example), and **pilot** (9th example). Favorable results were also obtained on test problems from the Boeing–Harwell sparse matrix collection. Detailed comparisons are being reported in a Technical Report and an external publication [7].

Table 1. Examples from linear and quadratic programming applications.

identifier/n/nz	method	nz ( $R^T+R$ )	fill-in ( $R$ )	elimination tree height
share1b/117/1885	rcm	3360	796	71
	mmd	2538	385	43
	pal	2737	426	46
israel/214/5682	rcm	25574	9946	187
	mmd	7234	776	60
	pal	7168	743	57
brandy/255/5273	rcm	18767	6747	160
	mmd	8893	1810	80
	pal	8835	1781	78
bandm/320/6848	rcm	21134	7143	242
	mmd	10848	2000	73
	pal	9180	1166	65
scfxm1/473/5613	rcm	22463	8425	306
	mmd	15083	4735	105
	pal	11409	2898	68
seba/529/7639	rcm	69157	30759	281
	mmd	9003	682	43
	pal	8851	606	32
fffff800/616/16446	rcm	160038	71796	482
	mmd	35638	9596	137
	pal	34922	9238	132
shell/651/3809	rcm	19435	7813	234
	mmd	8925	2558	75
	pal	8519	2355	58
pilot/1129/10733	rcm	151817	70522	751
	mmd	43181	16204	152
	pal	37451	13339	142
25fv47/1301/22307	rcm	253359	115526	807
	mmd	102797	40245	265
	pal	83501	30597	232

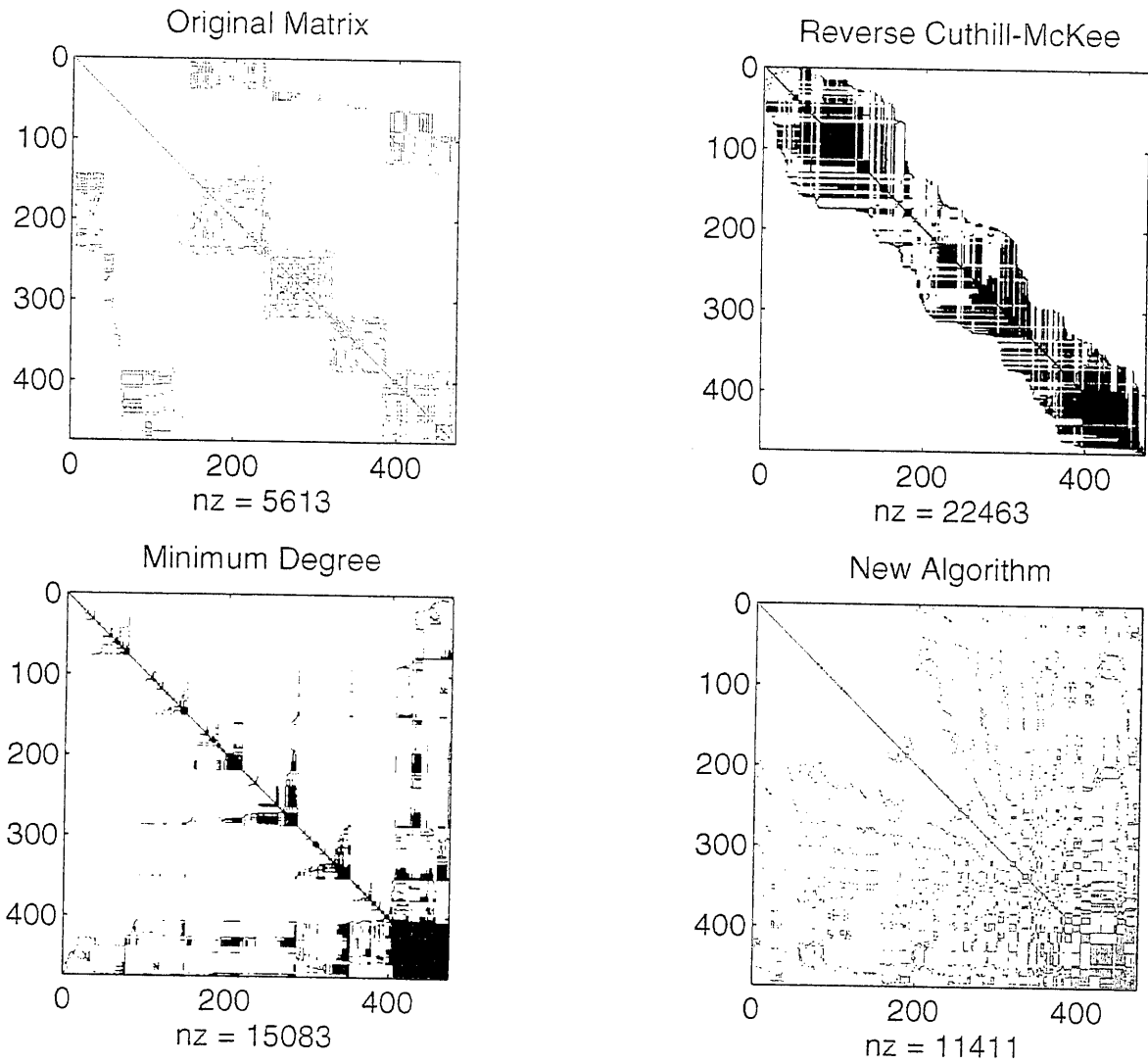


Figure 2. Sparsity structure of  $R^T + R$  for problem *scfxm1*.



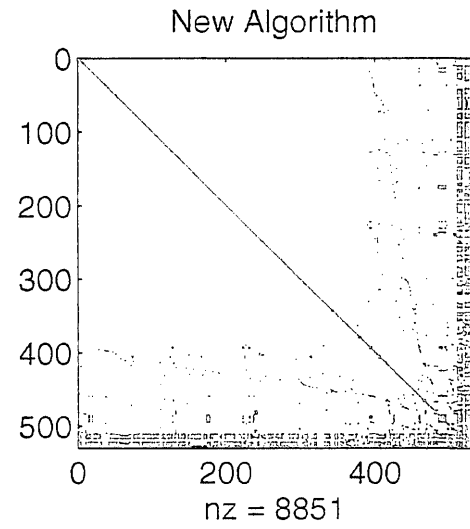
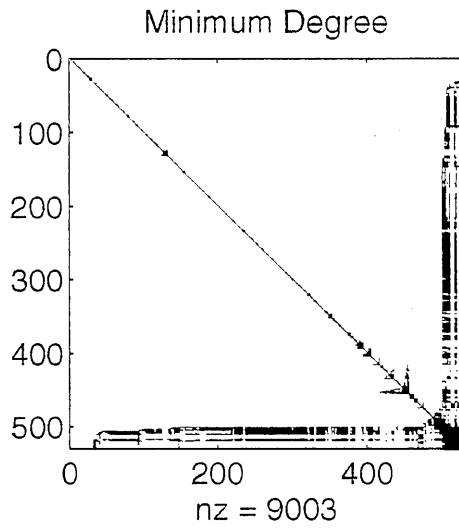
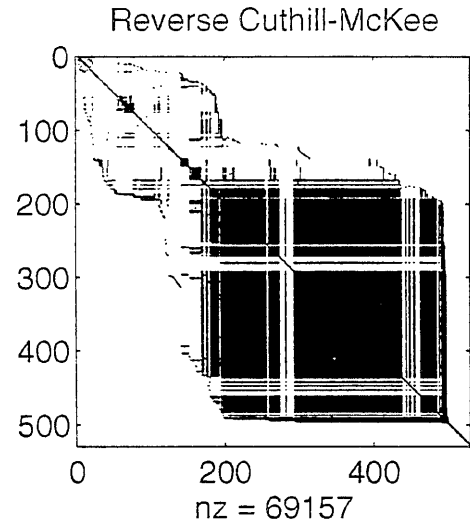
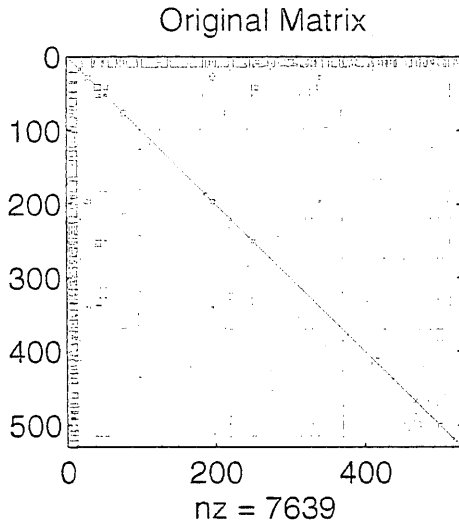


Figure 3. Sparsity structure of  $R^T+R$  for problem *seba*.



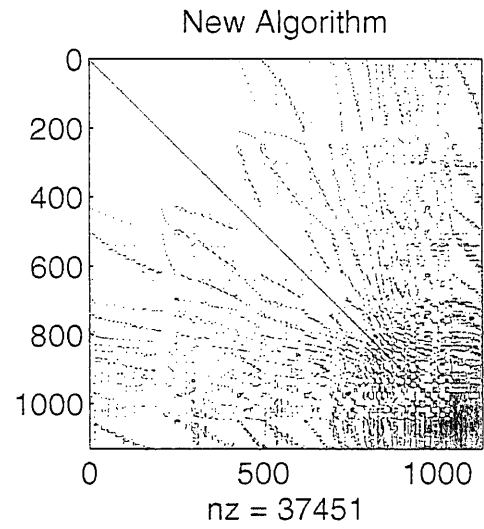
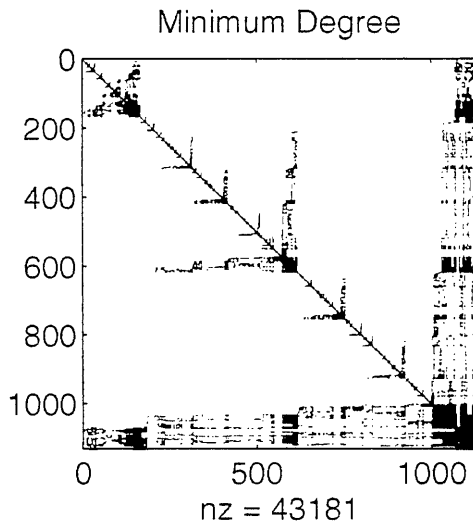
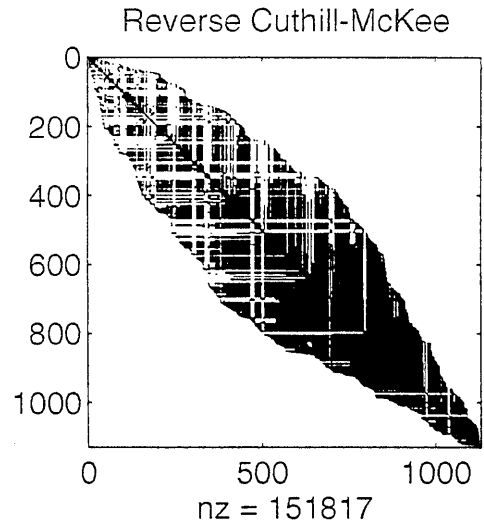
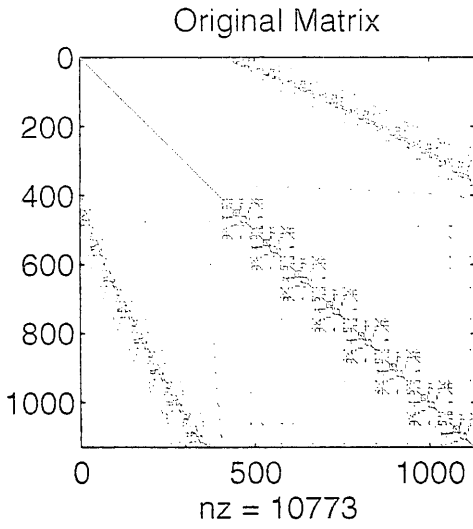


Figure 4. Sparsity structure of  $R^T+R$  for problem pilot.



## REFERENCES

- [1] Aho, A. V., J. E. Hopcroft, and J. D. Ullman. 1976. *The Design and Analysis of Computer Algorithms*, Reading, MA, Addison-Wesley, 3rd Printing.
- [2] Duff, I. S., R. G. Grimes, and J. G. Lewis. 1989. "Sparse Matrix Test Problems," *ACM Trans. Math. Software*, vol. 15, pp. 1–14.
- [3] George, A. and J. W.-H. Liu. 1981. *Computer Solution of Large Sparse Positive Definite Systems*, Prentice-Hall, Inc., Englewood Cliffs, New Jersey.
- [4] *Ibid.* 1989. "The Evolution of the Minimum Degree Algorithm," *SIAM Review*, vol. 31, pp. 1–19.
- [5] Gilbert, J. R., C. Moler, and R. Schreiber. 1992. "Sparse Matrices in MATLAB: Design and Implementation," *SIAM J. Matrix Anal. Appl.*, vol. 13, pp. 333–356.
- [6] Kevorkian, A. K. 1993. "Decomposition of Large Sparse Symmetric Systems for Parallel Computation. Part 1: Theoretical Foundations," NRaD TR 1572 (March). Naval Command, Control and Ocean Surveillance Center, RDT&E Division, San Diego, CA.
- [7] *Ibid.* 1995. "An Ordering Algorithm for Exposing Parallelism in Large Sparse Symmetric Matrices." NRaD TR 1697 (in preparation). Naval Command, Control and Ocean Surveillance Center, RDT&E Division, San Diego, CA. Also submitted to *SIAM Journal on Scientific Computing*.
- [8] Liu, J.W.-H. 1985. "Modification of the Minimum Degree Algorithm by Multiple Elimination," *ACM Trans. Math. Software*, vol. 11, pp. 141–153.
- [9] *Ibid.* 1986. "A Compact Row Storage Scheme for Cholesky Factors Using Elimination Trees," *ACM Trans. Math. Software*, vol. 12, pp. 127–148.
- [10] *Ibid.* 1989. "Reordering Sparse Matrices for Parallel Computation," *Parallel Computing*, vol. 11, pp. 73–91.
- [11] "The Mathworks." 1990. *Pro-MATLAB User's Guide*, South Natick, MA.
- [12] Pothen, A., H. D. Simon, and L. Wang. 1992. "Spectral Nested Dissection," Technical Report RNR-92-003, NASA Ames Research Center, Moffett Field, CA.
- [13] Saunders, M. A., Private communication, 1992–1993.
- [14] Schreiber, R. 1982. "A New Implementation of the Sparse Gaussian Elimination," *ACM Trans. Math. Software*, vol. 8, pp. 256–276.

Principal Investigator:  
Dr. A. K. Kevorkian

0601152N  
NRaD ZW62



# Evolving Artificial Neural Networks

**J. R. McDonnell**

*Variable topology, feedforward networks are constructed by training a population of hidden units and then incorporating the best hidden unit from the population into an artificial neural network's structure. Evolutionary search is employed in the optimization of both the hidden units' structure and weights. Unlike conventional methods, the newly incorporated hidden units are not necessarily fully connected to all previous inputs and hidden units in the net. Neural networks trained by the proposed technique are applicable to nonlinear system modeling and pattern recognition, as demonstrated here on sample time-series and pattern classification tasks, respectively. Parsimony is then further addressed with the formulation of a mixture-activation function so that hidden units can be either ridge- or kernel-type functions allowing for a combination of functions that best describes the data set.*

## INTRODUCTION

Although neural networks have found widespread usage as function approximators (e.g., pattern classifiers and nonlinear models), the design of neural network architectures remains largely an art guided by insight into the nature of the problem and/or the designer's past experience. The objective of this research is to evaluate the capabilities of evolutionary search for solving the dual problem of architecture selection and weight training. A primary benefit of using an automated design approach is realized by a reduction in the labor associated with evaluating various architectures until a trainable implementation is found. Additional benefits are accrued by incorporating a design approach that balances network's performance with its complexity. This report presents an overview of a computationally efficient implementation of evolutionary search to the problem of artificial neural network design.

Evolutionary optimization is a multiagent stochastic search process that emulates Darwinian evolution. Because evolutionary optimization is a direct search method, it does not rely on the assumptions (such as continuity) required by higher order search techniques. As with most global optimization techniques, evolutionary search sacrifices local knowledge of the search space, which may result in a loss of efficiency since the analytical form of the underlying model is not taken advantage of during the search process. Nevertheless, evolutionary search has proven to be an effective optimization technique on problems that are not analytically tractable and/or have many local extrema.

The evolutionary search method employed throughout most of this research is actually a hybrid combination of evolutionary programming (Fogel, 1992) and an evolution strategy (Bäck and Schwefel, 1993). However, based on investigations by McDonnell and Waagen (1995), an evolution strategy (ES), which combines attributes of both the original ES (Schwefel, 1981) and its later modification (Bäck and Schwefel, 1993), is recommended by the author. By combining attributes of both Schwefel's and Bäck and Schwefel's recommended algorithms into a single ES, faster and more reliable convergence to the global extremum was observed on a small set of real-valued surfaces (McDonnell and Waagen, 1995). The generic form of an evolutionary search algorithm is given below in figure NO TAG.

```

evolutionary search procedure
begin
k=0
initialize parent population P(k)
evaluate P(k)
do {
    generate offspring O(k) from P(k)
    evaluate O(k)
    select P(k+1) from {P(k) ∪ O(k)}
    k=k+1
} while (terminate criteria not met)
end

```

*Figure 1. A generic evolutionary search algorithm.*

The current project investigates the feasibility of evolutionary search for automatically generating general feedforward architectures, such as the example shown in figure 2. The design philosophy is to let the user define the desired input/output (I/O) mapping, thus specifying the number of input and output units, and let the number of hidden units and their interconnectivity be automatically determined. Many experiments were conducted that employed evolutionary search for generating both neural network structures and weights simultaneously. For example, investigations were conducted that pruned nodes in fully connected, feedforward networks. For simple functional mappings, it was demonstrated that evolutionary search could be employed for adding and deleting nodes until the optimal number of hidden units were attained. Relaxing the assumptions about network connectivity, additional investigations showed that the connectivity between layers could also be determined. However, if a static objective function accounted for network complexity, it was found that the network may rapidly prune away all of the connections unless some degree of learning immediately took place. This result occurred as a consequence of reducing the complexity cost at the expense of performance. The rapid pruning problem can be alleviated either by using a variable complexity penalty term (discussed subsequently) or, perhaps, by deterministically training the output weights to increase the overall learning rate. Finally, it is noted that the latter approach assumed the notion of layers of units and restricts connectivity as existent only between layers.

Preliminary investigations also revealed that high-performance computing resources are necessary for evolving a population of networks of substantial size. To circumvent this problem, subcomponents of a single network are trained because it is computationally more efficient to optimize a population of candidate hidden units than to search over a population of candidate artificial neural networks. The cascade-correlation learning algorithm (CCLA) serves as the basis for implementing this idea. The CCLA and the application of evolutionary search to cascaded networks are presented below.

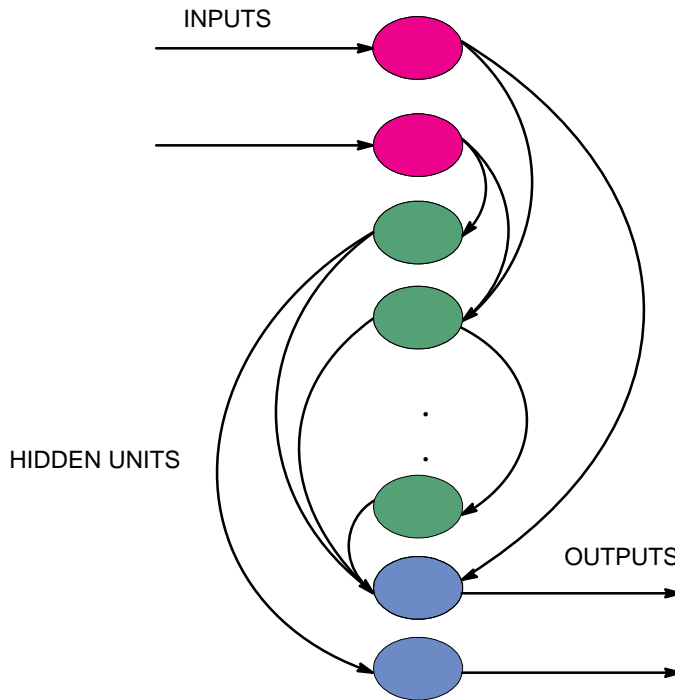


Figure 2. A general feedforward network.

## CASCADE-CORRELATION LEARNING ARCHITECTURES

The cascade-correlation learning algorithm was developed as a means of automatically constructing feedforward networks by adding hidden units until a desired mapping could be achieved (Fahlman and Lebiere, 1990). The network is initialized with only the input units feeding directly to the output units. New hidden units are added on an individual basis (one-by-one) into the network until a termination criterion is met. Each new hidden unit is selected from a pool of candidate units and is incorporated into the network with its input weights frozen. Using a pool of candidate units increases the likelihood of finding a good hidden unit by reducing the susceptibility to poor initial conditions.

The CCLA is amenable to population-based evolutionary search algorithms since a population of candidate hidden units is typically used during the CCLA construction process. The goal of each candidate unit in the population pool is to maximize the correlation between its output and the residual output error of the network. This is the correlation aspect of the cascade-correlation algorithm. Each newly incorporated hidden unit is connected to *all* input and previously generated hidden units in the network, as shown in figure NO TAG. Likewise, each newly incorporated hidden unit is also fully connected to all of the output units. Since a node is “frozen” into the network, it is imperative that only good nodes be added. After each hidden unit is inserted into the network, training takes place on the output layer weights with the hidden unit weights remaining fixed.



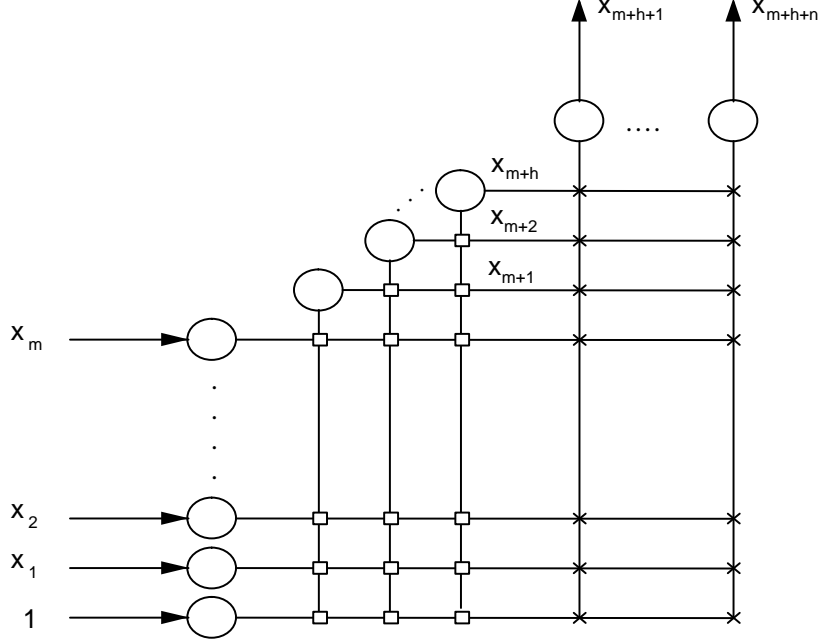


Figure 3. The cascade-correlation network structure. The boxes  $\square$  indicate weights that are frozen when the unit is incorporated into the network. The crosses  $\times$  indicate weights that are modified after a new hidden unit is incorporated.

The hidden and output units achieve the following mappings:

$$\text{hidden unit:} \quad x_i = g_i \left[ \sum_{j=1}^{i-1} \alpha_{ij} x_j \right] \quad m < i \leq m + h,$$

$$\text{output unit:} \quad x_i = g_i \left[ \sum_{j=1}^{m+h} \alpha_{ij} x_j \right] \quad m + h < i \leq m + h + n,$$

where  $h$  represents the number of hidden units,  $m$  the number of inputs, and  $n$  the number of outputs. The cascade-correlation learning approach appears quite similar to projection pursuit regression (Huber, 1985) when, assuming linear outputs, the output equation is broken down into its linear and nonlinear components

$$x_i = \mathbf{a}_i^T \mathbf{u} + \sum_{j=m+1}^{m+h} \alpha_{ij} g_j(\alpha_j, \mathbf{u}).$$

where  $\mathbf{u} = x_i \forall i \in \{1, \dots, m\}$ , and  $\alpha_i = \alpha_{ij} \forall j \in \{1, \dots, m\}$ . However, this view oversimplifies the repeated nonlinear transformations that actually occur as described by

$$x_i = \mathbf{a}_i^T \mathbf{u} + \sum_{j=m+1}^{m+h} \alpha_{ij} g_j \left( \mathbf{a}_j^T \mathbf{u} + \sum_{k=m+1}^{j-1} \alpha_{jk} g_k(\alpha_k, \mathbf{u}) \right).$$

## NEURAL NETWORK COMPLEXITY

In accordance with Occam's razor, networks that are parsimonious usually generalize better on new data. A variety of techniques can be used to avoid overfitting training data, and parsimony is not requisite in achieving good generalization capabilities. However, adaptive networks have demonstrated superior performance over fixed-topology networks on certain benchmark problems. Techniques employed for determining network structures include increasing network size by the addition of hidden units/layers or pruning an oversized, trained network to generate a smaller network. The CCLA falls into the former class of approaches.

Since it is desirable to construct parsimonious architectures, a risk or objective function is used that incorporates both system performance and model complexity. The common form of such a risk function is given by Haykin (1994) as  $R(\mathbf{w}) = E_s(\mathbf{w}) + \lambda E_c(\mathbf{w})$  where  $E_s$  is the performance measure (usually the sum-squared error),  $E_c$  is the complexity penalty, and  $\lambda$  is the regularization parameter. As noted by Haykin, there exists a similarity between the risk function  $R(\mathbf{w})$  and the composition of statistically derived complexity terms like the minimum description length (MDL) criterion.

Initially,  $\lambda = 0$  so that performance is not sacrificed at the expense of complexity. Many approaches may be taken in adapting  $\lambda$  during the training process. One approach is to train for an arbitrary number of cycles, or until a specified condition is met, and then set  $\lambda$  to a positive constant. Successful implementation of this strategy may require *a priori* knowledge about  $E_s$  and  $E_c$  to achieve the desired balance between performance and parsimony. An alternative approach is to continually adapt the regularization parameter  $\lambda$  during the training process. Weigend et al. (1992) have formulated a set of heuristics that guide the adaptation process. Although Weigend et al. (1992) incorporate an additional lower bound estimate, only the current and previous risk values  $R(k)$  and  $R(k-1)$ , and the running average risk value as defined by  $R_{ave}(k) = \gamma R_{ave}(k-1) + (1-\gamma)R(k)$ ,  $0 < \gamma < 1$ , are considered here as the heuristic decision variables. Thus, the following heuristics are used in the present investigation for adaptively modifying the regularization parameter

- *Increment  $\lambda$* : If learning is progressing satisfactorily  $R(k) < R(k-1)$ , then  $\lambda$  may be incremented by some small amount  $\delta$  on the order of  $10^{-2}$ .
- *Decrement  $\lambda$* : If learning is not progressing satisfactorily, as judged by both  $R(k) \geq R(k-1)$  and  $R(k) < R_{ave}(k)$ , then  $\lambda$  may be decremented by some small amount  $\delta$  on the order of  $10^{-2}$ .
- *Drastically decrement  $\lambda$* : If learning is not progressing satisfactorily as judged by  $R(k) \geq R(k-1)$  and  $R(k) \geq R_{ave}(k)$ , then  $\lambda$  may be decremented by, say, 10 percent.

It is noted that besides leaving out the lower bound estimate in the adaptation process, the amount  $\delta$  by which  $\lambda$  is changed is significantly larger than the value given by Weigend et al. (1992) where  $\delta = 10^{-6}$ . The larger  $\delta$  employed in the present study facilitates a faster relaxation process on the candidate hidden unit structures.

## EVOLVING CCLA

Evolving the weights and connectivity structure of a population of candidate hidden units in a cascade-correlation network is computationally less demanding than evolving the weights and connectivity of a population of neural networks. A valid criticism of this approach is that, in exchange for these computational savings, one is solving only small parts of a large problem, thereby reducing the benefits associated with using global search methods on large-scale optimization problems. However, the combinatorial optimization properties of evolutionary algorithms remain beneficial for determining both the input weights and connections of individual candidate nodes.

Pruned CCLAs have also been constructed by Klagges and Soegtrop (1993) and Hansen and Pedersen (1994). Klagges and Soegtrop randomly connect an arbitrary number of fan-ins to each candidate node, and then train the population of nodes. Hansen and Pedersen use the optimal brain surgeon (OBS) technique for determining the fan-in structure of each candidate node. It is speculated that the evolutionary search approach proposed in the present investigation sacrifices the diversity maintained in training a multitude of independent (i.e., no interaction) candidate nodes since the candidate hidden units may tend to converge to very similar, if not the same, architectures as the search progresses.

A population of  $\mu$  candidate hidden units is randomly initialized with full connectivity as in the traditional CCLA. The same optimization objective (the absolute value of the covariance between the hidden unit and the residual error) used to train CCLA units is employed to represent the fitness of each candidate node

$$S(a_i) = \sum_o \left| \sum_p (z_{i,p} - \bar{z}_i)(e_{p,o} - \bar{e}_o) \right|,$$

where  $z_p$  represents the output of each candidate node for pattern  $p$ , and  $e_o$  is the residual error as measured at the network's output unit  $o$ . Weights for each candidate unit are modified using the perturbation equation

$$w'_{ij} = w_{ij} + \sqrt{Sf/S(a_i)} \cdot N_j(0, 1),$$

where  $Sf$  represents an arbitrarily selected scaling factor. Recombination of each weight vector takes place according to

$$\mathbf{w}_k = \mathbf{w}_i + \alpha(\mathbf{w}_j - \mathbf{w}_i),$$

where the indices and scaling coefficient are selected at random such that  $i, j \in \{1, \dots, \mu\}$ ,  $i \neq j$ , and  $\alpha \sim U(0, 1)$ . Selection is deterministic so that a new parent set is formed from the best  $\mu$  members of the set composed of the  $\mu$  original parents, the  $\mu$  mutated offspring, and the  $\mu$  recombined offspring. After an arbitrary number of generations, the best candidate unit is then inserted into the network.

The objective function, which incorporates the unit's complexity, is formulated using the standard CCLA performance measure  $S(a_i)$  in the risk function  $R(\mathbf{w})$ . Thus, the objective function retains the general form of the risk function and is given by

$$\Phi(a_i) = -S(a_i) + \lambda E_{c,N}(\mathbf{w}, k),$$

where  $E_{c,N}(\mathbf{w}, k)$  represents the complexity cost for  $N$  samples and  $k$  parameters. The MDL complexity term  $E_{c,N}(\mathbf{w}, k) = 0.5 \cdot k \log N$  is employed since the connections are strongly specified. Modification of the variable complexity regularization parameter  $\lambda$  is based on the risk  $\Phi$  of the best candidate node in the population at each generation. No degree of optimality is implied by the given formulation of  $\Phi(a_i)$ . An MSE performance criterion can be used in lieu of the covariance in the weight perturbation and risk function equations such that

$$w'_{ij} = w_{ij} + \sqrt{Sf \cdot MSE(a_i)} \cdot N_j(0, 1)$$

$$\Phi(a_i) = MSE(a_i) + \lambda E_{c,N}(\mathbf{w}, k)$$

Meta-level evolutionary search techniques that do not rely on non-negative performance criteria can also be implemented.

As opposed to the conventional performance-driven stopping criteria, a reasonable stopping criterion is to test the current model performance and the newly generated model performance on a validation set. When the current model has superior performance to the newly created model, training is stopped and no more units are added. Likewise, since the architecture is dynamic, training can continue by incorporating additional hidden units with the topology corresponding to the lowest risk function selected as the best, since it balances both performance and complexity.

To achieve variable connectivity, the fan-in structure of each candidate unit is also subject to the mutation and recombination operators. Diversity is introduced in the mutation step of the algorithm by randomly selecting an input connection to a candidate node and flipping its bit (i.e., 1→0 or 0→1). Recombination of the connectivity arrays is limited to the bitwise logical ‘AND’ and ‘OR’ operators as illustrated in figure NO TAG. The AND operation reinforces common connectivity structures while the OR operation retains any connectivity that exists between two randomly selected candidate nodes. Structural modifications occur less frequently than weight perturbations as suggested by Yao (1993), who advises that different time-scales should be applied at different levels of evolution. That is, modifying the connectivity should be considered a larger evolutionary step and occurs less frequently than a smaller evolutionary step such as perturbing the weight.

Parent Node 1	Operation	Parent Node 2	Offspring
[1111 0010]	AND	[1110 0110]	→ [1110 0010]
[1111 0010]	OR	[1110 0110]	→ [1111 0110]

*Figure 4. Bitwise logical operations applied to the candidate node connectivity strings.*

The output weights are found in a deterministic manner. The inputs to the output layer of the cascade-correlation architecture for  $p$  patterns are described by

$$\mathbf{X}_p = \begin{bmatrix} x_1^{(1)} & x_2^{(1)} & \dots & x_m^{(1)} & x_{m+1}^{(1)} & x_{m+2}^{(1)} & \dots & x_{m+h}^{(1)} \\ x_1^{(2)} & x_2^{(2)} & \dots & x_m^{(2)} & x_{m+1}^{(2)} & x_{m+2}^{(2)} & \dots & x_{m+h}^{(2)} \\ \vdots & \vdots & \ddots & \vdots & \vdots & \vdots & \ddots & \vdots \\ \vdots & \vdots & \ddots & \vdots & \vdots & \vdots & \ddots & \vdots \\ x_1^{(p)} & x_2^{(p)} & \dots & x_m^{(p)} & x_{m+1}^{(p)} & x_{m+2}^{(p)} & \dots & x_{m+h}^{(p)} \end{bmatrix}.$$

Likewise, the outputs of the network are given by

$$\mathbf{Y}_p = \begin{bmatrix} x_{m+h+1}^{(1)} & x_{m+h+2}^{(1)} & \dots & x_{m+h+n}^{(1)} \\ x_{m+h+1}^{(2)} & x_{m+h+2}^{(2)} & \dots & x_{m+h+n}^{(2)} \\ \vdots & \vdots & \ddots & \vdots \\ \vdots & \vdots & \ddots & \vdots \\ x_{m+h+1}^{(p)} & x_{m+h+2}^{(p)} & \dots & x_{m+h+n}^{(p)} \end{bmatrix},$$

where  $Y_p = X_p V$ . The optimal (in a least-squares sense) output weight set  $V$  can be determined using the pseudoinverse  $V = (X_p^T X_p)^{-1} X_p^T Y_p$ . Iterative deterministic methods, such as the LMS rule, are also appropriate for determining the  $n \cdot (m+h)$  output weights.

## CASE STUDIES

### A Time-Series Modeling Example

Evolutionary learning was applied to the CCLA in an effort to model the sunspot time-series data set. The average relative sunspot number represents a daily mean value taken from up to 50 observing stations throughout the world. The sunspot data set is typically broken down into a training set (years 1700 to 1920) and two test sets (years 1921 to 1955 and 1956 to 1979). A distinction between the two test sets is made based on their different statistical characteristics. This data set has served as a benchmark for a variety of statistical (including neural network) models. For example, both Priestly (1988) and Tong (1990) include this data set in their studies on nonlinear time series. Tong suggests that combining both linear and nonlinear prediction on the sunspot series might be beneficial since both models capture different attributes of the data. Such capability is inherent in the employed neural network model. The normalized mean-squared error (NMSE) is used to evaluate the performance of the model that generates next step predictions. The NMSE for the sunspot data set is referenced as the MSE of each data segment scaled by the variance of the full data set

$$\text{NMSE} = \frac{1}{N \cdot \hat{\sigma}_{all}^2} \sum_{i=1}^N (y_i - \hat{y}_i)^2$$

where  $\hat{y}$  is the single-step prediction, and  $y$  is the observed value. An NMSE = 1 implies that the estimate is the average of the observed values.

Pruning was not employed in the initial CCLA-evolutionary search experiment, which consisted of 100 parents (candidate nodes) and 100 generations (evolutionary training iterations). The experiment was arbitrarily stopped after the addition of three hidden units. It is noted that, as hidden units are added, the performance of each model on a validation set could be used as the termination criterion. This idea is easily implemented since a new model is built on the existent one. Table NO TAG shows that the performance of the relatively more complex model (as demonstrated by the higher number of parameters) is comparable to results generated using regularization techniques (pruning) in other investigations.

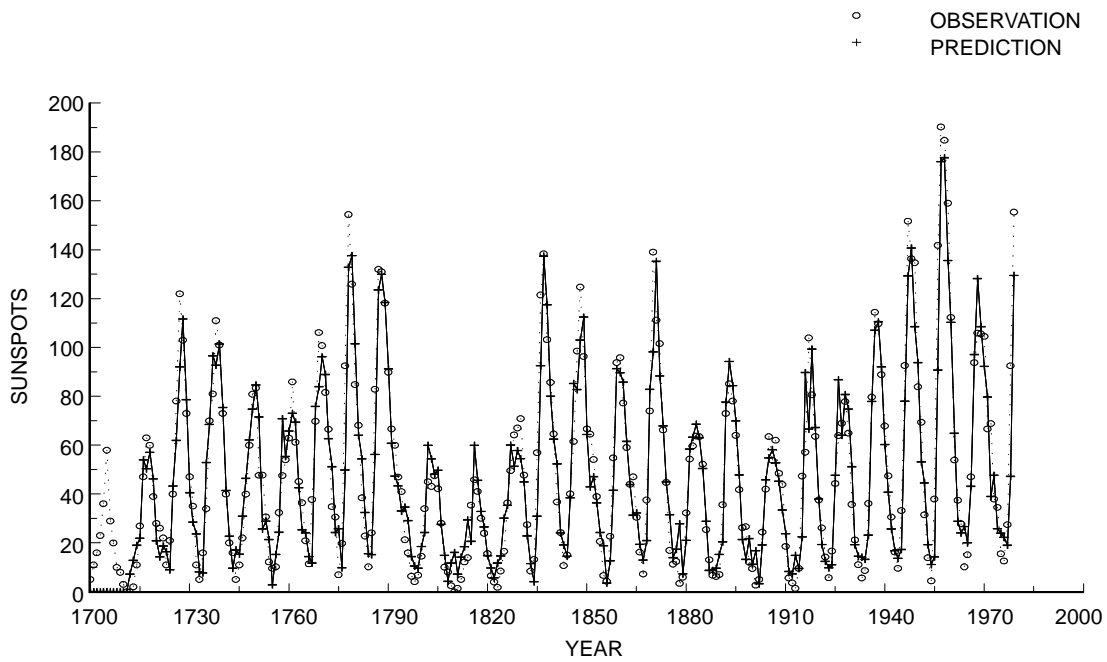
*Table 1. NMSE performance and complexity of various sunspot models.*

	NMSE Train: 1700–1920	NMSE Test: 1921–1955	NMSE Test: 1956–1979	No. of Parameters
Tong & Lim (1980)	0.097	0.097	0.28	16
Weigend et al. (1992)	0.082	0.086	0.35	43
Svarer et al. (1993)	0.090	0.082	0.35	12–16
Deco et al. (1994)	0.091	0.087	0.32	n/a
CCLA-EP (3 hidden nodes, not pruned)	0.084	0.082	0.36	58
CCLA-EP (4 hidden nodes, pruned)	0.094	0.083	0.25	27*

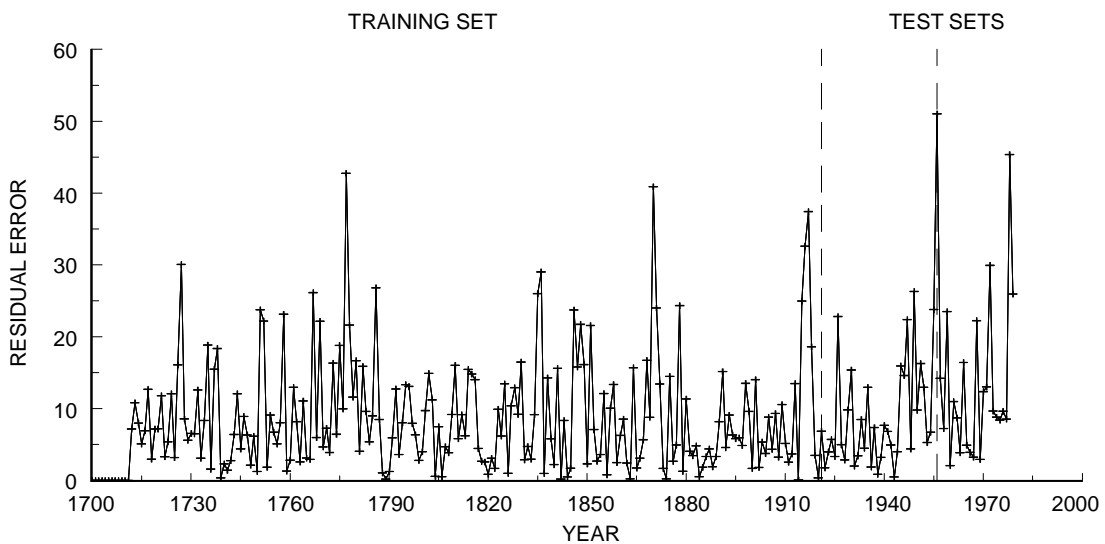
\*25 if output units are pruned. See text.

The next set of CCLA-evolutionary search experiments incorporated pruning during network construction and consisted of 50 parents with 100 generations. Training was arbitrarily stopped after four hidden units were added. For the pruned network, good generalization occurs on both test sets with roughly half as many parameters as the unpruned CCLA-EP network as given in table 1. Although not ardently pursued in the present investigation, additional pruning may take place on the output vector. For example, zeroing out the two smallest output weights yields essentially the same performance and reduces the model complexity to 25 parameters. Figure NO TAG shows the test and training results for the CCLA with complexity regularization. These results are the only results known to date that are better than Tong and Lim's threshold autoregressive model results for both testing sets.

The linear (AR) portion of the model describes most of the dynamics of the sunspot series. The linear model is augmented by the nonlinear (*tanh*) components of the CCLA as shown in figure NO TAG. The 10-year difference between the  $x(k-2)$  and  $x(k-12)$  inputs to the first hidden unit corresponds with the cycle with maximum power spectral content for the first 280 years (1700 to 1979). When more recent observations (1980 to 1987) of sunspot activity are included, the maximum power spectral content shifts to an 11-year cycle for the first 288 years (1700 to 1987). The sensitivity to additional observations illustrates the difficulty of building time-series models from a short data record (Marple, 1987).



(a) An approximation of the sunspot data over the years 1712 to 1799.



(b) The magnitude of the residual error for each year.

Figure 5. Results of the pruned, four hidden node CCLA with evolutionary learning.



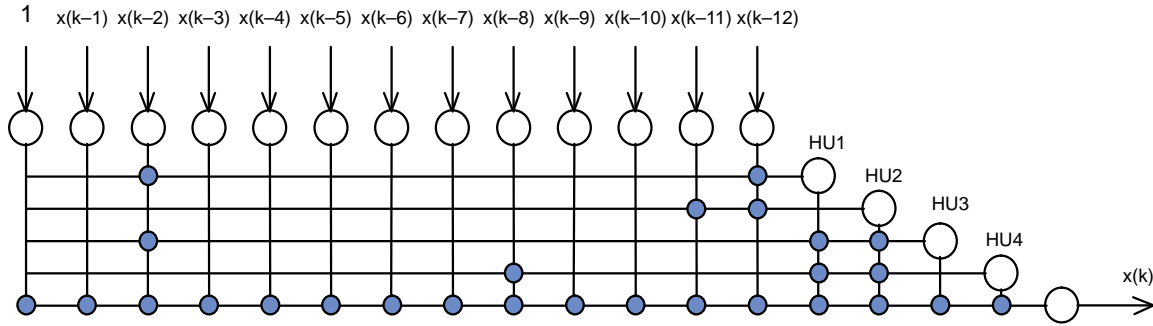


Figure 6. The resulting architecture for the CCLA-EP with complexity regularization. The solid circles represent active connections.

### A Pattern Classification Example

Consider the example taken from Flick et al. (1990) who proposed that two data classes exist on the unit square with the following probability density functions

$$p(x, y) = \begin{cases} 3.0 & [0.0] & 0 \leq y \leq 0.25 \\ 0.86 & [0.14] & 0.25 \leq y \leq b(x) \\ 0.14 & [0.86] & b(x) \leq y \leq 0.75 \\ 0.0 & [3.0] & 0.75 \leq y \leq 1 \end{cases}$$

where  $b(x) = 0.5 - 0.25 \cos(2\pi x)$ . Experiments were conducted with 100 parents for 500 iterations using 500 samples from each class. Figure 7 shows the learning curves for the best node among the pool of candidate units. From this figure, one can observe that after the first two hidden units, the fitness (correlation) values show a marked decrease in magnitude. For this example, only two hidden units are adequate as demonstrated by the contour plot of the decision surface as shown in figure 8(a). Figure 8(b) shows the shape of the decision surface.

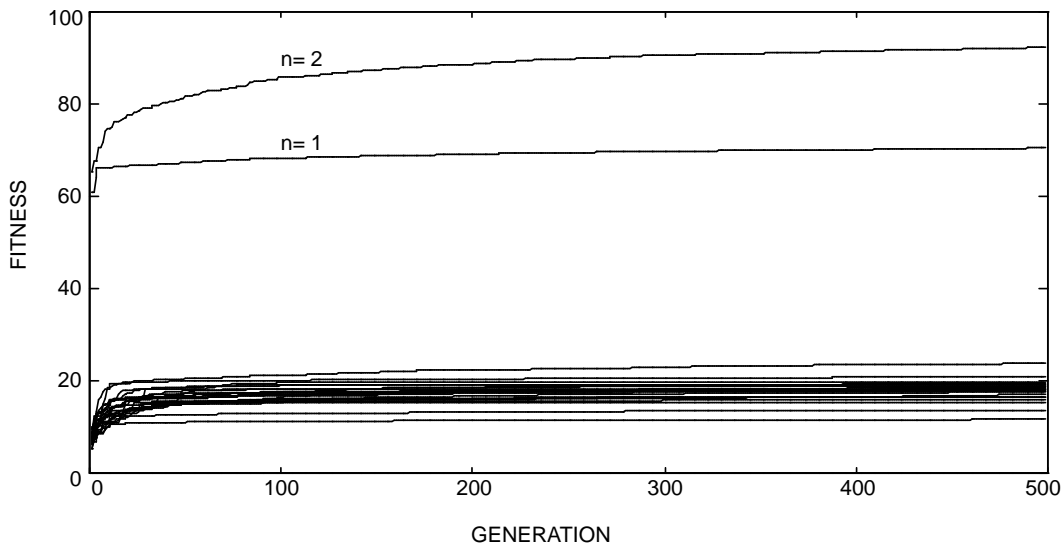


Figure 7. The correlation of the best candidate node in the population. The highest correlations correspond to the first ( $n = 1$ ) and second ( $n = 2$ ) hidden units.



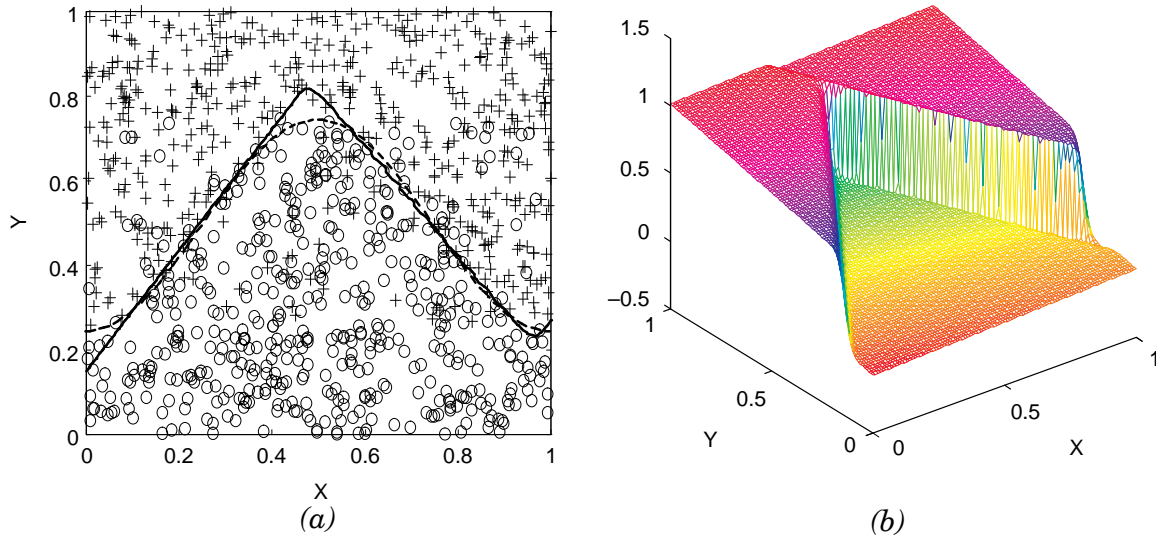


Figure 8. (a) A contour plot of the decision surface generated by the evolved cascaded network with two hidden units. The dashed line represents the optimal decision boundary. (b) The decision surface generated by the two hidden node CCLA.

## MIXTURE ACTIVATION FUNCTIONS

Although not commonly considered variable, the activation function(s) employed within a network may accentuate (or hinder) the ability to generate a parsimonious architecture since they are central in approximating the desired functional mapping. In fact, Donohoe and Johnstone (1989) have shown that a duality exists between projection-based ridge approximators and kernel-based methods. This duality is manifested in the ability of ridge-based approximators to parsimoniously model radial functions while kernel-based approximators are superior for modeling harmonic functions. Mixture activation functions are inspired by this duality and how it pertains to pattern classification tasks. Intuitively, portions of a particular data set may be amenable to kernel-based discriminators while other parts of the same data set may be partitioned using a ridge-type discriminator (e.g., the Iris data set). Kernel-based approaches are likely to perform poorly in high dimensions since a finite kernel set typically describes only a sparse portion of the data space. Likewise, ridge-type functions are not predisposed to parsimoniously model data clusters. The complementary nature of both types of functions can be taken advantage of during network construction.

The mixture activation function  $f$  is formulated from a proportionate mixture of kernel and ridge functions

$$f(\mathbf{x}, \mathbf{w}, \alpha) = \alpha \cdot g(\mathbf{w}^T \mathbf{x}) + (1 - \alpha) \cdot h(\|\mathbf{w} - \mathbf{x}\|),$$



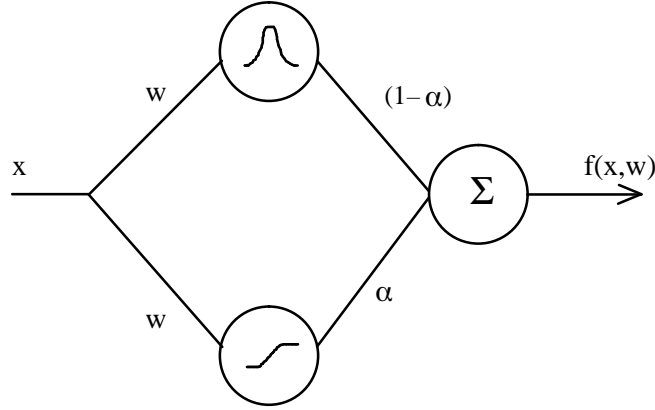


Figure 9. The mixture activation function model employs a combination of kernel and ridge-type functions.

where  $\alpha$  is the mixing proportion  $0 \leq \alpha \leq 1$ . Figure 9 shows that a mixture activation function is simply the equivalent of a two-node system with different activation functions. However, it is noted that the activation function can switch between either a kernel or ridge function by the addition of only a single parameter to the search space.

The mixture activation function can be bipolar with a projection-based function given by

$$g(\mathbf{x}, \mathbf{w}) = \tanh(\mathbf{w}^T \mathbf{x})$$

and a kernel-based function given by

$$h(\mathbf{x}, \mathbf{w}) = 2\exp\left(-\frac{1}{2\sigma^2} \|\mathbf{x} - \mathbf{w}\|^2\right) - 1.$$

In the event that unipolar activations are desired, the bipolar expressions can be respectively replaced with

$$g(\mathbf{x}, \mathbf{w}) = \frac{1}{1 + \exp(-\mathbf{w}^T \mathbf{x})}$$

and

$$h(\mathbf{x}, \mathbf{w}) = \exp\left(-\frac{1}{2\sigma^2} \|\mathbf{x} - \mathbf{w}\|^2\right).$$

Though not yet incorporated into the candidate unit optimization process, it is a reasonable exercise to ascertain the potential of the mixture activation function (MAF) concept and the viability of evolutionary learning on this variable activation function. A set of experiments was conducted using 100 data points, which were linearly separable for the first test and then clustered for the second test. A bipolar activation function of the form

$$f(\mathbf{x}, \mathbf{w}, \alpha) = \alpha \cdot \tanh(\mathbf{w}^T \mathbf{x}) + (1-\alpha) \cdot \left\{ 2\exp\left(-\frac{1}{2\sigma^2} \|\mathbf{x} - \mathbf{w}\|^2\right) - 1 \right\}$$

was used for both tests.



Since the first test involved data that was linearly separable, it was expected that a hyperplane would be evolved with the mixture coefficient  $\alpha \approx 1$ , as was the case. The slope of the separation line shown in the contour plot of figure 10 was within 3 percent of optimal while the bias difference was negligible. The mesh plot also shown in figure 10 shows the surface of the activation function for this data set. The same data set was then redesignated so that all of the points within 0.32 units from the center (0.5,0.5) belonged to one class, while those outside this range belonged to the other class. The same training algorithm was rerun yielding the results shown in the contour and mesh plots of figure 11. This particular set of experiments embedded a variety of offspring perturbation techniques in the evolutionary search algorithm.

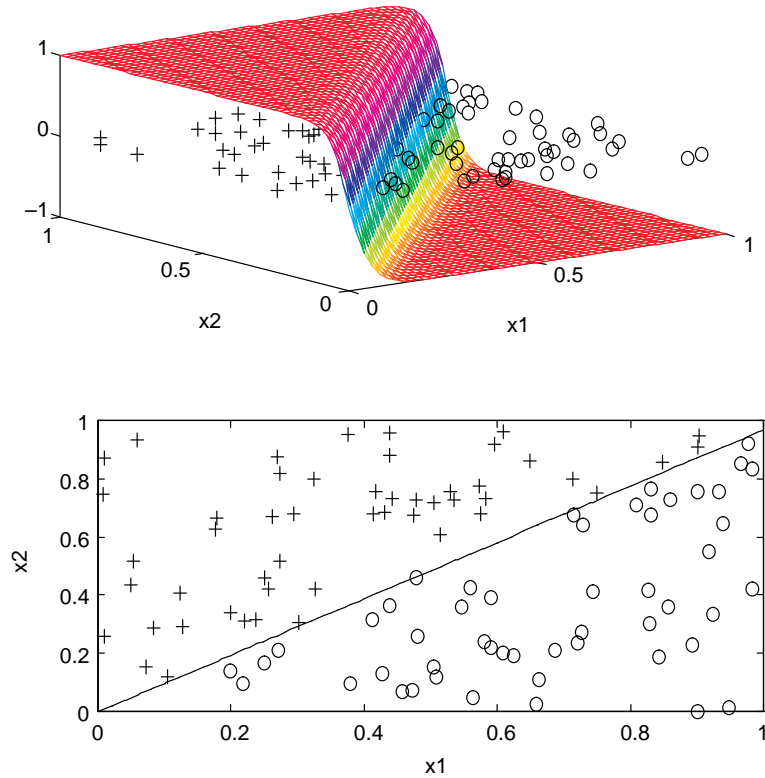


*Figure 10. The mesh and contour plots of the decision surface generated by the mixture activation function for the linearly separable data set.*



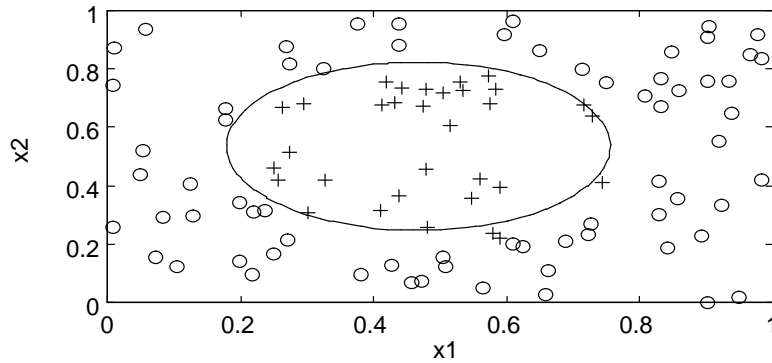


*Figure 11. The mesh and contour plots of the decision surface generated by the mixture activation function for the clustered data set.*

## CONCLUSION

Evolutionary search should not be regarded as a panacea for all problems, but rather as another tool for one's optimization toolbox. When intelligently applied, evolutionary search methods may yield good results on problems that are not tractable when using traditional optimization techniques. Although good results have been shown, the algorithm presented here is but one (albeit, very efficient) approach in applying evolutionary search to artificial neural networks. Other evolutionary computation approaches to neural networks can be found in Yao (1993) and Whitley and Schaffer (1992). Further development of the presented algorithm will include the integration of mixture activation functions in an effort to better represent the data in a parsimonious fashion, implementation of the automatic stopping criteria, and the evaluation of other objective functions (such as mean-squared error as well as correlation).

As a multi-agent stochastic search process, evolutionary optimization is amenable to a wide range of difficult problems. Other problems addressed using evolutionary search include training recurrent perceptrons (McDonnell & Waagen, 1994), generating probability density mixture models using a generalized kernel instead of just a Gaussian basis function (Waagen, Parsons, McDonnell, & Argast, 1994), and generating the threshold coefficients for wavelet-based image compression (Waagen, Argast, & McDonnell, 1994). Evolutionary search is considered appropriate for tackling a wide range of other difficult problems such as designing filters for communication systems and controlling nonlinear plants, determining fuzzy logic membership functions, mission planning, and resource allocation (operations research).



## REFERENCES

- Bäck, T., and H.-P. Schwefel. 1993. "An Overview of Evolutionary Algorithms for Parameter Optimization," *Evolutionary Computation*, vol. 1, no. 1, pp. 1–24.
- Deco, G., W. Finnoff, and H. G. Zimmermann. 1994. "Unsupervised Mutual Information Criterion for Elimination of Overtraining in Supervised Multilayer Networks," submitted to *Neural Computation*.
- Donohoe, D. L., and I. M. Johnstone. 1989. "Projection-Based Approximation and a Duality with Kernel Methods," *The Annals of Statistics*, vol. 17, no. 1, pp. 58–106.
- Fahlman, S. E., and C. L. Lebiere. 1990. "The Cascade-Correlation Learning Architecture," Technical Report CMU-CS-90-100, Carnegie Mellon University, Pittsburg, PA.
- Flick, T. E., L. K. Jones, R. G. Priest, and C. Herman. 1990. "Pattern Classification Using Projection Pursuit," *Pattern Recognition*, vol. 23, no. 12, pp. 1367–1376.
- Fogel, D. B. 1992. *Evolving Artificial Intelligence*. Ph.D. Dissertation, University of California, San Diego.
- Hansen, L. K., and M. W. Pedersen. 1994. "Controlled Growth of Cascade Correlation Nets," *International Conference on Artificial Neural Networks (ICANN)*.
- Haykin, S. 1994. *Neural Networks: A Comprehensive Foundation*, MacMillan.
- Huber, P. J. 1985. "Projection Pursuit," *The Annals of Statistics*, vol. 13, no. 2, pp. 435–475.
- Klagges, K., and M. Soegtrop. 1993. "Limited Fan-in Random Wired Cascaded-Correlation," *Proceedings of the Third International Conference on Microelectronics for Neural Networks*, pp. 6–8, Edinburgh, Scotland.
- Marple, S. L. 1987. "Digital Spectral Analysis with Applications," Prentice-Hall.
- McDonnell, J. R., and D. E. Waagen. 1994. "Evolving Recurrent Perceptrons for Time-Series Modeling," *IEEE Transactions on Neural Networks*, vol. 5, no. 1, pp. 24–38.
- McDonnell, J. R., and D. E. Waagen. (forthcoming in) 1995. "An Empirical Study of Recombination in Evolutionary Search," *Proceedings of the Fourth Annual Conference on Evolutionary Programming*, J. R. McDonnell, D. B. Fogel, and R. G. Reynolds (eds.), MIT Press.
- Priestley, M. B. 1988. *Non-linear and Non-stationary Time Series Analysis*, Academic Press.
- Schwefel, H.-P. 1981. *Numerical Optimization of Computer Models*, John Wiley & Sons.
- Svarer, C., L. K. Hansen, and J. Larsen. 1993. "On Design and Evaluation of Tapped-Delay Neural Network Architectures," *IEEE International Conference on Neural Networks*, pp. 46–51, San Francisco.

- Tong, H. 1990. *Non-linear Time Series: a Dynamical System Approach*, Oxford Science Publications.
- Tong, H., and K. S. Lim. 1980. "Threshold Autoregression, Limit Cycles and Cyclical Data," *Journal Royal Statistical Society*, vol. B42, pp. 245–292.
- Waagen, D. E., J. R. McDonnell, and J. D. Argast. 1994. "Stochastic Determination of Optimal Wavelet Compression Strategies," *SPIE Conference on Visual Communications and Image Processing*.
- Waagen, D. E., M. D. Parsons, J. R. McDonnell, and J. D. Argast. 1994. "Evolving Multivariate Mixture Density Estimates for Classification," *Neural and Stochastic Methods in Image and Signal Processing III*, SPIE vol. 2304, pp. 175–186.
- Weigend, A. S., B. A. Huberman, and D. E. Rumelhart. 1992. "Predicting Sunspots and Exchange Rates," in M. Casdagli and S. Eubank (eds.), *Nonlinear Modeling and Forecasting*, pp. 395–432, Addison-Wesley.
- Whitley, L. D., and J. D. Schaffer, eds. 1992. *Proceedings of COGANN-92 International Workshop on Combinations of Genetic Algorithms and Neural Networks*, IEEE Computer Society Press.
- Yao, X. 1993. "A Review of Evolutionary Artificial Neural Networks," *International Journal of Intelligent Systems*, vol. 8, no. 4, pp. 539–567.

Principal Investigator:  
J. R. McDonnell

0601152N  
NRaD ZW67

## Photonic Silicon Device Physics

S. D. Russell, W. B. Dubbelday,  
R. L. Shimabukuro, and P. R. de la Houssaye

*This program investigated the fundamental mechanisms involved in light-emitting silicon structures, fabricated silicon-based photonic devices, and examined the electrical device properties. The approach evolved into the study of three distinct areas of interest: porous silicon layers, silicon microplasmas, and silicon nanostructures. These three areas are related by the need for understanding materials properties on the nanometer size scale and the need for applying microelectronic-device-fabrication techniques to aid in elucidating the emission mechanisms and to ultimately transition such knowledge into practical electronic devices. The following paragraphs summarize the work completed to date in each of these areas.*

### BACKGROUND AND OBJECTIVE

Silicon, because of its process maturity, low cost, high yield, and reliability, is the material of choice for large levels of electronic device integration. Recent research and development of novel silicon-based technologies (e.g., silicon-germanium alloys, silicon on insulator (SOI), silicon on sapphire (SOS)) have resulted in high-speed performance approaching that offered by group III–V and II–VI semiconductors. The remaining limitation of silicon for optoelectronic applications is the indirect band gap, which has, heretofore, prevented direct optical transitions that could provide an efficient photonic (light-emitting) source compatible with silicon processing. The availability of a photonic silicon source would allow a breakthrough in optoelectronic integrated circuits with applications in optical computing, high-speed communications, and integrated sensor and smart sensor technology. Additional applications include light-emitting diodes (LEDs), flat-panel displays, and optical interconnections critical for advances in future generation Navy C<sup>4</sup>I platforms and systems.

### POROUS SILICON DEVICES

Since the discovery of photoluminescent porous silicon (Canham, 1990), porous silicon has emerged as a potential photonic source compatible with silicon microelectronics. The light emission mechanism, however, is still not fully understood. The predominant theory is related to the confinement of electrons and holes in a silicon wire or particle with dimensions on the order of tens of nanometers. In such cases, it is hypothesized that the electrons and holes may recombine and efficiently emit light if there are few nonradiative mechanisms competing for the charge carriers. This theory, called quantum confinement, has been observed in other materials systems and has been theoretically modeled in silicon (Ohno et al., 1992; Sawada et al., 1994). These silicon nanoparticles or nanowires are predicted to have a direct band gap, thus allowing efficient electron-hole recombination without employing the less efficient phonon-assisted transitions. Other theories note that silicon compounds such as amorphous silicon, silicon oxides, and siloxene derivatives also luminesce in the visible region of the spectrum and propose those models as a source of the luminescence (Perez et al., 1992; Milewski et al., 1994; Brandt et al., 1992).

Typically, the method of fabricating porous silicon layers in bulk silicon wafers uses an anodic oxidation process with a backside contact to the silicon anode and a platinum (Pt) counter-electrode in a hydrofluoric acid (HF) and ethanol solution (Canham, 1990; Bsiesy et al., 1991). By using low current densities, silicon wafers are made porous by the electrochemical dissolution of silicon, as schematically

shown in figure 1. Figure 1(a) schematically shows a plan view of partially anodized (100)-oriented silicon with 25-percent porosity (i.e., the silicon has been removed from one-quarter of the volume). Figures 1(b) and 1(c) show the effect of increased etching, which enlarges the pores or voids until they subsequently intersect leaving a matrix of isolated wires. Porosity exceeding approximately 65 percent is required to observe photoluminescence. In reality, the electrochemical dissolution is not as uniform, and the result is a dendritic structure of silicon wires in a complex matrix. A scanning electron microscope (SEM) photomicrograph of the cross-section of an anodically oxidized porous silicon layer is shown in figure 2.

In this project, we explored novel thin films of porous silicon on transparent insulating substrates (sapphire and quartz), which allowed the elimination of interactions with and contribution from the bulk by etching the entire silicon layer. This aided in the elucidation of the photoluminescence mechanism by independently allowing the examination of the porous layer. In addition, the transparent substrates allowed for unique analysis of the optical properties from either side of the porous layer and allowed the design of photonic devices using conventional (opaque) metals.<sup>1,2</sup> Due to the insulating nature of the transparent substrates, the studies described here typically use a stain etch composed of HF, nitric acid (HNO<sub>3</sub>), and distilled water in a ratio of 1:5:10 (Fathauer et al., 1992; Sarathy et al., 1992) to form the porous layers without need for electrical contact to the backside of the wafer. An alternative technique was developed in this program by using optical excitation rather than electrical contact to form porous silicon. Details have been published in Dubbelday et al. (*MRS Proc.*, 1993a) and Dubbelday et al. (1993b). Figure 3 shows a cross-sectional SEM photomicrograph of ~10 micron thick porous silicon layer on a sapphire (Al<sub>2</sub>O<sub>3</sub>) substrate fabricated using the purely chemical or stain-etching process. Figure 4 shows the photoluminescence spectra of a porous SOS film. The porous SOS sample shows photoluminescence signals comparable to those published for porous bulk silicon. The two curves shown are the emission spectra obtained when the sample is illuminated and emission collected at the silicon side (dotted line) and at the sapphire side (solid line) of the wafer. The photoluminescence maximizes in intensity at ~700 nm with a width of ~100 nm. The luminescence from the Cr<sup>+3</sup> impurity (695 nm) is pronounced in the sapphire-side emission spectrum. This peak occurs since the sapphire substrate used in this case was from a Czochralski (CZ) grown boule that had trace impurities from the growth of ruby laser crystals (chromium-doped sapphire). This peak does not occur in edge-fed-growth (EFG) sapphire available from other manufacturers. The similarity in the front and backside porous silicon spectra suggests uniformity in the porous structure with depth, and that strain effects due to the lattice mismatch between the silicon and the sapphire are minimal. Photoluminescent films were obtained in porous films ranging in thickness from 10 microns to as thin as 90 nm (NRaD's ultrathin SOS, see Offord, 1992). Further analyses of the morphological differences and strain effects of porous SOS structures have been published (Dubbelday et al., 1993b).

---

<sup>1</sup>Russell, S. D., W. B. Dubbelday, R. L. Shimabukuro, P. R. de la Houssaye, and D. M. Szaflarski, "Photonic Silicon on a Transparent Substrate," Navy case 75,292, filed 9 September 1993; patent pending.

<sup>2</sup>Dubbelday, W. B., R. L. Shimabukuro, and S. D. Russell, "Electroluminescent Devices in Porous Silicon on Sapphire," Navy case 76,291, disclosure submitted 26 January 1993.

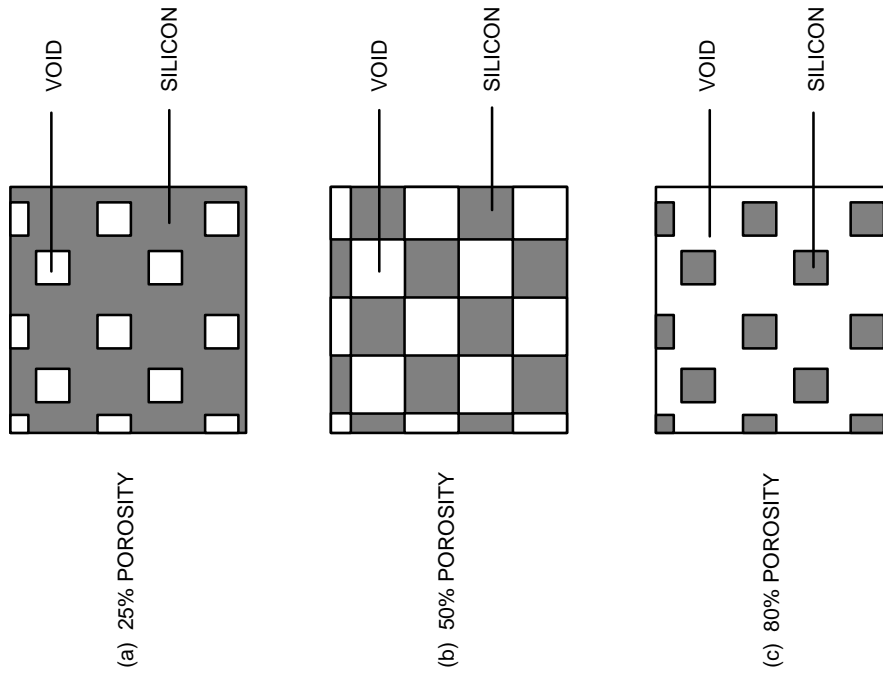


Figure 1. Schematic plan view of porous silicon.

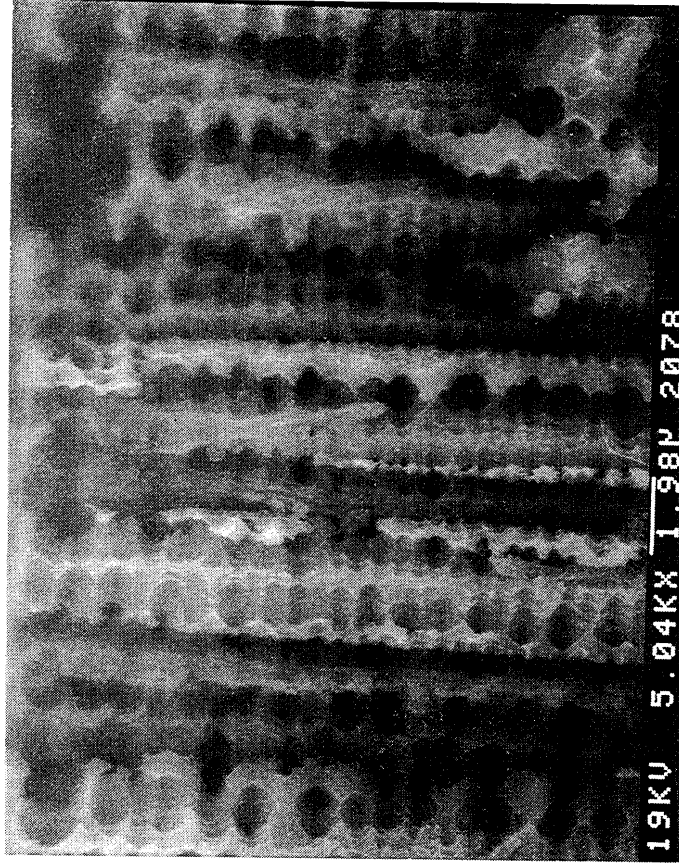


Figure 2. SEM cross section of porous silicon.

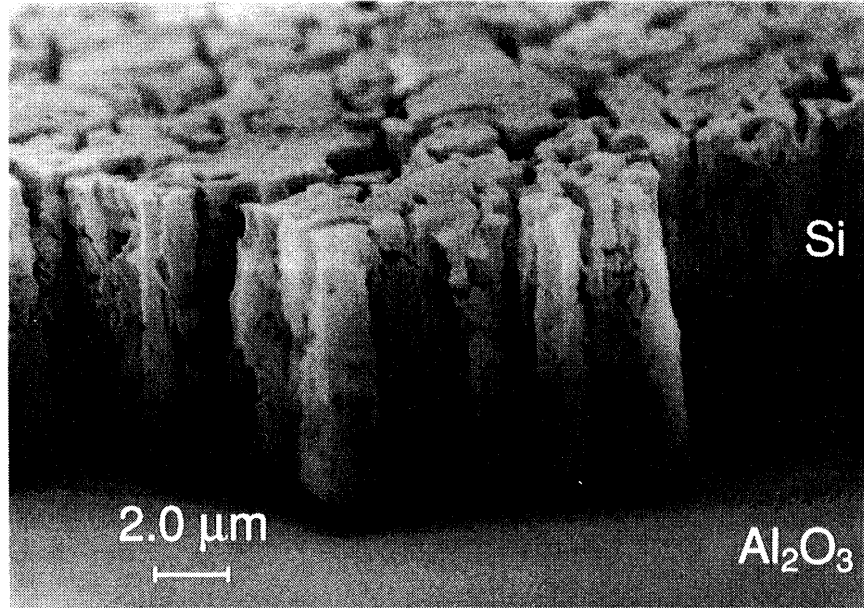


Figure 3. SEM cross section of porous SOS.

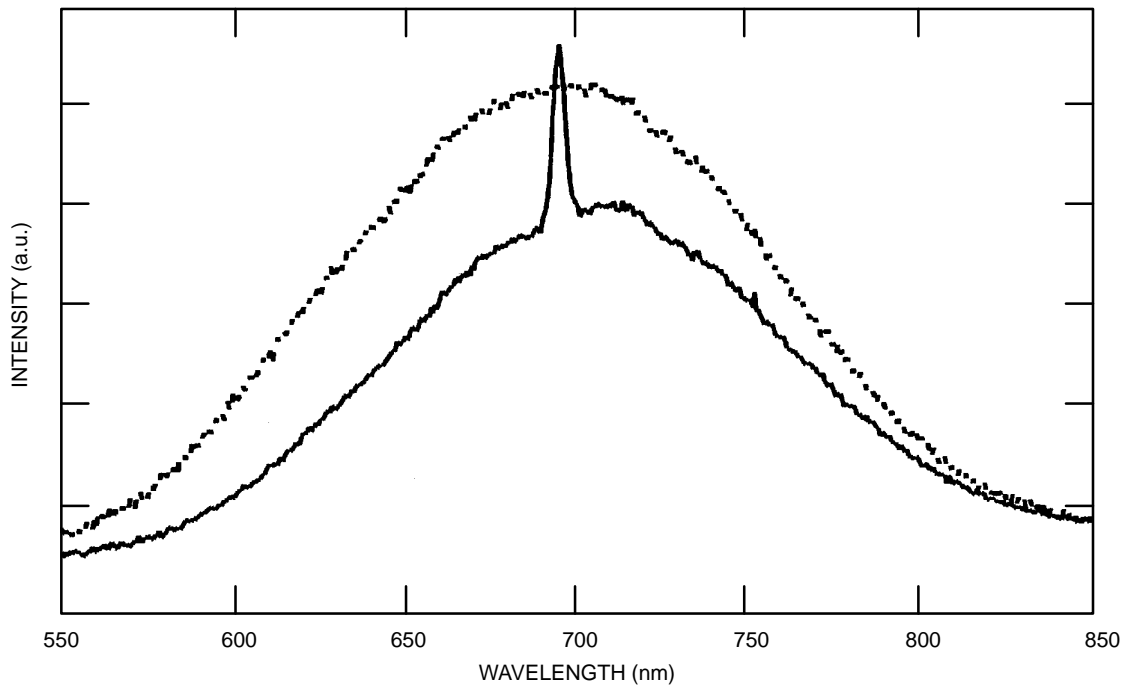


Figure 4. Photoluminescence spectra of porous SOS.

An investigation into the dependence of porous silicon photoluminescence on the crystallinity of the starting silicon layers was completed to elucidate the light emission mechanism by decoupling the surface species formed by the chemistry from the crystalline state of the nano-structures. This study applied identical etch procedures to crystalline, damaged, and amorphous silicon layers to examine the emission mechanism. Ion implantation was employed to control the degree of crystalline damage prior to the fabrication of the porous layer. The data indicated that crystalline order is required for photoluminescent porous silicon. The lack of photoluminescence from an amorphous silicon layer etched identically to bulk silicon is consistent with the absence of photoluminescence from porous silicon layers fabricated in heavily ion-damaged amorphous silicon. These results are inconsistent with an amorphous silicon or siloxene emission mechanism, and suggest quantum confinement plays a role in the light emission of the porous silicon (Dubbelday et al., 1993a). The effects of etchant composition and microstructure on the photoluminescence of porous silicon has also been reported (Dubbelday et al., 1995). An alternative etchant using HF-sodium nitrite ( $\text{NaNO}_2$ ) was developed with freely available  $\text{NO}_2$  ions, which reduced the accelerated etching effects from ion implantation damage. Transmission electron microscopy (TEM) analysis of the porous silicon layer (figure 5a) shows lattice images of the crystalline portions. Figure 5b shows the electron diffraction pattern obtained, characteristic of a crystalline porous region.

SOS was fabricated in the as-deposited, improved (Garcia et al., 1986), and bonded wafer forms. Each of the fabrication techniques imparts characteristic microcrystalline defects in the silicon layer. Microstructural defects such as microtwins and threading dislocations in the starting material had no observed effect on the light-emitting properties of porous SOS. Vacancies imparted by ion implantation damage, however, can amorphize the material resulting in a quenching of the photoluminescence. An apparent increase in the density of light-emitting structures leading to enhanced photoluminescence can also be obtained by limited ion damage of the material prior to the fabrication of the porous layer (Russell et al., 1994a). This may be employed to enhance light emission from porous silicon devices.<sup>3</sup>

Porous silicon LEDs have been reported using transparent (indium tin oxide known as ITO) and semitransparent (gold) electrodes (Koshida & Koyama, 1992; Namavar et al., 1992; Steiner et al., 1993). The electroluminescence spectra are similar to that of the photoluminescence spectra (i.e., peaked in the visible with broadband emission). Avoiding the use of nonstandard metals, such as ITO and gold, is a major manufacturing advantage offered by the transparent substrates studied in this project. Evaluation of microfabrication processes and their effect on the light emission of porous silicon was also performed. Thermal processing above about  $300^\circ\text{C}$  destroys the light-emitting properties of porous silicon by desorbing hydrogen from the surface passivation. Similarly, ion damage from dopant incorporation, reactive ion etching, and photoresist removal also permanently destroy the light emission. Chemical treatments using solvents can have a temporary quenching effect, but the light emitting properties return after the solvents desorb from the porous layer.<sup>4</sup> Patterning of the porous silicon layers can be readily achieved using standard photolithographic techniques, avoiding high-temperature bakes, and using

---

<sup>3</sup>S. D. Russell, W. B. Dubbelday, R. L. Shimabukuro, and D. M. Szaflarski, "Method of Controlling Photo-emission from Porous Silicon Using Ion Implantation," Navy case 75,726, patent pending; Notice of Allowance 7 February 1995.

<sup>4</sup>S. D. Russell and W. B. Dubbelday, "Liquid Level Sensor and Detector," NCCOSC case 183.



*Figure 5a. TEM lattice images of porous silicon.*



*Figure 5b. Electron diffraction pattern of porous silicon.*

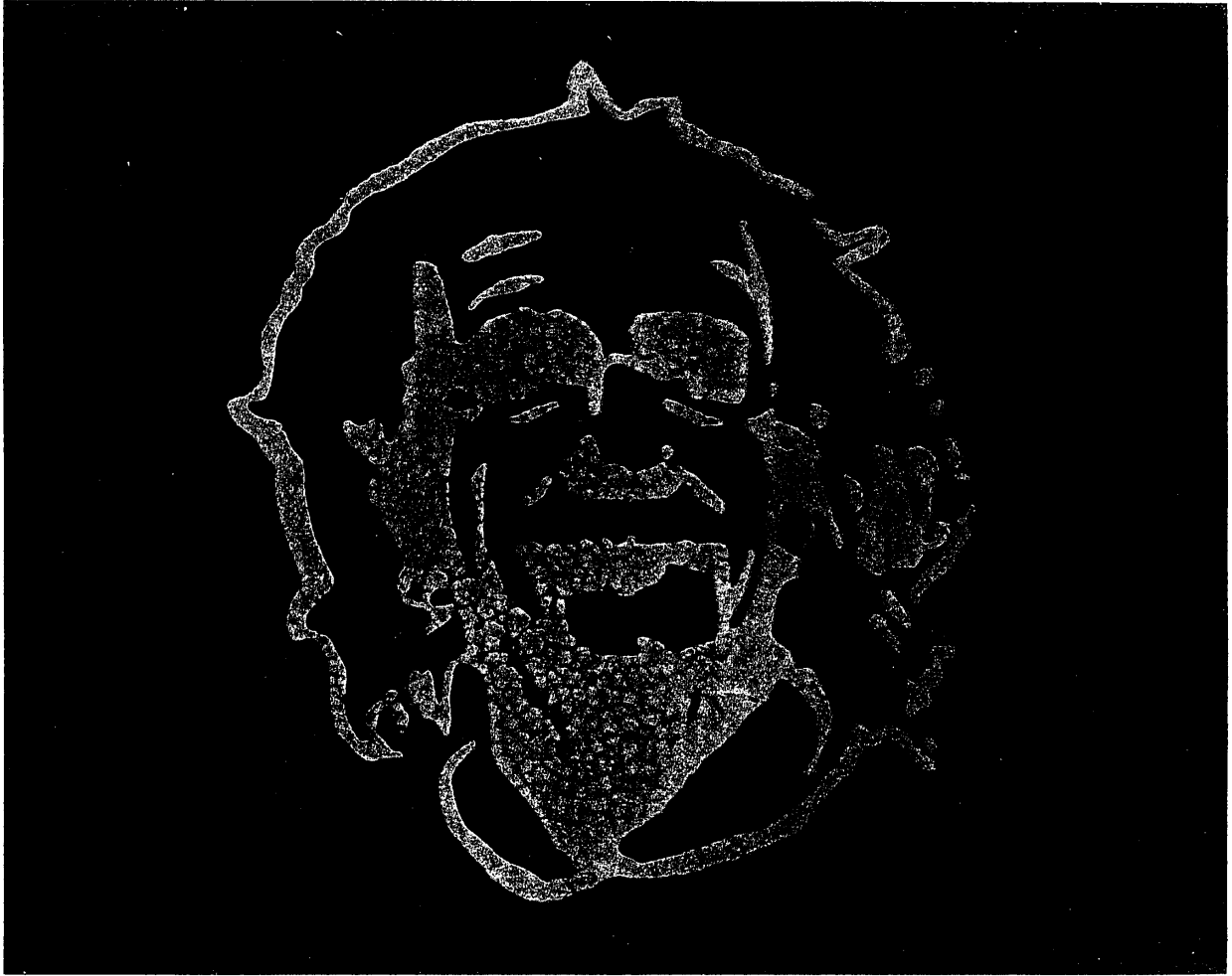


*Figure 6. Photolithographically patterned porous silicon.*



chemical rather than ion-assisted resist removal techniques. An example of a photolithographically patterned porous SOS film is shown in figure 6. Deposition of transparent metal ITO on porous silicon and porous SOS and porous silicon on quartz (SOQ) was performed, in part, to replicate previous reports. Despite having good electrical resistivity and rectifying I-V behavior, no measurable electroluminescence has been observed on our devices to date. Photoluminescence of the underlying porous layer was still evident after ITO deposition suggesting that the porous nanostructures were undamaged by the processing and that improvement in charge injection efficiency is required in our porous silicon device design. Unlike a variety of solvents, use of aluminum to make electrical contact to porous silicon layers does not quench the photoluminescence (Russell, 1994b). Initial tests, however, have not demonstrated electroluminescence from simple device structures using aluminum. Figure 7 shows one design for a porous silicon LED currently in the early stages of fabrication. Variation in the device geometry (both lateral and vertical junction designs) have been employed in the newly designed photolithographic mask set, which will allow further examination of these devices.

## SILICON MICROPLASMA DEVICES

Light emission from avalanche breakdown of silicon p-n junctions has been known since the early days of semiconductor research (Newman et al., 1955; Chynoweth & McKay, 1956; Rose, 1957; Davies & Storm, 1961). The light emitted from reverse-biased diodes is attributed to a phonon-assisted recombination of hot (high energy) electrons and holes in the region where avalanche breakdown is initiated. These avalanche regions have a high concentration of hot charge carriers that are produced by ionization of the silicon in large applied electric fields and are referred to as microplasmas. The characteristic emission spectra, while exhibiting high-energy visible photons (as high as  $\sim 3$  eV), peak near the silicon bandgap at 1.1 eV in the infrared. An alternative interpretation of the emission mechanism (Figielski & Torun, 1962) is that of bremsstrahlung of hot carriers, rather than recombination, in the microplasma regions.

Microplasma emission is unlike the reported light emission from SOS diodes reverse biased into second (thermal) breakdown (Dumin, 1969). In such cases, the diode exhibits a current-controlled negative resistance region in the I-V characteristics with the formation of a filament of high local current density. This effect occurs after the onset of the weaker emitting silicon microplasmas. While light emitted from diodes in the second breakdown does not have the spectra characteristic of an incandescence, the emitted intensity increases in the infrared region near 1.1 eV, similarly to those reported for the microplasmas. Most importantly, these effects occur prior to the onset of incandescence, and are not simply blackbody emission from a thermal body.

In this program, we have fabricated microplasma devices in the ultrathin layers of SOS described previously. The devices employ a simple p-n rectifying junction through which charge injection occurs. Conventional opaque metal (aluminum) is used for electrical contact; therefore, light emitted from these devices is detected through the transparent sapphire substrate. Forward-biased ultrathin SOS devices do not emit light, whereas reverse-biased devices emit broadband light. The onset of light emission occurs at voltages as low as 4 volts. Characteristic I-V curves, shown in figure 8, do not show the negative resistance regions observed in second (thermal) breakdown. Signatures of microplasma behavior, however, do exist, in addition to the reverse biasing required for light emission. Figures 9(a) and (b) show optical photographs of the emitted light along a junction of the SOS microplasma LED. The observed distribution of discrete microplasmas along the junction is typical of the previously reported microplasmas. Increase in



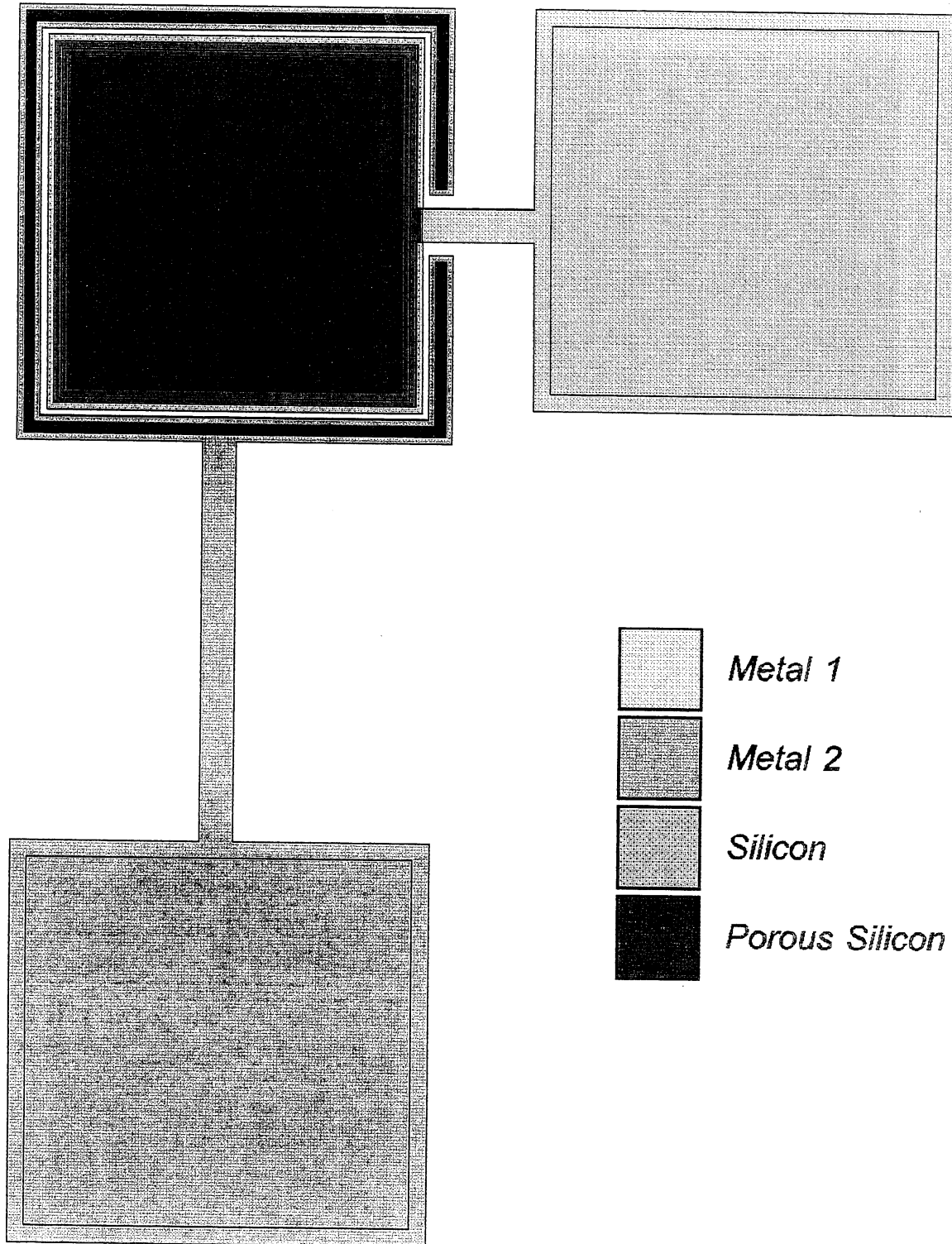


*Figure 7. Porous SOS LED design.*



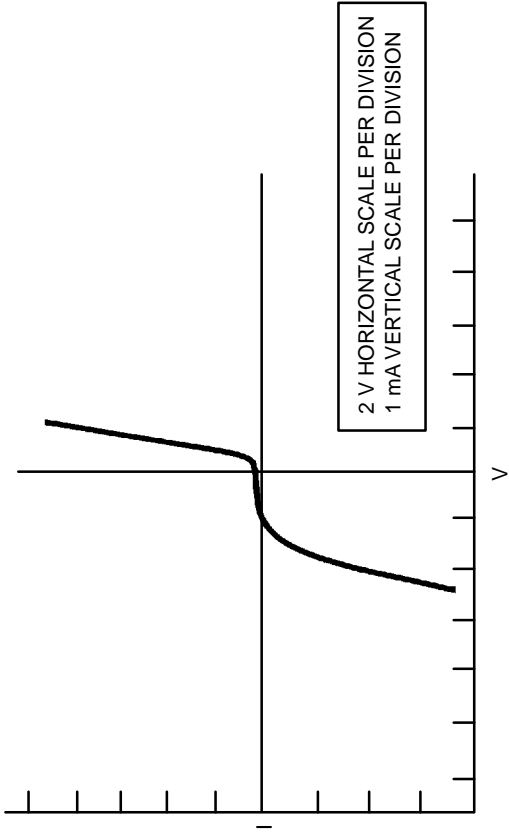


Figure 8. Microplasma LED I-V characteristics.

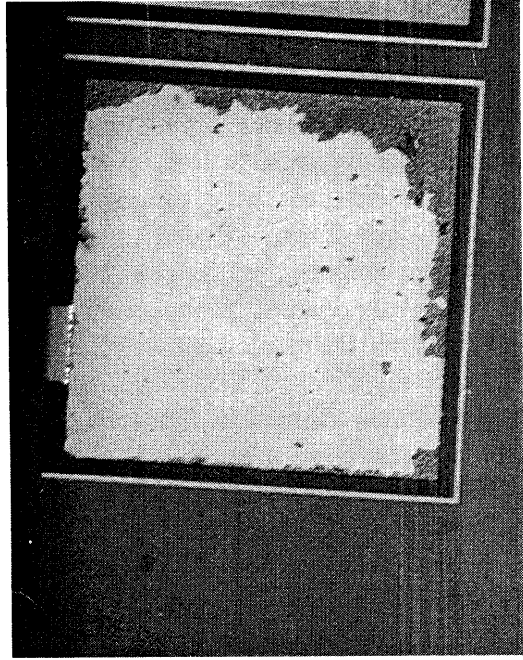


Figure 9a. Light emission from SOS microplasma LED.

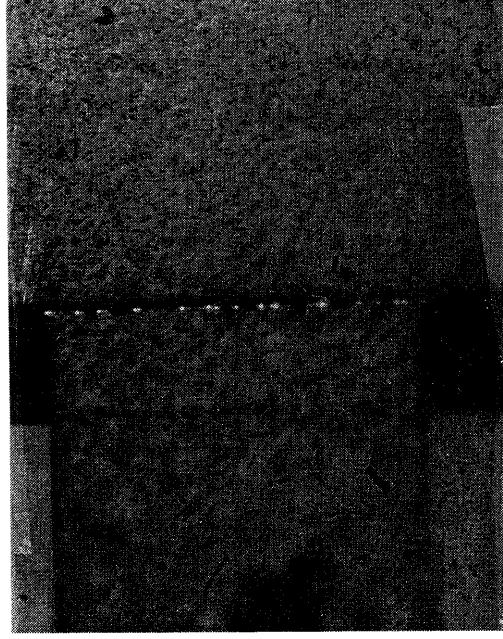
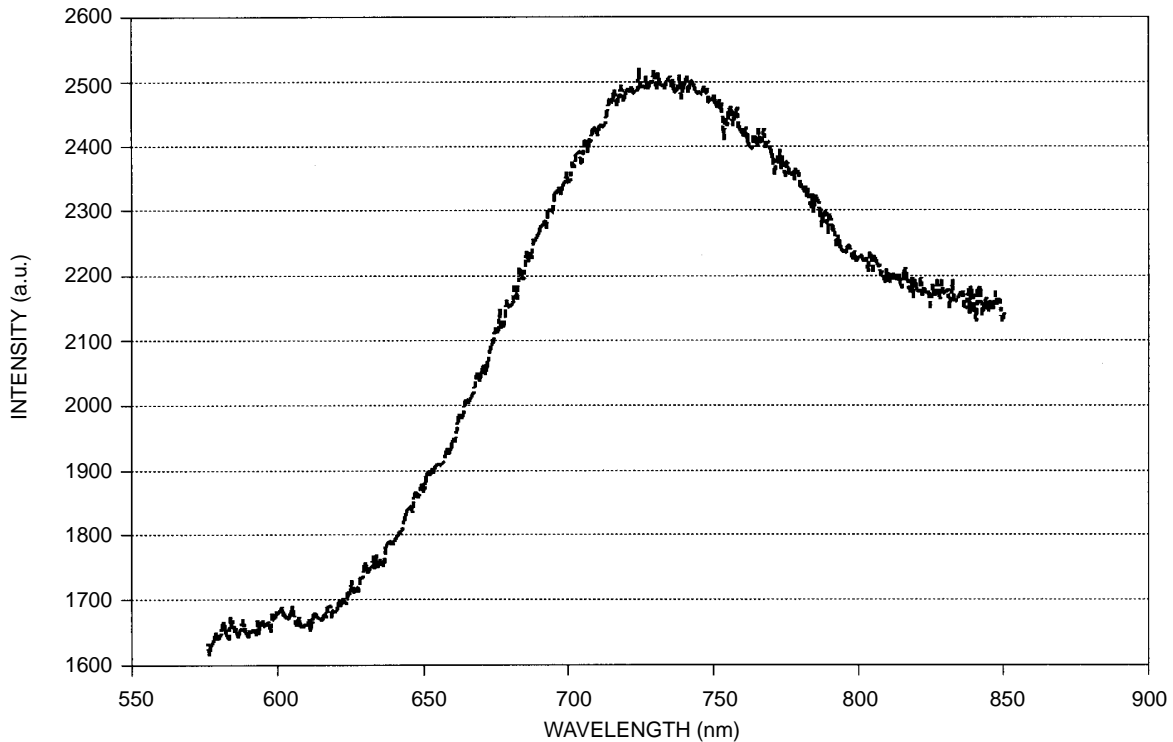


Figure 9b. Closeup view of microplasma emission.



*Figure 10. SOS microplasma LED emission spectrum.*

reverse-bias voltage (and corresponding increase in drive current) produces an increase in light emission, corresponding to an increase in the number of microplasmas. However, we have discovered new features that differ from earlier reports. The emission spectrum from the reverse-biased SOS microplasma LED are shown in figure 10 (corrected for spectrometer response). The peak of the light emission is in the visible region, unlike that previously reported for diodes in avalanche or thermal breakdown. In addition, a temperature dependence in opposition to prior reports (Kosyachenko et al., 1990; Lanzoni et al., 1991) of silicon hot-carrier light emission is observed. The integrated intensity (between 550 and 850 nm) at room temperature (296 K) is greater than four times that of the device at liquid nitrogen (77 K) temperature. When the device is heated to 398 K, the integrated intensity further increases to greater than 15 times the emission at cryogenic temperatures. The peak intensity also follows similar behavior. These deviations from previously reported microplasmas are, at this time, attributed to the highly stressed ultrathin silicon film and the reduced carrier lifetime in the ultrathin SOS. Since the charge carrier lifetime is substantially shorter in SOS compared to bulk silicon due to defect scattering, the increased electron-phonon scattering will affect the ionization rate (Wolff, 1954). Raman spectroscopic measurement of stress in ultrathin SOS films (Dubbelday et al., 1993a, b) shows that the silicon layer is under a large compressive stress ( $\sim 5 \times 10^9$  dynes/cm<sup>2</sup>). Such stresses are sufficient to modify the electronic band structure, which has been demonstrated with increased hole mobility and decreased electron mobility compared to bulk silicon (Garcia & Reedy et al., 1986). This intrinsic stress, caused by the thermal expansion mismatch between the silicon and the underlying sapphire, may be sufficient to shift the peak of the emission spectrum of the hot carriers into the visible region. Further experiments are in progress to fully identify these anomalous microplasma results. Figure 11 shows one design for an ultrathin SOS microplasma LED currently in the early stages of fabrication. Variations in junction and device geometry

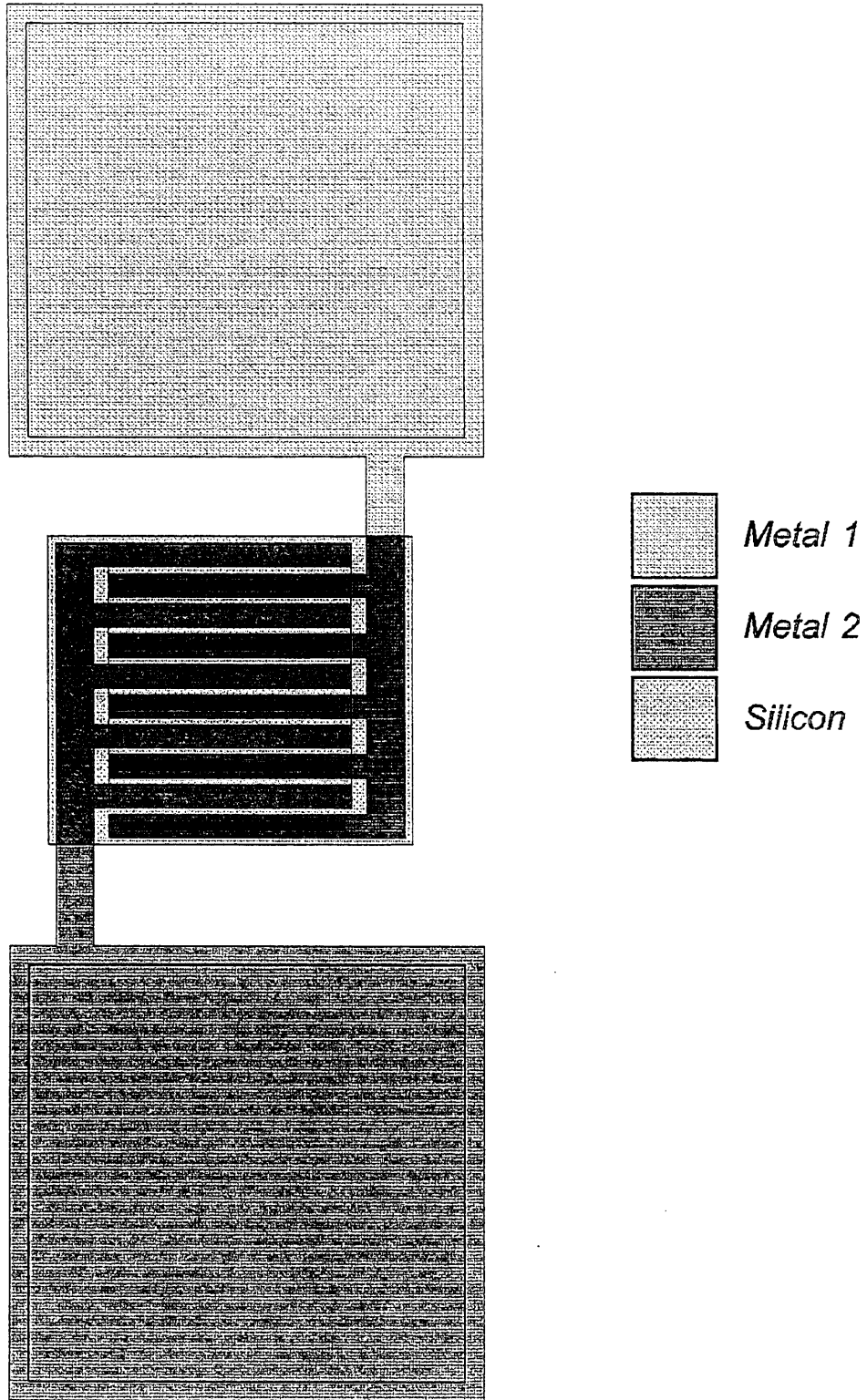


Figure 11. Ultrathin SOS microplasma LED design.



have been employed in the newly designed photolithographic mask set which will aid in the elucidation of these questions.

## SILICON NANOSTRUCTURED DEVICES

As requirements for increased speed and performance push silicon fabrication methods to smaller dimensions, nanofabrication techniques and quantum effects in semiconductors become important technological issues. The recent developments in photoluminescent porous silicon and porous SOS discussed above have hinted that possible quantum confinement effects may alter the 1.1-eV indirect bandgap structure in silicon to allow for the efficient emission of visible light as described above. Fabrication of vertical nanowires in an attempt to directly test this theory has been reported in bulk silicon crystals (Lui et al., 1993). One of the disadvantages of this technique results from the nonuniformity of the thinning oxidation, which produces a structure of varying width.

In this work, NReD, in collaboration with the Physics, Chemistry, and Electrical Engineering Departments at the University of California, San Diego; the Department of Materials Science and Materials Engineering at the University of California, Berkeley; and Digital Instruments harnessed the unique properties of a high-quality single crystal film of silicon on sapphire and used the film thickness as one of the confinement dimensions. Lateral arrays of silicon nanowires were fabricated in the thin (5- to 20-nm) silicon layer and studied (Dubbelday et al., 1994). This technique offers simplified contact to individual wires and provides wire surfaces that are more readily accessible for controlled alteration and device designs.<sup>5</sup> (100)-oriented silicon was deposited by chemical vapor deposition (CVD) on crystalline sapphire and crystal quality was improved using solid-phase epitaxy techniques (Garcia & Reedy, 1986). The silicon layer was subsequently thinned by oxidation and etching of the oxide layer. The thinned silicon layer on sapphire chips was coated with an electron-beam-sensitive photoresist, and individual lines 50 nm wide and 20 microns long were written in an array using a JEOL JSM-6400 electron-beam lithography system, which provided a 3-nm spot size. After resist development, the pattern was reactively ion-etched into the thin silicon using an oxygen-dichlorodifluoromethane ( $\text{CCl}_2\text{F}_2$ ) plasma to form the lateral nanowires. The resist was removed prior to examination. An alternative technique using monolayer etching of the silicon using an oxide mask and single layers of adsorbed chlorine was also tried to eliminate potential reactive ion-etch damage. This technique was extremely selective, i.e., there was little reaction with the  $\text{SiO}_2$ , so that undesired oxide-micromasked regions prevented uniform etching, which resulted in severe surface roughening.

The initial reactive ion-etched patterns were observed using scanning electron microscopy, and the larger arrays could be seen through an optical microscope (figure 12). Individual wire details were examined using atomic force microscopy (AFM). Figure 13 shows an AFM analysis of a single silicon nanowire with dimensions of less than 18 nm in height and approximately 100 nm across. To date, no visible photoluminescence has been observed from these lateral nanostructures. Controlled oxidation studies for thinning these 100-nm wires down to sub-10-nanometer sizes are underway. Subsequent examination of the light-emitting properties from individual nanowires will be performed using near-field microscopic techniques (Diaspro, 1994).

---

<sup>5</sup>S. D. Russell, R. C. Dynes, P. R. de la Houssaye, W. B. Dubbelday, A. S. Katz, and R. L. Shimabukuro, "Silicon Nanostructures in Silicon on Insulator," Navy case 76,969, disclosure submitted 22 November 1994.



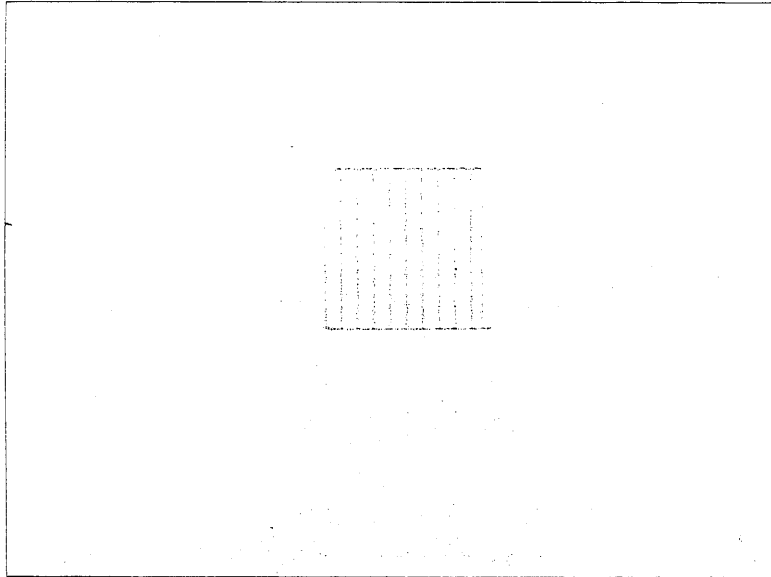


Figure 12. Optical micrograph (1000X) of nanowire array.

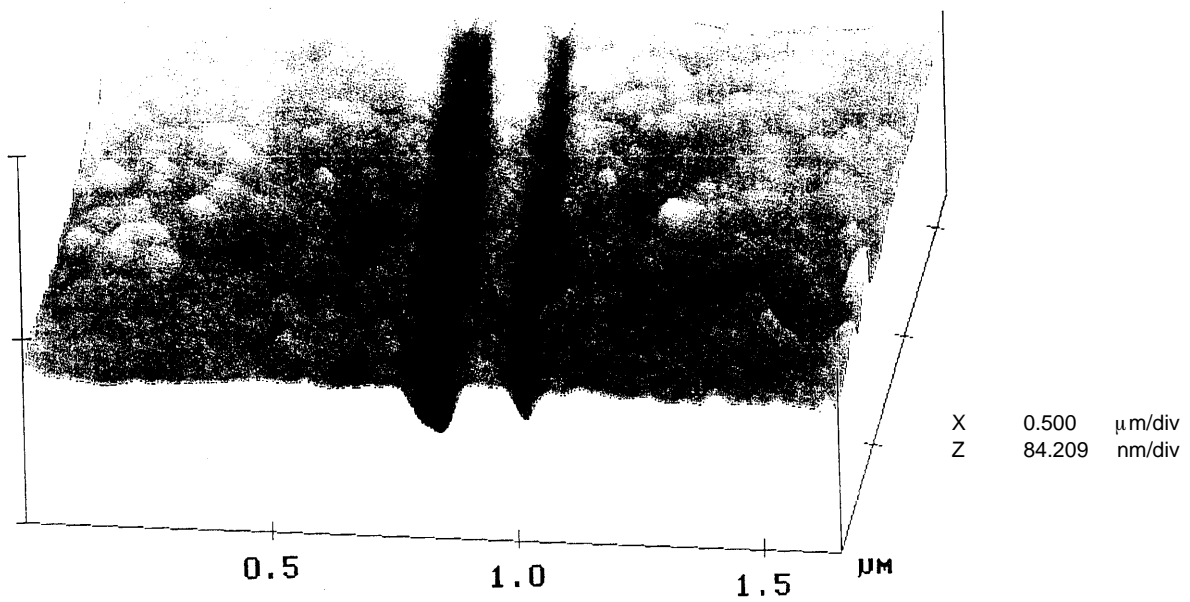


Figure 13. AFM profile of one nanowire.



## SUMMARY AND NAVY SIGNIFICANCE

A variety of novel silicon devices have been fabricated and their light-emitting properties studied during this project. Porous silicon, porous SOS, and porous SOQ exhibit strong photoluminescence with quantum efficiencies as large as 10 percent; however, this project has yet to demonstrate electroluminescence due, in part, to difficulties in making efficient electrical contact to the porous structures. We hope that modified device designs, currently in fabrication, will overcome this limitation. Lateral silicon nanowires on sapphire have been fabricated, and future tests will be performed on the validity of the quantum confinement theory in this materials system. Long-lived SOS microplasma LEDs have been fabricated that exhibit visible light emission at low voltages. Improvements in device design have been completed, and further study of the anomalous emission spectrum will be finished following completion of the current wafer lot.

These preliminary results have generated interest from several Navy sources. The Office of Naval Research (ONR) Solid State Materials program supported preliminary research on porous silicon device processing for potential solid-state, laser-pumping applications (Russell et al., 1993). ONR's Microelectronics program is interested in the technology for use in advance optical interconnection systems. The Strategic Systems Program Office is currently evaluating the technology as a chemical sensor for use in real-time environmental diagnostics and reliability tests and enhancements to guidance systems.<sup>6,7</sup>

## ACKNOWLEDGMENTS

The principal investigator gratefully acknowledges M. J. Sailor (Department of Chemistry, University of California, San Diego) for use of his CCD-based spectrometer system during the course of this project. P. Georgief (San Diego State Foundation) and D. M. Szaflarski (ONR/ASEE Postdoctoral Fellow) are acknowledged for assisting in the fabrication of porous silicon samples during portions of this program. Additional gratitude is given to those who have assisted in the fabrication and characterization of the nanowire structures including: R. C. Dynes and A. S. Katz (Department of Physics, University of California, San Diego), M. Winton (National Defense Science and Engineering Graduate Fellow, Department of Materials Science and Mineral Engineering, University of California, Berkeley), M. A. Wendman (Digital Instruments, Santa Barbara, CA), K. L. Kavanagh (Department of Electrical and Computer Engineering, University of California, San Diego) and A. C. Kummel (Department of Chemistry, University of California, San Diego). Lastly, startup funding was provided by ONR Solid-State Materials program during FY 92 and FY 93.

## REFERENCES

- Brandt, M. S., H. D. Fuchs, M. Stutzmann, J. Weber, and M. Cardona. 1992. "The Origin of Visible Luminescence from 'Porous Silicon': A New Interpretation," *Solid State Communications*, vol. 81, no. 4, pp. 307-312.
- Bsiesy, A., J. C. Vial, F. Gaspard, R. Herino, M. Ligeon, F. Muller, R. Romestain, A. Wasiela, A. Halimaoui, and G. Bomchil. 1991. "Photoluminescence of High Porosity and of Electrochemically Oxidized Porous Silicon Layers," *Surface Science*, vol. 254, pp. 195-200.

---

<sup>6</sup>S. D. Russell, "Energy Converting Porous Silicon Optical Element," Navy case 76,947, disclosure submitted 19 October 1994.

<sup>7</sup>S. D. Russell and W. B. Dubbelday, "Liquid Level Sensor and Detector," NCCOSC case 183.

- Canham, L. T. 1990. "Silicon Quantum Wire Array Fabrication by Electrochemical and Chemical Dissolution of Wafers," *Applied Physics Letters*, vol. 57, no. 10, September, pp. 1096–1098.
- Chynoweth, A. G., and K. G. McKay. 1956. "Photon Emission from Avalanche Breakdown in Silicon," *Physical Review*, vol. 102, no. 2, April, pp. 369–376.
- Davies, L. W., and A. R. Storm, Jr. 1961. "Recombination Radiation from Silicon under Strong-Field Conditions," *Physical Review*, vol. 121, no. 2, January, pp. 371–387.
- Diaspro, A. 1994. "Application of Near-Field Optical Interactions to Microscopy," *USA Microscopy and Analysis*, July, pp. 21–24.
- Dubbelday, W. B., S. D. Russell, A. S. Katz, M. Winton, M. A. Wendman, P. R. de la Houssaye, R. C. Dynes, K. L. Kavanagh, A. C. Kummel, R. L. Shimabukuro & R. Gronsky. 1994. "Fabrication of Single Crystal Silicon Nanowires on a Sapphire Substrate," *27th Annual Symposium of the Southern California Chapter of the American Vacuum Society Abstracts*, 13 September, p. 27.
- Dubbelday, W. B., S. D. Russell, K. L. Kavanagh. 1995. "The Effect of Starting Silicon Crystal Structure on Photoluminescence Intensity of Porous Silicon," *Materials Research Society Proceedings*, to be published.
- Dubbelday, W. B., D. M. Szaflarski, R. L. Shimabukuro, and S. D. Russell. 1993a. "Study of Thin Film Porous Silicon on Sapphire," *Materials Research Society Proceedings*, vol. 283, pp. 161–166.
- Dubbelday, W. B., D. M. Szaflarski, R. L. Shimabukuro, S. D. Russell, and M. J. Sailor. 1993b. "Photoluminescent Thin Film Porous Silicon on Sapphire," *Applied Physics Letters*, vol. 62, no. 14, April, pp. 1694–1696.
- Dumin, D. J. 1969. "Emission of Visible Radiation from Extended Plasmas in Silicon Diodes During Second Breakdown," *IEEE Transactions On Electron Devices*, vol. ED-16, no. 5, May, pp. 479–485.
- Fathauer, R. W., T. George, A. Ksendzov, and R. P. Vasquez. 1992. "Visible Luminescence from Silicon Wafers Subjected to Stain Etches," *Applied Physics Letters*, vol. 60, no. 8, pp. 995–997.
- Fgielski, T., and A. Torun. 1962. "On the Origin of Light Emitted from Reverse Biased p-n Junctions," *Proceedings of the Sixth International Conference on Physics of Semiconductors*, London: Institute of Physics, pp. 863–868.
- Garcia, G. A., and R. E. Reedy. 1986. "Electron Mobility Within 100 nm of the Si/Sapphire Interface in Double-Solid-Phase Epitaxially Regrown SOS," *Electronics Letters*, vol. 22, no. 10, May, pp. 537–538.
- Koshida, N., and H. Koyama. 1992. "Visible Electroluminescence from Porous Silicon," *Applied Physics Letters*, vol. 60, no. 3, January, pp. 347–349.
- Kosyachenko, L. A., E. F. Kukhto, V. N. Sklyarchuk, and V. A. Shemyakin. 1990. "Semiconductor Emitter Having the Spectrum of a Type A Source," *Soviet Journal of Optical Technology*, vol. 57, no. 6, June, pp. 385–386.

- Lanzoni, M., E. Sangiorgi, C. Fiegna, M. Manfredi, and B. Ricco. 1991. "Extended (1.1-2.9 eV) Hot-Carrier-Induced Photon Emission in n-Channel Si MOSFETs," *IEEE Electron Device Letters*, vol. 12, no. 6, June, pp. 341–343.
- Lui, H. I., P. K. Biegelsen, N. M. Johnson, F. A. Ponce, R. F. W. Pease. 1993. "Self-Limiting Oxidation of Si Nanowires," *Journal of Vacuum Science and Technology B*, vol. 11, no. 6, pp. 2532–2537.
- Milewski, P. D., D. J. Lichtenwalner, P. Mehta, A. Kingon, D. Zhang, and R. M. Kolbas. 1994. "Light Emission from Crystalline Silicon and Amorphous Silicon Oxide (SiO<sub>x</sub>) Nanoparticles," *Journal of Electronic Materials*, vol. 23, no. 1, pp. 57–62.
- Namavar, F., H. P. Maruska, and N. M. Kalkhoran. 1992. "Visible Electroluminescence from Porous Silicon np Heterojunction Diodes," *Applied Physics Letters*, vol. 60, no. 20, May, pp. 2514–2516.
- Newman, R., W. C. Dash, R. N. Hall, and W. E. Burch. 1995. "Visible Light from a Si p-n Junction," *Physical Review*, vol. 98, pp. 1536–1537.
- Offord, B. W. 1992. "Fully-Depleted Silicon-on-Sapphire and Its Application to Advanced VLSI Design," 4th NASA Symposium on VLSI Design, pp. 4.3.1–4.3.7.
- Ohno, T., K. Shiraishi, and T. Ogawa. 1992. "Intrinsic Origin of Visible Light Emission from Silicon Quantum Wires: Electronic Structure and Geometrically Restricted Exciton," *Physical Review Letters*, vol. 69, no. 16, October, pp. 2400–2403.
- Perez, J. M., J. Villalobos, P. McNeill, J. Prasad, R. Cheek, J. Kelber, J. P. Estrera, P. D. Stevens, and R. Glosser. 1992. "Direct Evidence for the Amorphous Silicon Phase in Visible Photoluminescent Porous Silicon," *Applied Physics Letters*, vol. 61, no. 5, August, pp. 563–565.
- Rose, D. J. 1957. "Microplasmas in Silicon," *Physical Review*, vol. 105, no. 2, pp. 413–418.
- Russell, S. D., W. B. Dubbelday, P. Georgief, R. L. Shimabukuro, and P. R. de la Houssaye. 1994a. "The Effects of Microcrystalline Structure on the Photoluminescence of Porous Silicon on Sapphire," *Journal of Applied Physics*, vol. 76, no. 10, November, pp. 6012–6013.
- Russell, S. D., W. B. Dubbelday, P. Georgief, R. L. Shimabukuro, and P. R. de la Houssaye. 1994b. "Porous SOS, BESOS, and SOQ for Flat Panel Emissive Displays," *1994 IEEE SOI International Conference Proceedings*, pp. 105–106.
- Russell, S. D., W. B. Dubbelday, and R. L. Shimabukuro. 1993. "Porous Silicon for Pumping Solid-State Lasers," NRaD TD 2461 (March). Naval Command, Control and Ocean Surveillance Center, RDT&E Division, San Diego, CA.
- Sarathy, J., S. Shih, K. Jung, C. Tsai, K. H. Li, D. L. Kwong, J. C. Campbell, S. L. Yau, and A. J. Bard. 1992. "Demonstration of Photoluminescence in Nonanodized Silicon," *Applied Physics Letters*, vol. 60, no. 13, pp. 1532–1534.
- Sawada, S., N. Hamada, and N. Ookubo. 1994. "Mechanisms of Visible Photoluminescence in Porous Silicon," *Physical Review B*, vol. 49, no. 8, pp. 5236–5245.

Steiner, P., F. Kozlowski, and W. Lang. 1993. "Blue and Green Electroluminescence from a Porous Silicon Device," *IEEE Electron Device Letters*, vol. 14, no. 7, July, pp. 317–319.

Wolff, P. A. 1954. "Theory of Electron Multiplication in Silicon and Germanium," *Physical Review*, vol. 95, September, pp. 1415–1420.

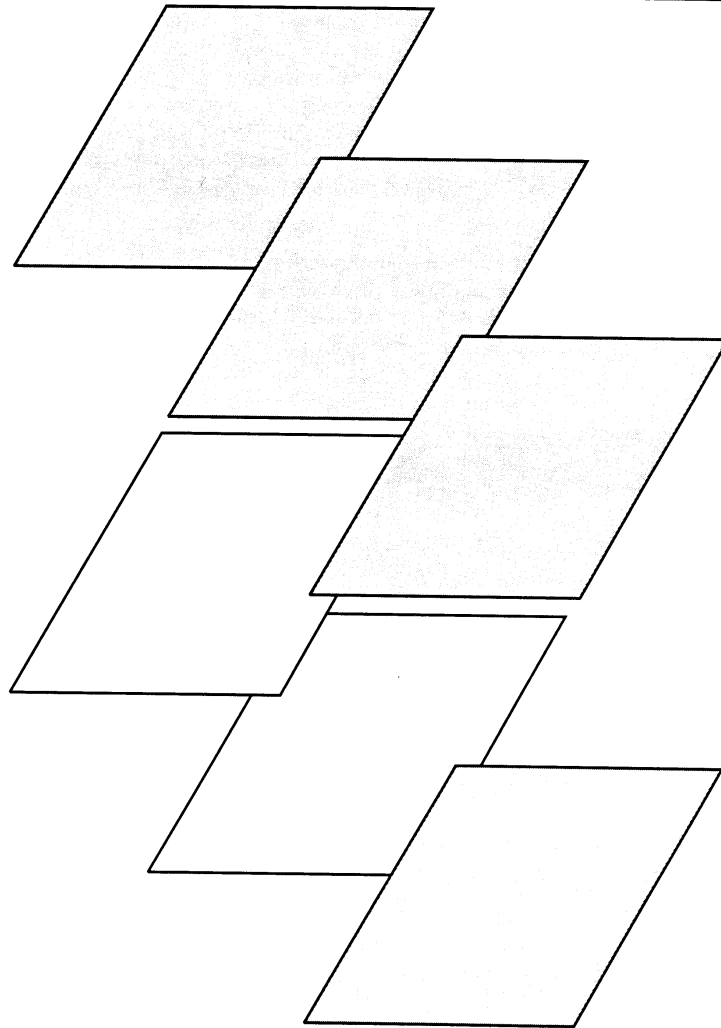
Principal Investigator:  
Dr. Stephen D. Russell

0601152N  
NRaD ZW70

---

## APPLICATIONS FROM PAST IR/IED PROJECTS

---





## Quantum-Well Electroabsorption Optical Modulators

Bandwidth requirements for future antenna-based radar surveillance and communication systems pose significant technology challenges for Navy systems architects. Distribution and reception of ultra-wideband microwave antenna information conventionally uses electrical transmission lines. These electrical transmission lines suffer from high RF loss and are bulky, expensive, and difficult to shield. Analog photonic links are required for transferring the broadband RF information to practical, efficient, optical modulation techniques capable of ultra-wideband operation.

In FY 89, an IR project (NOSC ZW12) entitled “Electroabsorption and Electroreflection in InGaAs/InP and InGaAs/InAlAs Quantum Wells” was initiated in an attempt to optimize semiconductor material properties and device geometry for maximum modulation efficiency. Optimum-well and barrier-material choices, as well as thicknesses, were theoretically predicted and experimentally verified for maximizing the electroabsorption and electrorefraction effects in single quantum wells. An efficient, high-speed optical modulator operating at a wavelength of 1.55 microns was fabricated based on the results obtained from this effort. The quantum-well, optical-device work related to this effort was transitioned into an ONR-funded project (NRaD EE04) to further develop high-speed optical modulators. This ONR program has since been transitioned to the University of California, San Diego (UCSD), where it is continuing.

In FY 92, a follow-on IR effort (NOSC ZW56) entitled “High-Sensitivity Optical Modulators using Asymmetric Coupled Quantum Wells” was initiated to demonstrate that by modifying the potential profile, enhanced electroabsorption could be obtained. Using asymmetric coupled InP/InGaAs/InAlAs quantum wells, an order of magnitude enhancement in the quantum-well electroabsorption effect was demonstrated. This program was transitioned into the ONR-funded program (NRaD CM41) to develop a broadband, photonic, EM field probe. An ARPA-funded optoelectronic effort to modify the semiconductor superlattice potential and refractive index profile by ion-beam mixing, solid-phase regrowth, and the use of the photoelastic effect was also motivated by this IR effort. In cooperation with UCSD, electroabsorption modulators suitable for monolithic integration with other optoelectronic devices have been fabricated by using these material modification techniques. A Phase II SBIR effort entitled “Millimeter Wave Optical Modulator” was also initiated as a result of the FY 93 IR and EM field probe programs. In this program, electroabsorption modulators with bandwidths in excess of 40 GHz are being developed.

Contact:  
Dr. S. A. Pappert

## **Optical Properties of Single-Mode, Fiber-Fused, Biconically Tapered Couplers**

This IR project (NOSC ZT24) began in FY 85 to develop the theoretical modeling and the experimental techniques needed to fabricate reliable and reproducible fused, tapered, single-mode fiber couplers suitable for optical power division and wavelength division multiplexing (WDM). A computer-controlled fabrication process for fused, tapered, single-mode optical-fiber couplers was developed. This process enabled controlled experiments to be performed to develop new fabrication techniques and investigate the material and optical properties of couplers produced by this method. In addition to providing a reproducible, reliable, and efficient means for the production of various types of couplers, including power splitters and wavelength division multiplexers, new insights into the actual optical-coupling mechanism were discovered. Understanding of the fundamental properties of optical couplers was demonstrated in the paper "Core Dopant Profiles in Weakly Fused Single-Mode Fibers," *Electronic Letters*, vol. 24, January 1988. Patent number 4,557,553, "Method of Wavelength Multiplexing in Fused Single-Mode Couplers," was issued 10 December 1985.

The project, initially transitioned to the Diode Array Amplifier program (NOSC CH37) at the end of FY 86, used fiber couplers to obtain coherent summation of single-mode lasers. Another transition to the ONT/ONR Wide Area Undersea Technology program in FY 89 continues through FY 96. In the program, polarization independent narrow channel (PINC) WDM couplers have been developed that enable multiplexing and demultiplexing of optical signals separated by small wavelength differences, on the order of 8 to 40 nanometers. This allows for multiple, and/or bidirectional, signal transmission in fiber telemetry links using a single optical fiber. The PINC WDM fiber couplers can be made to operate in the 1550-nm region where fiber loss is a minimum and Erbium Doped Fiber Amplifiers operate. The PINC WDMs also have been demonstrated at 1310 nm, the second fiber low-loss window. These devices are unique in that they perform the multiplexing/demultiplexing functions independent of the polarization of the optical signals. An invention disclosure, "Method for Producing Polarization Independent Narrow Channel Wavelength Division Multiplexed Fiber Couplers," was filed on 13 August 1990. The PINC WDMs are described in a paper "Polarization Independent Narrow Channel Wavelength Division Multiplexing Fiber Couplers for 1.55 $\mu$ m," *Journal of Lightwave Technology*, vol. 9, no. 4, April 1991. The use of the PINC WDMs in a brassboard system is described in a paper "Bidirectional Transmission at 1.55 Microns Using Fused Fiber Narrow Channel Wavelength Division Multiplexers and Erbium-Doped Fiber Amplifiers," published in *IEEE Photonics Technology Letters*, vol. 6, no. 4, April 1994.

NRaD is seeking to transition its WDM coupler technology to industry for use in both military and commercial fiber-optic and photonic systems. Both Litton Guidance and Control Systems and Honeywell have used NRaD WDMs for implementation of proprietary designs of their interferometric fiber-optic gyroscopes (IFOGs) developed under the ARPA-sponsored Global Positioning System (GPS) Guidance Package (GGP) program. NRaD is negotiating a Cooperative Research and Development Agreement to design, develop, and demonstrate PINC WDMs in fiber-optic hydrophone based, all optical towed arrays. Also, NRaD is seeking with industry partners under the Federal Defense Laboratory Diversification Program to further develop the PINC WDM technology for commercial applications such as long-haul telecommunications networks, and fiber-to-the-home segregation of services such as telephone, NTSC video, HDTV video, and broadband computer networking. Finally, NRaD is addressing the issues

associated with the low cost, high volume production of PINC WDMs in an ONR-funded manufacturing technology and science program (NRaD ET65).

Contact:

M. N. McLandrich

## Robotic Sensor-Motor Transformations

The application of computer technology in the military arena, whether in actual combat, or in peace-keeping functions, is limited by the lack of adaptability of computer-controlled systems. A human observer or operator is invariably required to make critical decisions, often with inadequate information or feedback due to the person's remoteness or isolation from the site of action. Because the original limiting factor was the human operator, the only acceptable solution is to improve the adaptability of the machine. We have approached this objective by creating machines with both sensor and effector capability, and concentrated on the development of computer algorithms that emulate the adaptive biological mechanisms of sensor-motor control.

This research area was initiated in FY 88 under IED support (ZE62). An efficient algorithm was developed for motion analysis of the optic flow based upon mechanisms discovered in the retinas of frogs and rabbits. This algorithm was tested with video camera input and achieved a frame rate of 4 Hz using a 10-MHz 80286 PC, adequate to assess the velocity of a walking human at a range of 10 feet. Subsequent IR support in FY 89 and FY 90 (ZW07) permitted the production of control algorithms for target acquisition based on the frog optic tectum, and the first stages of pattern analysis in the mammalian primary visual cortex. Again using video camera input, the algorithms could learn to scan simple images in search of recognizable features. ONR began supporting this research in FY 91 on a project to emulate biological mechanisms of perceptual invariances in the visual domain. The problem of perceptual invariances must be solved for applications of machine vision to the real world where uncertainty abounds. This issue was pursued with IR funding in FY 92 (ZW07) resulting in the elaboration of theory and in the production of algorithms for the modulation of visual pattern by visual motion through secondary and tertiary cortical visual processing areas. Products from this work transitioned to a joint ONR/ARPA funded project in FY 93 to further explore perceptual invariances using active perceptual mechanisms. During the same time, IED support (ZF25), in collaboration with another code, allowed the implementation of the vision algorithms on a mobile robot equipped with video pan and tilt capability. This new testbed proved concepts of target acquisition and segmentation based on low-level vision while operating in a visually complex environment.

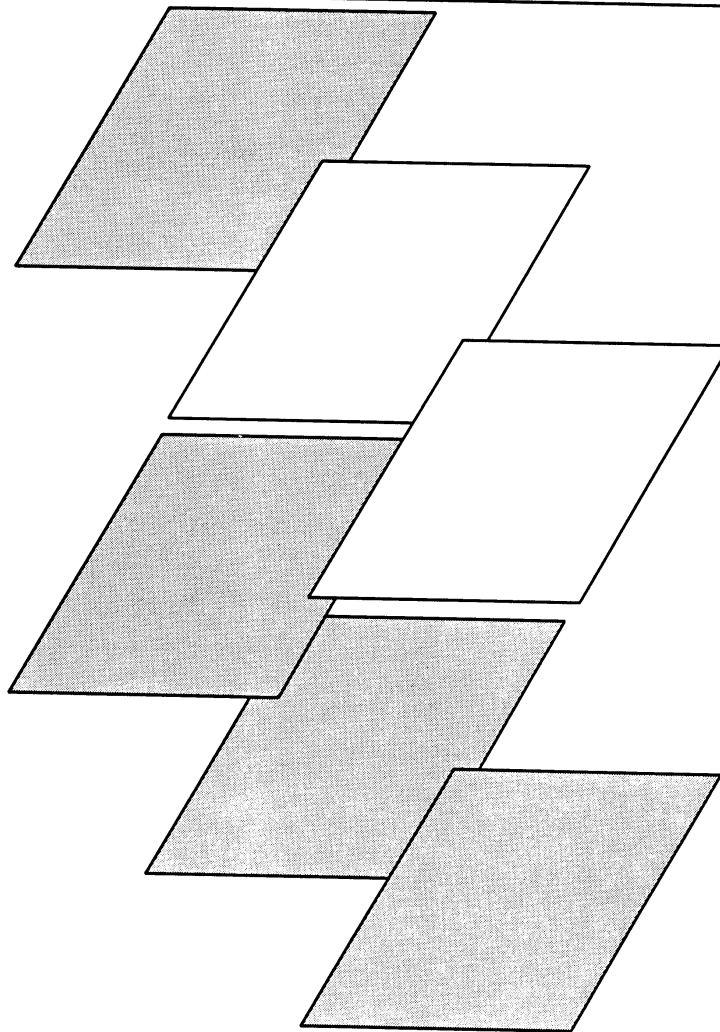
This approach to machine vision is significant because it builds capability from the bottom up, following proven biological methods. This secure foundation in elementary perceptual mechanisms favors the development of more advanced processes that will be analogs of both the functional design and the capabilities of higher vertebrates. Several Navy projects currently in force at NRaD could benefit from the target acquisition, maintenance, and adaptive-recognition algorithms developed through this work. The projects include the Mobile Detection and Response System (MDARS), the Mobile Inshore Underwater Warfare System (MIUW), the Waterside Security System, and the Air Mobile Ground Security and Surveillance System (AMGSSS). Commercial applications of the products of this research include the autonomous navigation of automobiles, autonomous robotic material handling in industry and in agriculture, and domestic robots.

Contact:  
M. R. Blackburn

---

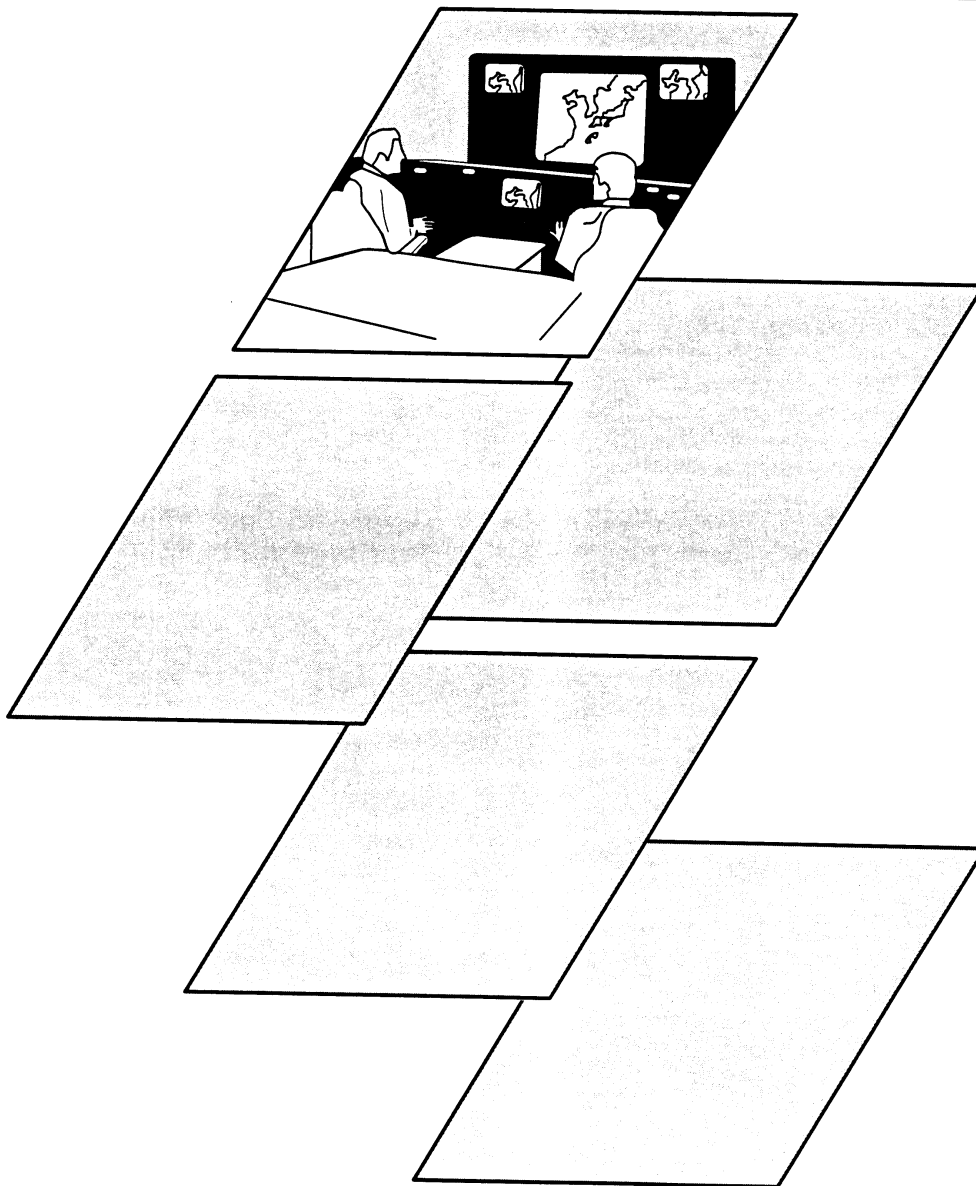
## INDEPENDENT RESEARCH: PROJECT SUMMARIES

---





# COMMAND AND CONTROL





## Deductive Inference in a Nonmonotonic Logic

*Objective(s).* Develop a logic that will enable computers to have the “common sense” to recognize when generalizations have exceptions and, thereby, avoid applying those generalizations “blindly.”

*Accomplishment(s).* Developed a logic of generalizations and exceptions based upon Ernest Adams’ logic of conditionals and a heuristic principle.

In classical logic, the conclusions inferred from premises are guaranteed to be correct. This means that it is impossible for the premises to be true and the conclusions false. However, in many situations where a human being would draw tentative conclusions that have high probability of being correct, classical logic concludes nothing because none of the potential conclusions are 100-percent certain. What is needed for use in computers is a new logic in which conclusions need not be certain, but do have a high probability of being correct. Because such a logic would occasionally infer incorrect conclusions, it should have the property of “nonmonotonicity.” This means that the logic should have the capability of retracting old conclusions when new information casts doubt on them. To accomplish this, the logic would need to be able to recognize exceptions to general rules.

A logic was constructed by first converting Ernest Adams’ logic of conditionals into a logic of syllogisms. The logic was given the property of nonmonotonicity by the following technique. Conclusions are inferred not from premises alone but from premises plus default assumptions. Currently, there are many default assumptions that could potentially be adopted. A heuristic principle was developed for selecting those default assumptions that presumably have high probability of being correct given the premises. Only the default assumptions selected by the heuristic principle are adopted. Thus, when the premises change, the default assumptions change. The resulting logic delivers conclusions that appear reasonable to human intuition. Still to be done is an analysis showing that the conclusions always have a high probability of being correct.

Principal Investigator:  
Dr. D. E. Bamber

0601152N  
NRaD ZW84

## **Further Investigations into the Effects of Using Lasers in Display Devices: Colorimetry and Laser Speckle**

*Objective(s).* Establish the extent to which the use of lasers in display devices affects perceived color and display legibility. Document the perceived effect of color mixing with monochromatic sources, and the effect of speckle on symbol legibility.

*Accomplishment(s).* Showed that the accepted color-mixing equations work less well at predicting color matches between coherent laser and incoherent cathode-ray tube (CRT) color fields when the laser wavelengths are long (deep red) and short (deep blue). Documented that the presence of laser speckle reduced an observer's ability to recognize symbol orientation, especially when the average speckle size approaches the symbol feature size.

Small, powerful visible lasers are now being developed under DoD, ARPA, and commercial funding, to provide sources for large displays. To date, however, work has not been found that pertains to the visual aspects of using coherent sources. To remedy this, we continued FY 93 efforts into FY 94 to establish the extent to which Commission Internationale de l'Eclairage (CIE) color and luminance predictions can be applied to laser images in the presence of multicolor speckle. In addition, we began the process of establishing the extent to which speckle noise in an image reduces legibility.

The setup for our colorimetry experiment was described in the FY 93 IR/IED Annual Report. Basically, we provided the subject with a dual-circle visual field, half of which presented incoherent light from a CRT, the other half presented light from a mixture of red (670 nm), green (532 nm), and blue (458 nm) laser sources. By adjusting the power of the red, green, blue (R, G, B) lasers, subjects produced a visual match between the two fields. Radiance measurements were then made and the CIE color and luminance predictions tested. This comparison was made at the three CRT primary colors as well as white and yellow.

Results from six subjects tested to date indicate that the laser power requirements predicted by the CIE equations (1) underestimated the need at 670 nm by approximately 25 percent; (2) were approximately correct at 532 nm; and (3) underestimated the need at 458 nm by about 15 percent. The intersubject variation was most notable for the 670 nm, which is very deep red. Later experiments (with the author as the subject) using 633-nm red indicated much less discrepancy between the predicted and measured values. These data indicate that designers of laser display systems that will be used in conjunction with other types of displays would be better off avoiding the deep red, not only because much more power is required for a given luminance, but also because its color-mixing properties are less predictable.

The above color-matching experiment was performed both with and without laser speckle. We were surprised to find that there was little difference in the average error between the two cases, even though the difference between the visual field was quite obvious. For example, in the test matching to white, the laser field with speckle appeared as multicolor speckles of virtually every hue, and generally appeared brighter with speckle than without. Yet, when the subjects produced a closest match to the uniform CRT white, the measured radiances were not much different than in the experiment without speckle (with the exception that the standard deviation in measurement was somewhat higher). It is unclear to the authors as to why this is so.

A second experiment was performed to test the affect of laser speckle on legibility. A 35-mm slide projector was modified to allow light from an argon ion laser to replace that from the original lamp. Slides containing the standard Landolt "C" at various orientations were used to project images onto a

diffuse screen. Eight slides, each containing a “C” with the gap either up, down, left, or right, were projected one at a time, and the subject was asked to identify the gap location. The sequence was performed twice, once with speckle present, and once with speckle removed by slightly vibrating one piece of a specially designed laminated screen. Differences between the frequency of correct responses for the two cases indicate the effect of speckle.

Experimental results to date have shown a clear reduction in performance with speckle present, if the viewing conditions produce speckle with average diameter nearly equal to the Landolt-C gap size. The difference in performance between tests with speckle present and tests without speckle varied greatly with distance. For short distances, the difference was negligible; at larger distances, the difference was extreme. This is due to the fact that the angular symbol size decreases with distance. The deterioration with range was much more noticeable when involuntary subject head motion was constrained with a chin rest. This effect might be expected, since the speckle pattern noise appears to move across the image as the head is moved; thereby increasing the visibility of the static target.

All our goals with the speckle experiment have not yet been obtained. Originally, we planned to set up a speckle recording testbed to document the size and contrast of the speckle field by using a charge-coupled device (CCD) camera. We hoped to devise a metric to establish the extent to which speckle must be removed for it to have negligible impact on display legibility. Since visual laser speckle exists only in the eye of the subject, a useful recording would need to duplicate the scene in terms of speckle statistics and image size. Using optical data for a standard eye, we approximated values for the expected speckle size, contrast, and luminance distributions. No affordable CCD cameras were found with suitable resolution and sensitivity to match the human vision system. We have been working toward a film-based solution, but the problem is unresolved.

To extend this work, we would more extensively vary the viewing distance (which changes the apparent speckle diameter compared to the image size), vary the luminance and chrominance of the image (which changes the actual speckle diameter in the eye), continue toward a means of documenting the speckle conditions that are present during the experiment, and perhaps develop methods for removing speckle in the image.

Principal Investigator:  
T. E. Phillips

0601152N  
NRaD ZW73

## Combining Combinatorial Search with Learning for Command Control

*Objective(s)*. Develop a general decision-making procedure capable of making good decisions in cases where information is incomplete and inaccurate.

*Accomplishment(s)*. Developed a method combining Bayesian decision making, Markov Random Fields, and game tree search.

Game tree search methods have proven to be very effective for making good decisions in some types of problems. A well-known example is in the game of chess, where computer chess programs rival even the best human players. However, such successes occur exclusively in cases where the program has “perfect information” about the current state of the task environment. In the case of chess, the locations and types of all the pieces are available from the current board position, and all legal moves for both players are known.

Unfortunately, in a typical Command and Control ( $C^2$ ) problem, the decision maker does not possess perfect information about the task environment. In a conflict, the decision maker is lucky to know the locations and readiness of his own forces, much less those of the opponent. Inaccurate and inadequate information is the norm. In such environments, computers are typically used only to accumulate and display information, providing little assistance for actually making the decisions. The objective of this research is to develop a method that will enable a computer program to recommend good decisions in such  $C^2$  environments.

Game tree search methods would be extended to enable them to make the correct decisions, in a Bayesian sense, given information whose accuracy and completeness can be roughly characterized probabilistically. A method that uses Markov Random Fields has been developed. This method, which can make such decisions for theoretical problems, is currently being tested on perfect information problems and, during FY 95 will be tested on imperfect information problems.

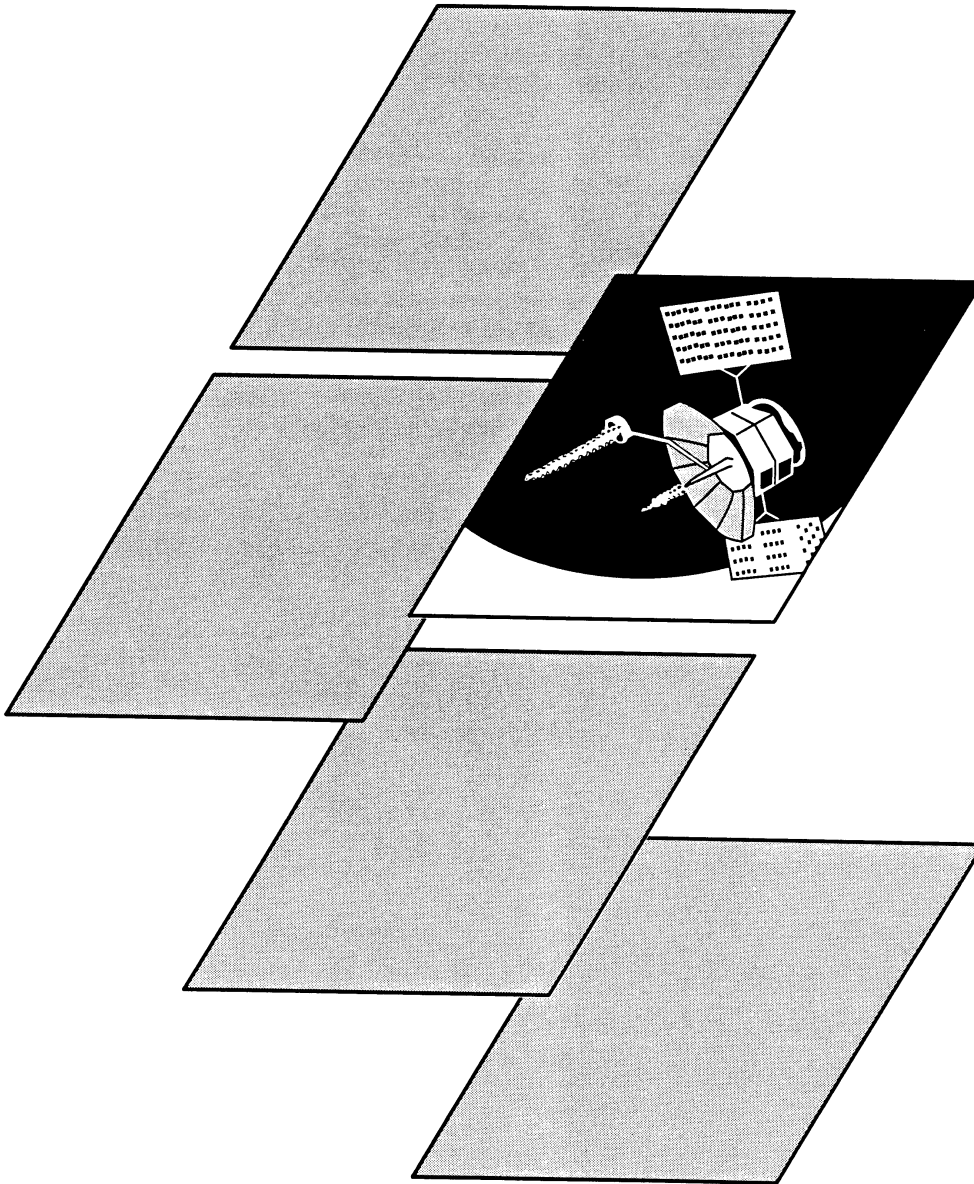
Principal Investigator:  
M. J. Gherrity

0601152N  
NRaD ZW87

---

# COMMUNICATIONS

---





## Ultra-Wideband Impulse Radio Propagation

*Objective(s).* Determine whether ultra-wideband impulse radio is feasible for non-line-of-sight communication.

*Accomplishment(s).* Constructed a transmitter and a transmitting and receiving antenna. Made numerous short-range measurements.

Impulse radio refers to an ultra-wideband communication technology that conveys information using pulse-position modulation of nanosecond pulses. The bandwidth is a result of the gaussian shape of the pulses and the pseudorandom spacing. Typical bandwidths are on the order of 100 percent of center frequency. This gives impulse radio the features of conventional spread-spectrum using a much simpler technique.

This project is designed to measure propagation characteristics of impulses over a non-line-of-sight path. The VHF band was selected to maximize diffraction while avoiding the environmental noise found in the HF band. The impulse transmitter was designed to operate with a center frequency of 100 MHz with a 100-MHz bandwidth. Impulse generation is accomplished by driving a transistor into avalanche mode. The transmitting antenna is biconical while the receiving antenna is a conical monopole. Signal reception is via a digital sampling oscilloscope and samples are downloaded to a computer for analysis.

Measurements have, for the most part, been conducted on the NRaD model range. Results have been good for short line-of-sight tests. Precise clocks are being constructed to allow synchronization for non-line-of-sight and long-range measurements.

Principal Investigator:  
J. L. Coleman

0601152N  
NRaD ZU01

## Blue-Green Iso-Index Filter Material Development

*Objective(s).* To characterize the birefringent properties of a family of chromium-doped fluoride crystals, model the dependence of birefringence on crystal composition, and assess their suitability for use in an iso-index type birefringent filter.

*Accomplishment(s).* In FY 93, eight chromium-doped fluoride crystals of varying composition were procured from the Center for Research in Electro-Optics and Lasers (CREOL) at the University of Central Florida, and sent to Lightning Optical of Tarpons Springs, Florida, for fabrication into prisms. Five useful prisms were prepared from these samples, spanning the range from 100-percent calcium to 100-percent strontium (the other crystals being unsuitable for prism preparation due to cracking from internal stresses). Measurements were completed on these samples using an Abbe refractometer that confirmed that the birefringence changed sign with composition. These measurements also indicated that the appropriate composition for an iso-index point at the sodium D line (589.29 nm) was a composition with slightly less than 60-percent calcium. A procedure for measuring the index of refraction of these samples was perfected based on the classical "Method of Least Deviation," but using discrete laser wavelengths instead of an arc lamp. Measurements were completed with a HeNe (632.8 nm) laser and indicated the appropriate composition for an iso-index point was a composition with slightly more than 60-percent calcium.

Narrow-band, wide field of view, optical filters have been an area of interest for the Navy for decades. In the early 1980s, two birefringent filter-based receivers were developed under the Submarine Laser Communications Program. One of these receivers used traditional filters made of crystalline quartz, while the other was a novel design using cadmium sulfide (CdS) dispersive birefringent materials. Both filters showed significant improvements over preceding technical approaches but suffered some shortcomings. The small birefringence of quartz resulted in very long filters that had a correspondingly small field of view. In contrast, the CdS filters displayed excellent field of view characteristics; however, they suffered from poor optical transmission. In addition, problems with materials' growth and availability limited the size and number of CdS crystals available.

The iso-index filter is a variation on the dispersive birefringent filter design. In the iso-index design, the material used is still dispersive but has no birefringence at the desired operating wavelength. This provides several important advantages. Since the material is isotropic at the design wavelength, the filter uses parallel polarizers rather than crossed polarizers, resulting in improved overall transmission. In addition, since the filtering mechanism is no longer path-dependent at the design wavelength (the material is isotropic at this wavelength), the filter does not exhibit a bandwidth dependence on incident angle. This further improves the field of view characteristics of iso-index filters.

In the past, production of iso-index filters was limited by the availability of suitable materials. There were very few transparent materials with iso-index points in the 450- to 550-nm region, and those that were available were limited to operating at one specific wavelength. LiCAF (LiCaAlF<sub>6</sub>) and LiSAF (LiSrAlF<sub>6</sub>) crystal hosts doped with chromium 3+ ions have been under development by the Navy as solid-state laser materials. Measurements made on these materials showed that they are birefringent. Surprisingly, the birefringence of pure LiSAF is positive, while that of pure LiCAF is negative. The birefringence of a mixed crystal (80-percent strontium and 20-percent calcium) fell between the values measured for either pure crystal. Mixing an appropriate composition in these crystals should allow the

production of a dispersive birefringent material with an iso-index point at any wavelength in the blue-green.

After measuring both the ordinary and extraordinary indices of our samples over a range of wavelengths from 458 nm to 633 nm, the dependence of the iso-index point on material composition and wavelength will be tabulated, and the dispersion of the birefringence around these points measured. Once such data have been gathered, the information can be used to design iso-index filters at suitable wavelengths in the blue-green for use with various underwater laser systems. These include systems being proposed for communications, surveillance, underwater imaging, mine detection, and nonacoustic ASW applications.

Principal Investigator:  
G. L. Adams

0601152N  
NRaD ZW71

## Adaptive Equalization for High-Data-Rate Communications

*Objective(s).* Develop and evaluate adaptive blind equalization algorithms with improved convergence performance for the suppression of intersymbol and other additive interference in high-data-rate digital communications networks.

*Accomplishment(s).* Discovered the mechanism by which the constant modulus algorithm (CMA) for blind equalization can be caused to misconverge by a signal from a phase shift keying (PSK) or quadrature amplitude modulation (QAM) modem that employs a PN-reset data scrambler. Found that (1) the stationary points of the CMA algorithm can be altered by such a signal, and (2) that the impact of the scrambler on CMA convergence performance is minimized when certain relationships between the scrambler parameters and the modulation format are satisfied.

In order to provide ship-to-ship multimedia communications services, the Navy is investigating the development of high-data-rate (>1.544 Mbps) digital communications systems operating in both the military UHF (225 to 400 MHz) and SHF (1 to 10 GHz) ranges. These communications systems will include line-of-sight (LOS) links between the ships of a battlegroup configured in appropriate network topologies. A current SHF effort involves modifications to the existing Light Airborne Multipurpose System (LAMPS), which uses frequency shift keying (FSK). A current UHF effort is focused on the use of more bandwidth-efficient modulations such as  $M$ -ary phase shift keying (PSK) and quadrature amplitude modulation (QAM) for these links. Ship-to-ship radio links are plagued by over-water multipath propagation impairments, nonideal equipment frequency responses, and additive interference. In bandwidth-efficient digital communications systems, adaptive equalization is required to compensate for all three of these sources of performance degradation. The three characteristics of adaptive equalizers that are particularly relevant for use in maritime data network applications are the following: (1) whether or not the equalizer requires a training sequence of known data to adjust its coefficients; (2) the convergence rate; and (3) the degree to which the equalizer can reject additive interference while simultaneously compensating for multipath and nonideal equipment. Blind equalizers do not require training sequences. This property makes them desirable for application in multipoint data networks when it is required that any given node be able to access any of the other (available) nodes at random times. The Navy's proposed ship-to-ship LOS data network is an example of such a multipoint network and would benefit greatly from the use of blind equalization techniques. The single most important blind equalization algorithm for Navy applications is the constant modulus algorithm (CMA). CMA is relatively simple to implement. However, it has three shortcomings that need to be addressed before it can be applied to the Navy's ship-to-ship LOS data network. First, although CMA does not require training sequences, it converges more slowly than a trained equalizer, especially for the more bandwidth-efficient QAM signals. Furthermore, under some circumstances, CMA can "misconverge" to solutions that do not equalize the channel. Finally, it is also possible for CMA to be "captured" by an interfering signal and actually suppress the desired signal in the process.

The main accomplishment of this project in FY 94 was an investigation of the convergence behavior of CMA in blind equalization when the received  $M$ -ary PSK or QAM signal is not random. This situation can arise in practice when the input data port to a modem employing a PN-reset data scrambler is lightly loaded or idle. The limiting case in which the input data port is idle and continuous repetitions of complete maximal periods of a binary PN sequence are encoded into a continuous  $M$ -ary symbol sequence was considered. With these restrictions, the principal factor in determining the properties of the resulting pseudorandom  $M$ -ary symbol sequence is the greatest common divisor  $d$  of the period of the

underlying binary PN sequence and the number  $L_b = \log_2(M)$  of bits per symbol. A closed form expression was derived for the period  $P_M$  of the pseudorandom  $M$ -ary sequence as a function of  $P_N$  (or  $P'_N$ ),  $L_b$ , and  $d$ . When  $d = 1$  (i.e., when  $L_b$  and  $P_N$  (or  $P'_N$ ) are relatively prime), it is also possible to derive separate closed-form expressions for the probability mass function (pmf) of the transmitted constellation for both odd-period and even-period underlying binary pseudorandom sequences. When  $2 \leq d \leq L_b$ , it is not possible to derive such a closed-form expression because the resulting pmfs depend on the relative phase between the binary and  $M$ -ary sequences. The pmfs in these cases can be highly nonuniform, and may be determined by simply counting the number of occurrences of each symbol in the resulting  $M$ -ary sequence.

Given the above properties of the pseudorandom  $M$ -ary symbol sequence, it is possible to see which combinations of  $L_b$  and binary PN sequence period can cause more problems for the convergence performance of CMA than others. In general,  $M$ -ary sequences with short periods and/or highly nonuniform pmfs should be avoided. For some values of  $L_b$ , it is also possible to construct signals with very short periods and yet uniform pmfs. Simulations using pseudorandom 8-PSK sequences were used to illustrate that for nearly equivalent periods, the uniformity of the pmf can be a deciding factor in determining if the CMA blind equalizer will converge. By considering the effect of the nonuniform pmf on the expected value of the error-function component of the CMA tap-weight update after convergence, it was possible to predict that the introduction of a pseudorandom  $M$ -ary sequence after the equalizer had converged (in response to a random sequence) could cause it to move away from settings that equalize the channel. This was demonstrated via simulation for 16-QAM sequences derived from encoding the maximal odd- and even-period binary sequences from the same shift register with the same feedback connections. These simulations also served to illustrate that, given a fixed number of shift register stages in the scrambler, selecting the corresponding (odd or even) period of the PN sequence such that it is relatively prime to  $L_b$  has a strong impact on the convergence performance of CMA.

Principal Investigator:  
R. A. Axford

0601152N  
NRaD ZW80

## Observation of Ionospheric Dynamics

*Objective(s).* Investigate the possibility that solar X-ray flare precursors are detectable in the ionosphere. Develop an ionospheric F-region variability index.

*Accomplishment(s).* Developed a variability index using San Diego data for the ionospheric F-region parameters foF2, MUF(3000), hmF2, and ymF2.

Two main goals are included in this effort: One goal is to investigate experimentally, through a long-term, high-temporal-resolution ionospheric sounding effort, the possibility that ionospheric solar flare precursors may be detectable by vertical incidence sounding of the ionosphere. This effort has been severely hampered by the total lack of any large solar X-ray flares occurring this fiscal year. The sun has been extremely quiet during the current minimum in the solar sunspot cycle, and we have not observed any examples of solar flares with which to study the phenomenon, if it exists.

The second goal of this effort is to establish an ionospheric F-region variability index that quantifies the diurnal and seasonal periods of maximum variability. This information is of potential use to military systems that involve propagation through or reflection from the ionosphere.

A new variability index for the F-region parameters foF2, MUF(3000), hmF2, and ymF2 was developed by using San Diego ionospheric data. An example of the index for the MUF(3000) is shown in figure 1 for three winter months. The periods (near sunrise and sunset) of maximum variability are clear in the figure. Also evident is an almost linear decay of the index from sunrise, which continues for the remainder of the day. Quite different behavior is seen for the summer months and for other parameters.

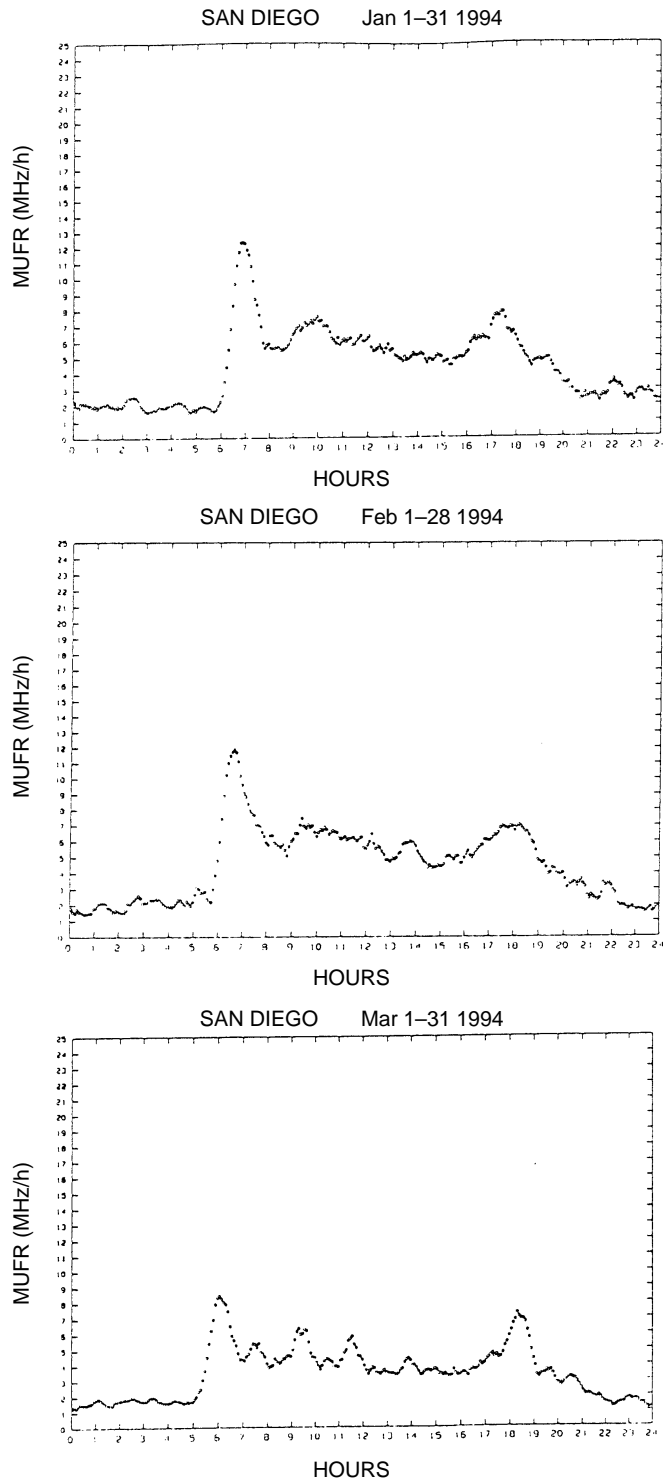


*Figure 1. Variability index for the parameter MUF(3000) for three winter months in 1994. Data for the derivation of the index were obtained from the San Diego sounder.*

Principal Investigator:  
R. A. Sprague

0601152N  
NRaD ZW82

## Quantitative Performance Evaluation of an ATM-Based Statistical Multiplexer

*Objective(s).* Derive a simple formula to estimate the transient cell-loss probability of an ATM statistical multiplexer subject to heterogeneous groups of on-off traffic sources.

*Accomplishment(s).* Derived an efficiently computable expression to estimate the transient cell-loss probability of the multiplexer. Derived the parameter region in which the expression is expected to be accurate. Developed a simulation model of the multiplexer to assess the accuracy of the derived expression. Designed an optimal algorithm to address the ATM buffer dimensioning problem.

Asynchronous Transfer Mode (ATM) networks will be the backbone of future information super-highways. Because of their ability to efficiently transport multiple traffic types, such as data, voice, and imagery, they are destined to revolutionize the global telecommunications industries. Despite their expected prominence, many of their basic design issues, such as buffer dimensioning, admission control, and routing, still have not been addressed. The resolutions of these issues will require a thorough understanding of the dynamic behavior of the ATM statistical multiplexer. Providing an analytical framework of the dynamic behavior of the ATM statistical multiplexer is precisely the objective of this work.

The statistical multiplexer subject to heterogeneous groups of on-off traffic sources is selected as the model of the analysis since it has relatively simple structures and yet captures the salient features of a real ATM multiplexer. The key performance measure of the multiplexer is its transient (time-dependent) cell-loss probability, as cell loss is the biggest concern for an ATM network; more specifically, the objective of this work is to derive an efficiently computable expression to estimate the transient cell-loss probability of the multiplexer. A set of partial differential equations (PDEs) is formulated to describe the transient behavior of the multiplexer. The transient cell-loss probability may then be obtained, in principle, from the solution of these equations. Unfortunately, the number of PDEs involved grows exponentially as the sizes of the parameters of the multiplexer increase. To overcome this combinatorial explosion, a discrete process that describes the multiplexer's behavior is approximated by a continuous one; the approximation is expected to be valid when the parameters of the multiplexer are set to match those found in a typical ATM environment. Effectively, the approximation reduces the number of PDEs involved to a two-dimensional PDE. The resulting PDE does not correspond to any PDE that has a close-form solution. Although the PDE may be solved numerically, doing so will not meet the objective of obtaining an analytical expression for the cell-loss probability. An approximation solution to the PDE is derived, and the cell-loss probability is expressed in terms of the approximation solution. The parameter region of the multiplexer, at which the approximation solution is expected to be valid, has also been derived. An optimal procedure to solve the ATM buffer dimensioning problem is formulated by using the derived estimation to the cell-loss probability. The procedure is also used in a numerical example to demonstrate the advantage of using an ATM-like network over the traditional Navy networks.

The quality of the cell-loss probability approximation is assessed through simulation studies. From the simulation studies conducted so far, the maximum relative error of the approximation is 115 percent. The large error may be attributed partly to the fact that the parameters set for the simulation studies fall outside the parameter region at which the approximation is valid. The parameters for the multiplexer must be large in order for the approximation to be accurate, but the computing requirement of a simulation study with large parameters is prohibitively excessive. The large error may also be attributed to the use of a one-term approximation to solution of the PDE. It is expected, that by using a multiple-

term approximation to the PDE, the accuracy of the approximation of the cell-loss probability would be improved. Also, the parameter region in which the approximation is valid would be expanded considerably, enhancing the applicability of this research. The multiple-term approximation to the PDE is being pursued under the IR Project of FY 95.

Principal Investigator:  
A. Shum

0601152N  
NRaD ZW96

## **Multiwavelength Ultraviolet (UV) Source Development**

*Objective(s).* Develop and characterize a high-repetition rate neodymium laser capable of operating at widely spaced wavelengths in the 1- $\mu$ m region.

*Accomplishment(s).* Characterized diode-pumped Nd:YAG and Nd:YALO lasers and demonstrated a novel approach for wavelength selection between 1064 and 1099 nm in Nd:YALO.

A high-repetition rate neodymium (Nd)-based laser that can be efficiently frequency quadrupled and used as a discretely tunable source at 266 nm and 275 nm has been demonstrated. The motivation of this work was to show that such a laser could have potential in an intentionally short-range communication (ISRC) system. A distinct benefit would result if the laser link could be operated at two wavelengths independently. The recent availability of high-power and high-duty-cycle, pulsed-laser, diode-pump arrays has made a neodymium-based laser an attractive approach for achieving this goal.

Nd:YALO exhibits the desired highly structured gain spectrum in the 1-micron region and has favorable thermal and mechanical properties. We made detailed and quantitative measurements of the anisotropic emission and absorption spectra and determined a suitable crystal orientation to achieve laser operation at either 1064 or 1099 nm. A novel filter based on the birefringent dispersion in crystal quartz was designed to allow wavelength selection of either laser line, in the same cavity, under high-gain pumping conditions.

Diode-pumped laser experiments were performed with both Nd:YAG and Nd:YALO with intracavity frequency doubling and external conversion to the fourth harmonic. The cavity geometry was verified using Nd:YAG, which also gave a reference level of performance. Over 4 W of Q-switched output at 1.33 kHz was obtained at 532 nm with an optical efficiency of 10 percent. The experiments with Nd:YALO were limited to repetition rates of a few hundred Hz due to the spectral details of the laser diodes and the Nd:YALO absorption. At 100 Hz, 2.5 and 1.4 mJ were obtained at 532 and 549.5 nm, respectively. Subsequent frequency conversion to the UV yielded 0.23 and 0.07 mJ at 266 and 275 nm. These results indicate that further power scaling and operation at higher repetition rates should be possible.

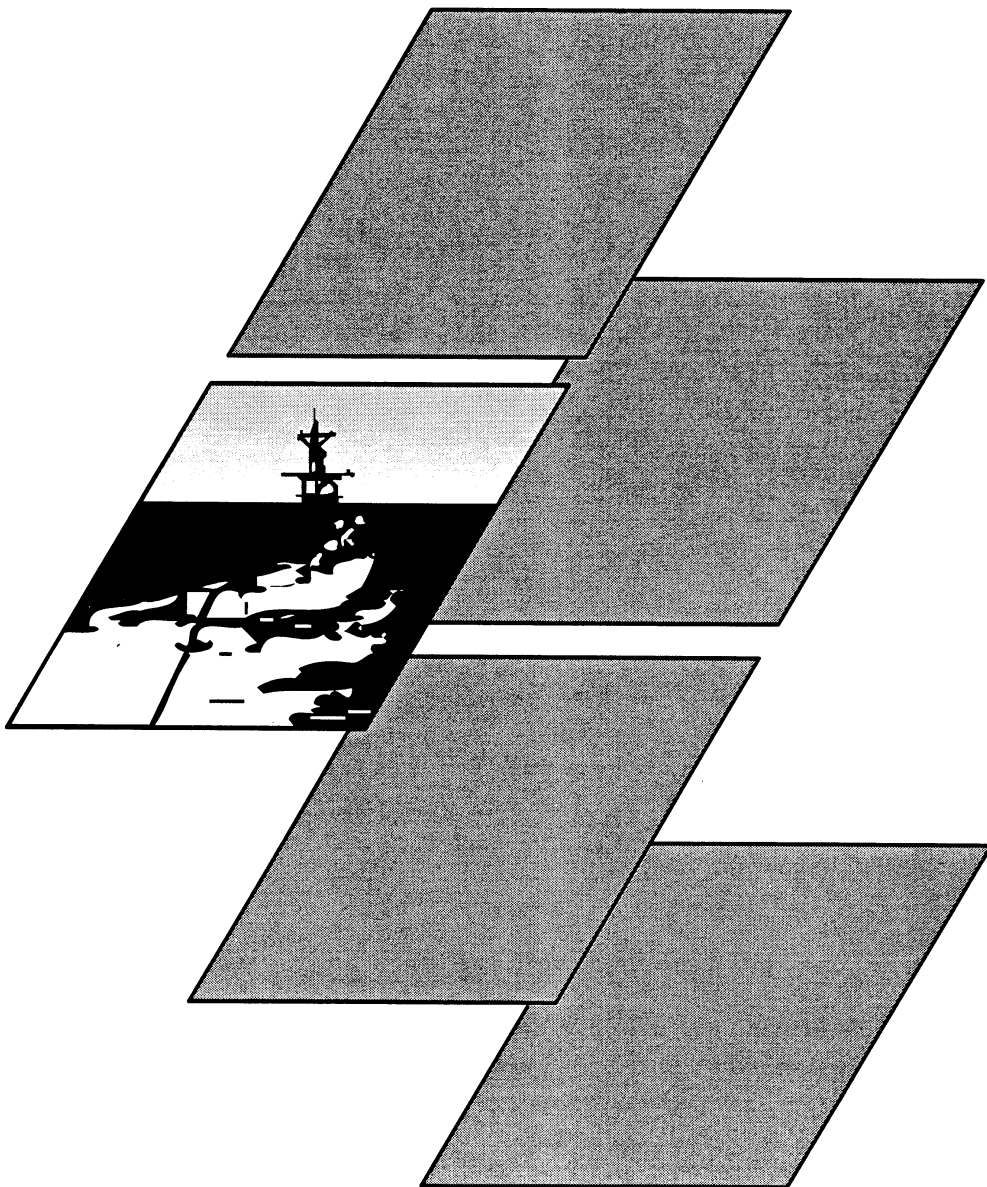
Principal Investigator:  
Dr. F. E. Hanson

0601152N  
NRaD ZW89

---

# OCEAN SURVEILLANCE

---





### **Three-Dimensional Electric Field Measurements in Shallow Water**

*Objective(s).* Develop a three-dimensional Electric Field Sensor Float (EFSF) that will allow measurements of the shallow-water noise field. Evaluate the background electric field and the motional induction source term.

*Accomplishment(s).* Negative results of prototype and repeated cost increases with loss of capabilities by contractor indicated work on EFSF development should not be pursued.

The development of the Electric Field Sensor Float (EFSF) and its deployment in the SoCal testbed allow us to place an emphasis on evaluation of E-fields from bottom-moored and drifting platforms. This evaluation would address the basic issue of contributions from motional induction (sea water motion through the earth's magnetic field). The governing equation says that  $\mathbf{v} \times \mathbf{F}$  (the motional induction source term) equals  $\text{grad } \phi$  (the electric field) plus  $\mathbf{J} / \rho$  (the electric current term). Motionally induced E-fields observations are obtained. This information is needed to determine if drifting sensors can observe E-fields in frequency bands where vessel signatures are expected.

The planned measurements will allow us to make a first-order characterization of the ambient E-field in a region of Navy interest and will help quell the ignorance of shallow-water fields near shorelines where significant ocean currents flow. Finally, important and basic questions about the technology to make E-field observations at mid-depth and near-surface will be answered by the various depths.

Principal Investigator:  
M. J. Morey

0601152N  
NRaD ZW91

## Matched-Field Tracking

*Objective(s)*. Develop new method for detecting quiet (i.e., diesel electric on battery power) submarines in shallow water.

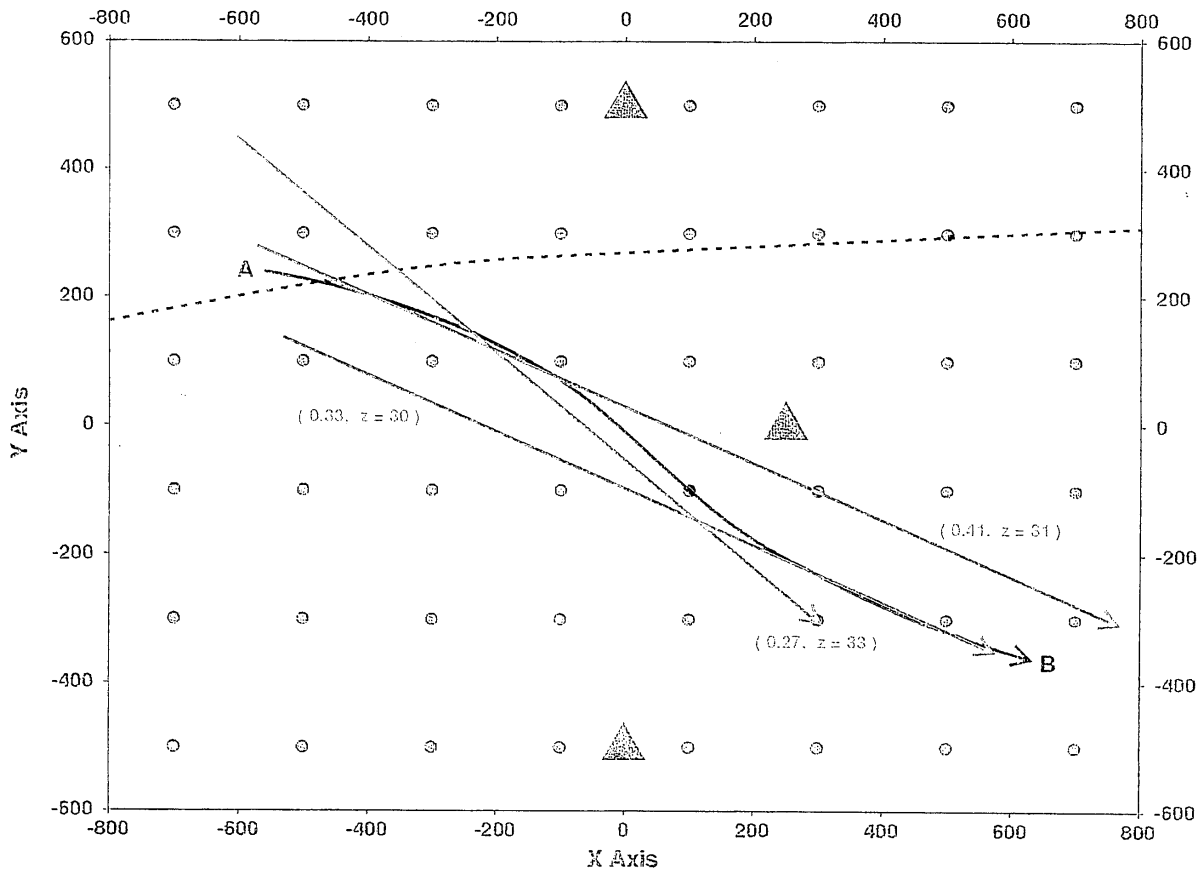
*Accomplishment(s)*. Developed an algorithm that allows coherent processing over a 3- to 5-minute period of time. This provides sufficient processing gain for the detection of very quiet targets.

Detection ranges for quiet targets in shallow water tend to be small (usually less than 10 km) because of high propagation loss and high ambient noise levels. When an acoustic source travels close to a sensor, the received signal has large fluctuations due to differential change in phase of the multipath arrivals as the range varies. In the matched-field-tracking algorithm, compensation is made for this signal fluctuation by calculation of the expected signal for a specified target location.

In the matched-field-tracking algorithm, the end points (A and B) of a possible track are specified (figure 1). Then, a correlation function,  $C_{AB}$ , is defined as the matched-filter between measured elements of the covariance matrix and corresponding elements calculated for the specified path A to B. The next task is to search the space of possible paths to find those with the highest correlation values. To do this, values of  $C_{AB}$  are calculated over a coarse search grid. Then, iterations are made on the locations of A and B to find the relative maximum values of likely tracks.

A paper published in the December 1994 issue of the *Acoustical Society of America* describes a realistic simulation of the algorithm where a quiet submarine target is detected in the presence of a much louder surface ship and high ambient noise levels.

The algorithm can be easily extended to the case of moving receivers. Therefore, simulations will be made to demonstrate its application using signals from two or more sonobuoys.



- ▲ Locations of 3 hydrophones
- Start or end point on coarse search grid
- A---B Path of submarine
- Path of surface ship (right to left)
- Three paths with highest correlations.

Figure 1. Plan view of sensors and targets.

Principal Investigator:  
Dr. H. P. Bucker

0601152N  
NRaD ZW85



## Shallow-Water Three-Dimensional Parabolic Equation Model

*Objective(s).* Develop and validate a high-speed, shallow-water, acoustic propagation model based upon the split-operator method for solving the parabolic wave equation.

*Accomplishment(s).* Extended the domain of applicability for the split-step parabolic equation (PE) algorithm by incorporating shallow-water bottom boundary conditions directly into the PE propagator. Developed a new method for efficiently extending the computational PE grid by using a boosted propagator. The ramifications of this are twofold: first, exact bottom conditions may now be incorporated into split-step Fourier PE codes just as in finite difference PE codes; second, large calculational domains can be covered at modest calculational expense, allowing PE computations at higher frequencies and larger areas.

The changing nature of the submarine threat has refocused the Navy's interests on shallow-water antisubmarine warfare (ASW). With this new emphasis has come a concomitant requirement for new ASW systems and tactics that are capable of exploiting and/or mitigating the effects of the shallow-water acoustic environment. To meet this challenge, one needs the capability to analyze and predict the propagation of acoustic wave fields in complex spatial-temporal environments and thereby impact the design of new sensors and robust signal-processing algorithms. In particular, the requirements of broadband matched-field processing in shallow-water applications has reinforced the requirement for full-wave propagation models.

The approach used in this work is to extend the two-dimensional split-operator spectral parabolic wave equation algorithm to three dimensions and incorporate generalized impedance- type boundary conditions to deal with the strong bottom interaction present in shallow-water environments. Along with the algorithm development is a rigorous error analysis based upon operator truncation analysis.

Principal Investigator:  
Dr. F. J. Ryan

0601152N  
NRaD ZW79

## Signal Detection Based on Limited Clues

*Objective(s).* Determine under what conditions, if any, two-state Markov change-point statistical methods have a higher probability of detecting targets for a set false-alarm value than the method currently in use.

*Accomplishment(s).* Compared the best of the parametric two-state Markov change-point methods, cumulative sum (CUSUM), with the “optimal” matched-filter detection method. Determined that the change-point statistical methods have a higher probability of detecting targets, even when the signal is time late or increasing in amplitude. Derived an extension of the CUSUM change-point method that will provide estimates of the signal start, end points, length, and amplitude. Performed Monte Carlo testing of the new statistic, the maximum CUSUM, to determine the error in these estimates. Rederived the dynamic programming algorithm, track-before-detect method, to include the maximum CUSUM statistic.

Current target detection and tracking algorithms fall into two classes: detect-before-track methods and track-before-detect methods. In both of these classes, the detection methodology embedded in the algorithms assumes that either the target is present in all of the observations, or the target is not present in all of the observations. The parametric matched-filter method in use in many systems and currently being implemented in the Shipboard Infrared Surveillance and Tracking System (SIRST) has been well documented. This method is, uniformly, the most powerful for the specified underlying conditions. Improvements in the signal-detection algorithms can only occur with a change in the assumption in the underlying conditions.

Recent work in manufacturing quality control by Siegmund, Hawkins, Woodall, B. James, K. James, and others, and by the principal investigator in medical sign monitoring has produced a new set of statistical methodologies. These methods assume that if a signal is present, it may start at some time after the initial observation. Of the parametric methods of this type, the CUSUM statistic provided the highest probability of detection. This statistic was tested against the matched-filter statistic. The probability of detection for the CUSUM statistic was the same or higher for all cases. As expected, the CUSUM statistic outperformed the “optimal” matched-filter algorithm when the signal was time late in arriving in the listen interval, or the data increased in amplitude with time.

An extension of the CUSUM statistic, maximum CUSUM, was derived, which removes the background noise that arrives before the onset of the signal, or after the signal has stopped. This method also provides estimates of signal start time and stop time, signal amplitude, and signal length. The additional information provided could be used to remove transients and would help in pruning unwanted paths in a track before detect algorithm.

The detect-before-track algorithms have a lower probability of detection for a given probability of false alarm than the track-before-detect methods. Of the track-before-detect methods, the dynamic programming algorithm (DPA) is considered to be the best. However, the DPA's computational burden is overwhelming. Current implementations, in an effort to decrease the computational burden, use banks of velocity filters. These implementations assume straight-line trajectories for the target over a small number of frames. Next-time-frame target searches are restricted to a linear search in the X direction and a linear search in the Y direction. The DPA algorithm adjusts for target appearance within a set of frames by starting a new set of algorithms at every frame. The detection method assumes the target is present or not present for all the frames viewed. These complications increase the computational burden of the DPA

and limit the number of integration frames. The DPA was rederived by using the hypotheses used to derive the maximum CUSUM statistic. A copy of Yair Barniv's DPA Fortran code was obtained, and work was initiated to make the changes in the algorithm. This work was not completed during FY 94.

This work has demonstrated that increases in the probability of detection are obtainable over the currently used statistic when the signal is either increasing in amplitude or is contained in only part of the data set. Estimates of signal start and stop time, signal amplitude, and signal length from this statistic would help in removal of transients and in setting the listen interval. This information, when used as part of the dynamic programming algorithm, would decrease its computational burden.

The use of a method that provides improvements in signal detection would benefit the Navy and Marine Corps surveillance sensors, weapons, and defense systems. Implementation of this technology in medical monitoring systems would help provide needed wartime medical logistic information as well as improvements in preventive medicine in civilian as well as military settings.

Principal Investigator:  
J. K. Pugh

0601152N  
NRaD ZW93

## Acoustic Bottom Interaction Using the Parabolic Equation

*Objective(s).* Develop theory, algorithms, and a computer code to model the propagation of acoustic energy near the liquid-solid interface, including elastic effects (such as shear waves) in the solid.

*Accomplishment(s).* Developed a preliminary theory and preliminary testbed computer code that use a Parabolic Equation (PE) approximation of two-dimensional acoustic propagation in elastic materials. Incorporated refinements to interface and backscatter conditions. A final full version is now being completed.

Navy emphasis has shifted from open-ocean, deep-water environments to littoral, or coastal, environments, since these environments are the most likely sites of naval operations and conflicts. The shallow-water littoral environment is a very demanding one for acoustic propagation: It requires accurately taking into account three-dimensional bathymetry, complex and high-level local noise fields, and intense bottom interaction. Advanced signal-processing techniques and safe naval operations in general require accurate signal representations, including this extensive bottom interaction.

In the shallow-water environment, there is extensive coupling of acoustic energy to the bottom sediments. Accurate handling of this bottom coupling and elastic effects in the bottom, including shear waves, is required to successfully understand the littoral environment.

To provide a stable formulation, which includes full-wave effect (as opposed to limited, often inaccurate approximations such as ray theory), an improved PE approximation was developed based on previous work of others in the field. The approach pursued allows development of an efficient, two-dimensional, viscoelastic PE that incorporates the necessary bottom interaction effects, including interface effects, shear wave propagation, range-dependent bottom bathymetry and bottom composition, water-column variation, and so forth. The “split-step Pade approximation” (M. D. Collins, *J. Acoust. Soc. Am.* 93, 1736–1742, 1993) can be applied through the formalism developed to yield improved accuracy and stability due to the unitary operators used. The possibility of using Fourier split-step propagation algorithms, which are intrinsically more stable than finite-element techniques, has also been explored using the formalism and algorithms developed. Other necessary refinements studied include improved boundary condition handling by developing corrections accounting for the fact that actual interfaces are never locally rectilinear, but involve finite slopes.

Accurately accounting for these bottom-interaction effects can produce significant differences critical to actual sensor performance prediction and signal processing, particularly for bottom-mounted or near-bottom sensors, which are a preferred configuration in shallow water. A simple example in a very simple scenario, which shows only the effects of including shear wave propagation and ignores any range variation or local scattering effects, is calculated and presented in figure 1. The scenario is of a detection target following a straight-line path past a bottom-mounted acoustic sensor in 73-m-deep water. The target’s closest approach is 2 km, and the operational range of the sensor is 6 km. The effective transmission loss, a logarithmic measure of the energy flux degradation at the sensor due to spatial propagation, is shown as a function of target location on its path while in the operational range. All range dependence is suppressed. Differences of up to 20 dB occur when shear is taken into account, which, when convolved with other detection factors, can dramatically alter the probability of detection of the target.

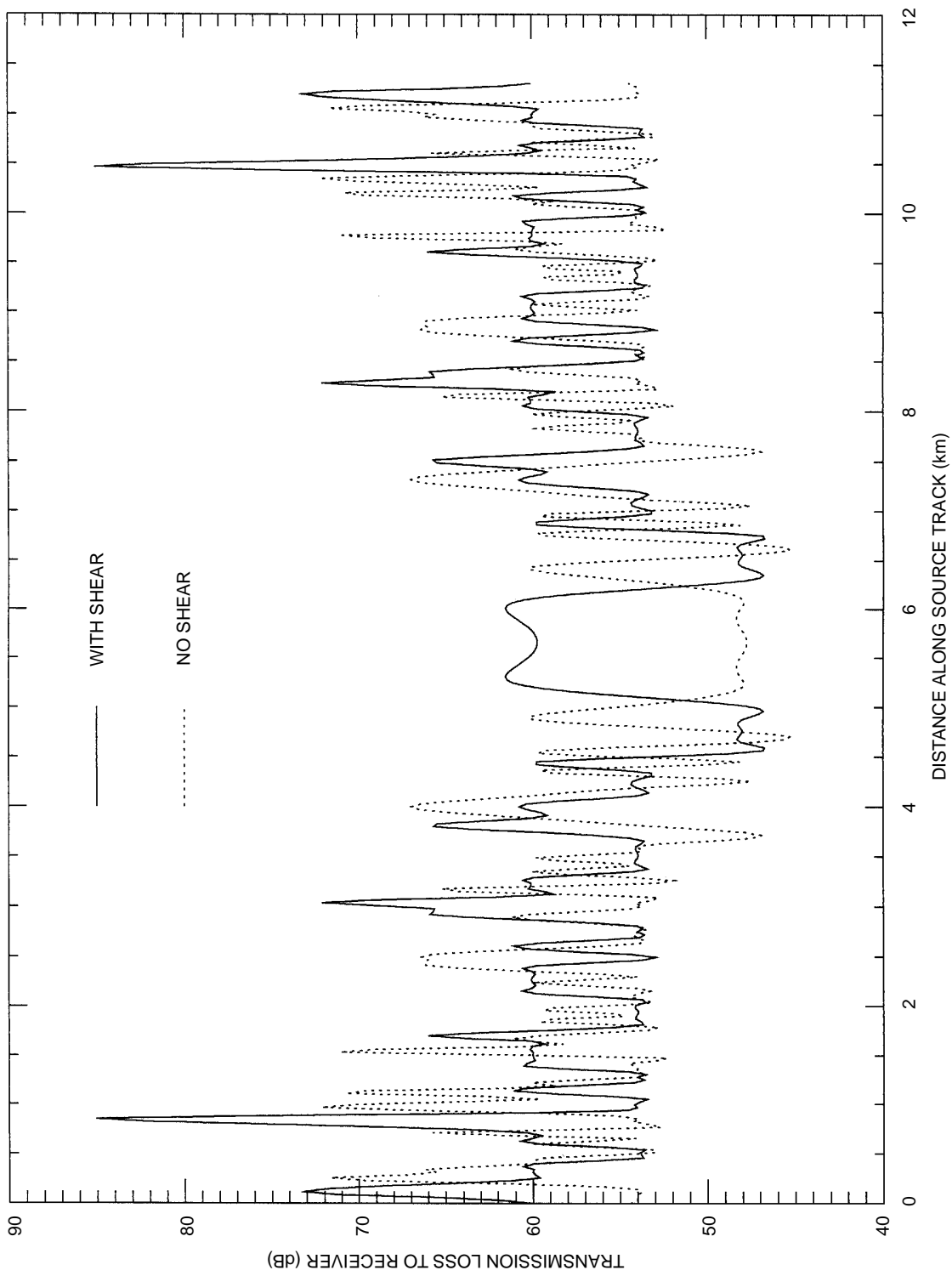


Figure 1. Propagation comparison with and without shear.

A final version of the theory, algorithms, and code is currently being produced. Results will be compared with the environmentally well-measured, complete Shallow Water Environmental Cell Experiment measurements recently conducted off the Southern California coast.

Principal Investigator:  
C. D. Rees

0601152N  
NRaD ZW94

## Wavelets for Ultrabroadband Radar

*Objective(s).* Develop and implement new wavelet algorithms for the processing of ultrabroadband radar.

*Accomplishment(s).* Developed a software package for Morlet wavelets. Formulated a general theory for the inversion of discrete nonorthogonal wavelets and published the results. Applied the software to ultrabroadband radar data.

This project has involved two concurrent efforts. The first consists of software development in order to interface the radar data, provide suitable graphics for the wavelet transforms, and enable interactive filtering in the wavelet domain. The second is the completion of suitable theory for the inversion of nonorthogonal wavelet transforms and its implementation. The project was completed in FY 94.

An extensive wavelet software package was developed with a MATLAB interface for visualization and interactive filtering in the wavelet domain. In particular, the user may experiment with different filters by using a mouse to excise regions in the wavelet domain and examine the result under the inverse wavelet transformation. Several sets of data were provided by the Radar Branch of NRaD. These data were examined and the following conclusions were reached: (1) RF interference may be dealt with by several classical techniques, but the wavelets appear to provide more efficient removal. (2) The highpass *à trous* wavelet filters, when used as matched filters for the return signals, appear to perform better than matched filters based on the emitted signals. (3) However, some indications exist that time-domain signal-processing techniques may be more relevant than time-frequency transforms, either FFT or wavelet. This is not too surprising considering the very short pulse duration.

The theoretical work, which was realized and applied in the above software, involved the derivation of discrete algorithms for the inversion of nonorthogonal wavelets. The standard inversion procedure for such transforms is a finite expansion in terms of the analyzing wavelet. While this approximation works quite well for many signals, it either fails to achieve good accuracy or requires an excessive number of scales for others. To overcome such difficulties, several new algorithms were derived that provide more adequate inversion. In the process, both practical and theoretical issues for the inversion of nonorthogonal wavelet transforms were addressed, and the results written up in several papers.

Principal Investigator:  
Dr. M. J. Shensa

0601152N  
NRaD ZW95

## Hydrodynamic Characterization of Bioluminescent Stimulus

### Part II—Prediction

*Objective(s).* Characterize the response of both laboratory and *in situ* luminescent organisms throughout a wide range of hydrodynamic stimuli. Predict whether a body moving through ocean waters, whose bioluminescent potential is known, will excite bioluminescence.

*Accomplishment(s).* Used a fully developed pipe flow to identify a general photomultiplier tube (PMT) vs. wall shear stress curve for both laboratory (0.1 to 200 dynes/cm<sup>2</sup>) and *in situ* (0.1 to 1000 dynes/cm<sup>2</sup>) luminous dinoflagellates. Combined these data together with conservative estimates on the shear stress resulting from a swimming dolphin to predict bioluminescent stimulation along most of its body.

Figure 1 is representative (in shape, magnitude changes throughout the year) of the average luminescent response to wall shear stress ordinarily found for the *in situ* measurements collected in San Diego Bay. Bioluminescence is observed, as it was the year before, to begin for  $\tau_{\text{wall}}$  values greater than about 1 dyne/cm<sup>2</sup>. With increasing  $\tau_{\text{wall}}$ , a conspicuous change in the rate of increase of average bioluminescence is normally found to occur between 10 to 20 dynes/cm<sup>2</sup>, with the greater rate of increase occurring initially. This is true regardless of whether the flow is laminar or turbulent. (The gap in the data shown in figure 1, between  $\tau_{\text{wall}}$  of 15 to 40 dynes/cm<sup>2</sup>, reflects transition from laminar to turbulent flow.) Again, as we found the previous year, between  $\tau_{\text{wall}}$  levels of 10 to 20 dynes/cm<sup>2</sup>, peak flash levels of individual cells become, after initially exhibiting a graded response (increasing with  $\tau_{\text{wall}} < 10$  dynes/cm<sup>2</sup>), approximately constant thereafter. The source of the San Diego Bay luminescence has been identified as the following dinoflagellates: Gonyaulax, Protoperidinium, Ceratium, and Noctiluca, occurring in various proportions throughout the year. With the exception of Noctiluca, laboratory cultures of all these organisms have been tested in similar pipe flows, and, where the range of shear stress can be compared (0.1 to 100 dynes/cm<sup>2</sup>), share similar traits with the *in situ* measurements. Figure 2 is a photograph (10-second exposure) of bioluminescent excitation. Gonyaulax polyedra,  $\sim 10^6$  cells per liter, was poured from a beaker over a model of a dolphin.

Bioluminescent threshold levels of the order 1 dyne/cm<sup>2</sup> indicate, contrary to numerous anecdotal reports, that swimming dolphins should excite bioluminescence over most of their bodies. This has been confirmed and filmed under controlled conditions. Recordings from a low- light-level ISIT camera were taken of a trained Navy dolphin swimming between floating pens. The pens were enclosed and draped with black cloth to reduce background light. Figure 3 is a photograph of a single frame, taken by the ISIT camera, of about the first third of the dolphin as he swam beneath us (swim speed about 2 m/s). Bioluminescence, which began around his blow hole, was observed over his remaining length.

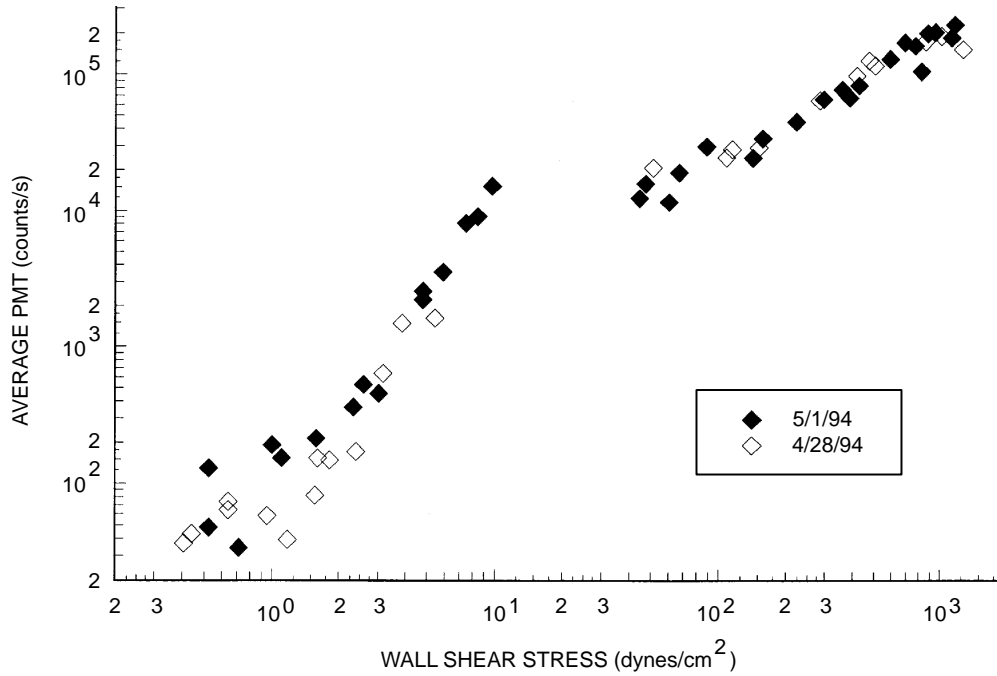


Figure 1. Representative San Diego Bay PMT levels as a function of wall shear stress.

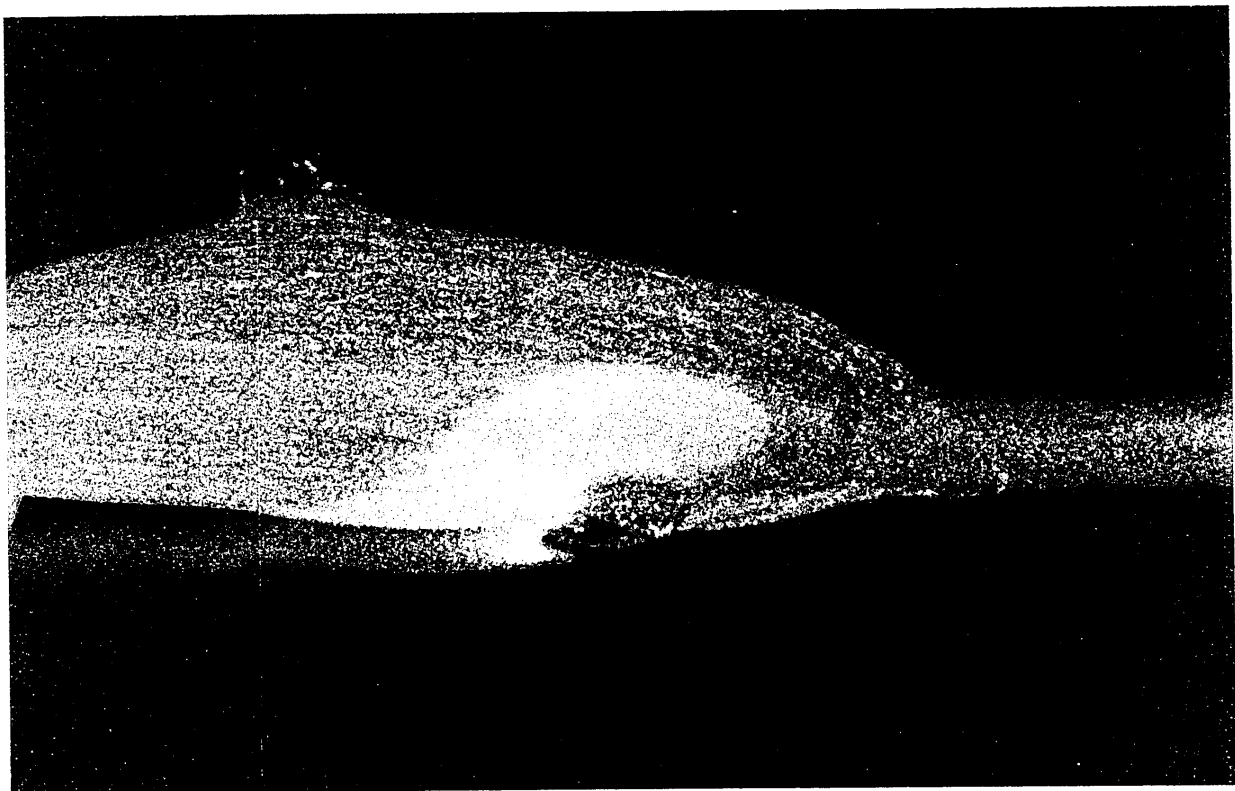
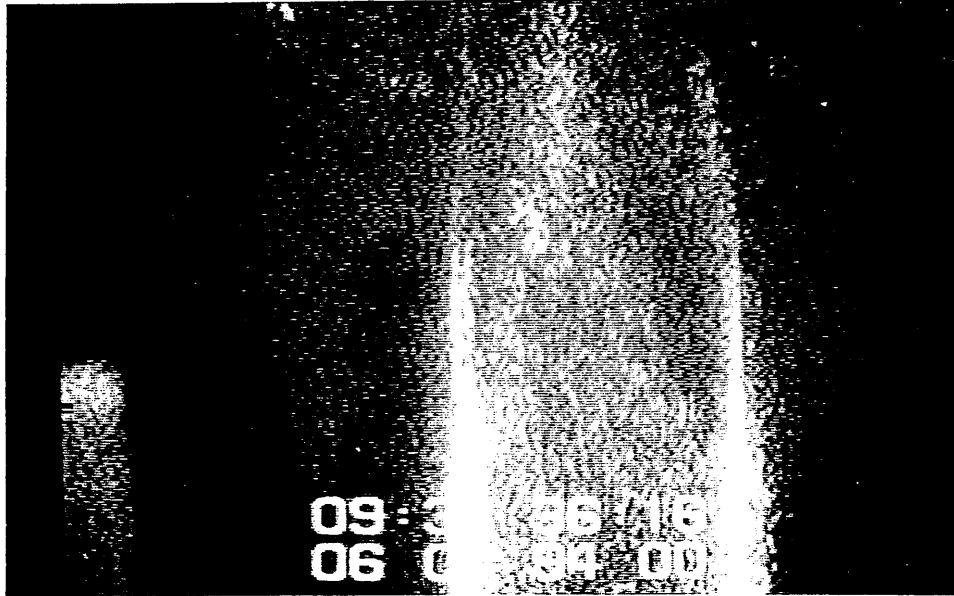


Figure 2. Photograph of bioluminescence. The marine bioluminescent dinoflagellate, *Gonyaulax polyedra*, are stimulated as they are poured over a 17.5-cm model of a dolphin.





*Figure 3. Bioluminescence, as recorded by an ISIT camera, excited along a swimming dolphin's body.*

Principal Investigator:  
Dr. J. J. Rohr

0601152N  
NRaD ZW77



## Real Solutions to Maximum Clique and Graph Coloring Patterns

*Objective(s).* Develop and implement adaptive algorithms and heuristic techniques for finding the maximum clique of a graph.

*Accomplishment(s).* Developed and implemented a recursive branch and bound algorithm for computing the maximum clique of a graph, incorporating several heuristics for assigning an order of traversal for the decision tree.

A graph  $G = (V(G), E(G))$  is an ordered pair of sets.  $V(G)$  is called the vertex set. The edge set,  $E(G)$ , is a subset of  $\{\{x, y\} | x, y \in V(G)\}$ . For  $U$ , a subset of  $V(G)$ , the induced subgraph of  $G$  with respect to  $U$  is the graph  $H = (U, E(H))$ , where  $E(H) = \{\{x, y\} | x, y \in U \text{ and } \{x, y\} \in E(G)\}$ . A *maximum clique* of  $G$  is a largest induced subgraph of  $G$  in which every pair of vertices is connected by an edge. The problem of finding a maximum clique in a graph belongs to the class of NP-Complete problems. This problem has found applications in areas of object recognition and single row routing problems.

We have implemented a recursive branch and bound algorithm for computing a maximum clique. The algorithm requires an initial order be specified on the vertex set. This order is used as the search order on the vertices. Heuristics for choosing the order include using the vertex degrees or the size and density of certain induced subgraphs to decide which path to pursue. Pruning techniques focus on computations that determine if the candidate subgraph could possibly have a clique larger than what has been found. Two such computations include testing the degrees of the largest vertices in the candidate subgraph, and second, using a vertex coloring of the candidate subgraph to get an upper bound on the size of the largest clique for the candidate. This latter technique has proven significant. Table 1 provides a list of benchmark graphs supplied by DIMACS, the NSF Science and Technology Center in Discrete Mathematics and Theoretical Computer Science. Columns 2 and 3 show the number of vertices and edges, respectively. Column 4 shows the size of a maximum clique, and column 5 is the time required by our algorithms to find a maximum clique.

We also ran our algorithms against a series of random graphs. Tables 2, 3, and 4 show the results of these experiments for graphs with 50, 100, and 200 vertices, respectively. The first column is the edge probability. The second column is the mean maximum clique size, and the third column is the mean time to compute a maximum clique.

Table 1. Benchmark graphs supplied by DIMACS.

Graph	Vertices	Edges	Clique Size	Time
c-fat200-1.clq	200	1534	12	0.25
c-fat200-2.clq	200	3235	24	0.85
c-fat200-5.clq	200	8473	58	10.17
c-fat500-1.clq*	500	4459	14	1.283
c-fat500-2.clq	500	9139	26	3.65
c-fat500-5.clq	500	23191	64	23.53
c-fat500-10.clq	500	46627	126	200.68
hamming6-2.clq	64	1824	32	1.5
hamming6-4.clq	64	704	4	0.15
hamming8-2.clq	256	31616	128	777.85
hamming8-4.clq	256	20864	16	1262.2
johnson8-2-4.clq	28	210	4	0.03
johnson8-4-4.clq	70	1855	14	3.68
johnson16-2-4.clq	120	5460	8	1951.53
san200_0.7_2.clq	200	13930	18	8947.77

Table 2. Results for graphs with 50 vertices.

Edge Prob	Mean Clique Size	CPU Time
0.1	3.1	0.01
0.2	4.0	0.02
0.3	5.0	0.04
0.4	6.1	0.09
0.5	7.3	0.17
0.6	9.1	0.42
0.7	11.3	1.15
0.8	14.7	4.06
0.9	21.8	8.20

*Table 3. Results for graphs with 100 vertices.*

<b>Edge Prob</b>	<b>Mean Clique Size</b>	<b>CPU Time</b>
0.1	3.9	0.06
0.2	5.0	0.16
0.3	6.2	0.42
0.4	7.8	1.06
0.5	9.2	3.23
0.6	11.4	13.32
0.7	13.8	88.01
0.8	20.0	902.17

*Table 4. Results for graphs with 200 vertices.*

<b>Edge Prob</b>	<b>Mean Clique Size</b>	<b>CPU Time</b>
0.1	4.3	0.38
0.2	5.8	1.18
0.3	7.5	3.75
0.4	9.0	15.68
0.5	11.0	78.00
0.6	13.8	700.43

Principal Investigator:  
Dr. J. F. Small

0601152N  
NRaD ZW97

## **Coupling Adaptive Beamforming and Adaptive Locally Optimal Detection Algorithms in Nonstationary Noise**

*Objective(s).* (1) Understand the conditions under which acoustic data from moving interferers in an ocean waveguide are better characterized by Gaussian mixture densities than by Gaussian densities. (2) Characterize and compare the performance of detection algorithms designed for Gaussian noise with those designed for Gaussian mixture noise.

*Accomplishment(s).* Developed techniques for analyzing the performance of both the locally optimum detector of random signals in Gaussian mixture noise and the power detector when the noise has a Gaussian mixture density. Showed, through the analysis of experimental data, that Gaussian mixture densities may apply to noise containing discrete sources. By using a solution of the wave equation having a moving source, this was shown to be due to the interference of modes of different horizontal wave numbers.

Statistical analysis of the sequences of the intensity of narrowband low-frequency hydrophone data, collected in 5000-m-deep water, showed that such data may be better described by exponential mixture densities than by exponential densities. The discrete Fourier transform of a solution of the wave equation with a moving source was calculated, and the sequence of the amplitudes of the Fourier coefficients at particular frequencies of hydrophone and beamformed data were shown to contain oscillatory terms, which depend upon the environment, source frequency, position and velocity, and the resolution of the DFT. These oscillations make the intensity of the response to moving sources have a density that is closer to an exponential mixture density than to an exponential density. Simulations showed that these characteristics should also be observed in shallow-water hydrophone and beamformed data. It was also shown that the range speed and heading of a moving source affect the goodness of fit of the exponential density, but that these parameters have substantially less impact on the goodness of fit of the exponential mixture density. As the sum of independent Gaussian-mixture distributed random variables has a Gaussian-mixture distribution, noise data, which is the response to more than one moving source, may also have a Gaussian-mixture distribution.

The locally optimal detection algorithm for random signals in correlated noise was derived and applied to independent circular Gaussian mixture noise. The algorithm was modified to detect signals that are not “vanishingly small.” To use the algorithm parameters of the noise, probability density function must be estimated, and a method for doing this by using the expectation and maximization (EM) algorithm was described. The error in the parameter estimates was shown to depend upon their values and the number of available samples. Probability density functions of the power detector in Gaussian mixture noise were derived. The moments of the mixture detector in Gaussian mixture noise were very accurately approximated by using piecewise polynomial approximations of the state weighting functions, and piecewise linear approximations of the state weighting functions were used to obtain approximations of the density functions of the mixture detector. These approximation techniques were compared with the “clairvoyant” mixture detector. The clairvoyant detector was shown to overestimate the variance of the mixture detector and, thus, to predict poorer performance than was predicted by either the piecewise polynomial or piecewise linear approximation techniques. For certain parameter values, the performance of the algorithm, as implemented by using the EM algorithm, was shown to be very close to the performance predicted by the piecewise polynomial and piecewise linear approximation techniques and to exceed the performance predicted by the “clairvoyant” approximation. The theoretical performance of the power and mixture detectors in the absence of parameter estimation error was then compared over a

wide range of noise parameters, and the mixture detector was seen to offer signal gains of 15 to 37 dB. For certain noise parameter values, the mixture detector was shown to be fairly insensitive to parameter estimation errors.

Principal Investigator:  
Dr. D. W. Stein

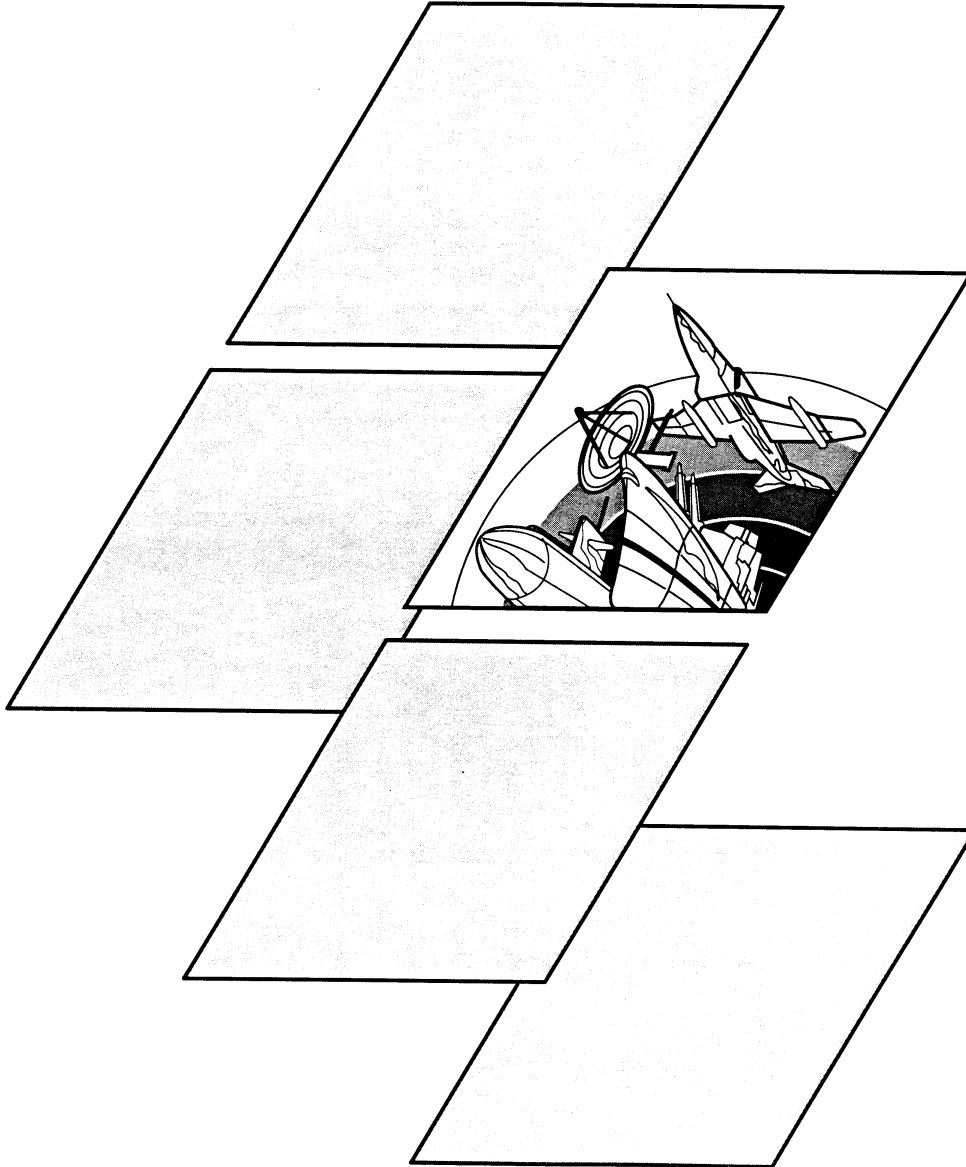
0601152N  
NRaD ZW98



---

# MULTIMISSION RESEARCH

---





## Studies of Optical Ringing in Seawater

*Objective(s).* Examine the temporal behavior of scattered light as an extremely short light pulse propagated through seawater. Such scattering is analogous to acoustical reverberation and, hence, is called “optical ringing” after Preisendorfer.

*Accomplishment(s).* Showed a possible link between optical ringing and the excess light that is often seen in actual LIDAR measurements.

This work represented an investigation into a possible, and as yet uninvestigated, cause of discrepancy between the signal-to-noise ratios (SNRs) modeled and measured for Navy underwater LIDARs, an immediately relevant problem.

A Monte Carlo model is used to examine the effect of water turbidity on the temporal storage of photons. Multiple scattering can store light in increasing scattering orders. It is hypothesized that this light will be present in a LIDAR gate when signal photons return from a distant target and will generally exceed the backscatter predicted by single scatter models. A photon’s mean survival time in a turbid medium is the product of the medium’s absorption coefficient at the photon’s wavelength times the speed of light in the medium. For very clear ocean water (absorption =  $0.023 \text{ m}^{-1}$  @ 480 nm), this is about 190 nanoseconds, the time that it would take a laser pulse to travel to and return from a target 20 meters distant. The model considers an unbounded body of water illuminated by light from a pulsed laser beam. An irradiance receiver collocated with the laser transmitter is the detector. Future studies will use radiance detectors of varying field subtenses. Results for the geometry modeled show multiply scattered light to surpass singly scattered light for paths of a few attenuation lengths or greater. The results show that this possible phenomenon must be more closely investigated to determine its potential impact on Navy underwater LIDAR systems.

Principal Investigator:  
Dr. G. D. Gilbert

0601152N  
NRaD ZW88

## Tidal Dispersion Mechanisms in a Coastal Embayment

*Objective(s).* Identify and quantify processes that are responsible for the dispersion of natural and anthropogenic substances in a tidally influenced coastal embayment.

*Accomplishment(s).* Reviewed existing literature, developed one-dimensional scaling model of dispersion mechanisms, formulated experimental design for field experiments, successfully performed field experiments at three locations in San Diego Bay, and performed preliminary data reduction and analysis of field data.

The Navy must provide an uncompromised level of defense capability without undue stress on the shoreline and marine environment. This issue is especially acute in coastal estuaries and embayments, such as San Diego Bay, where the impact of large numbers of Navy ships, submarines, support craft, and shoreside facilities must be balanced against a background of ecological, recreational, and aesthetic conservation. Since zero discharge is not technically possible, the inevitable question becomes, at what level can wastes be assimilated by the coastal ocean, and, from a scientific perspective, what are the fundamental processes that determine the fate of these substances. The first step towards answering this question lies in understanding the mechanisms, interactions, and scales of motion that control circulation and mixing in estuaries. For a tidally driven system, it has been hypothesized that large-scale circulation and turbulence features that lead to enhanced mixing are generated primarily by mechanisms associated with the topography of the embayment. These mechanisms include shear dispersion, tidal trapping, and tidal pumping. In San Diego Bay, as in most systems, areas exist where all of these processes may be active. Thus, this system provides an accessible, representative, field-scale model on which these hypotheses can be tested. The ability to perform field observations on the time and spatial scales required to resolve these mixing processes is due, in large part, to the recent development of sophisticated current and hydrographic mapping technologies. This includes instrumentation such as the Acoustic Doppler Current Profiler (ADCP), which allows rapid, accurate, underway measurement of water velocities through the entire water column; fast-response, reliable towed conductivity temperature detector (CTD) systems; and high-resolution Global Positioning System (GPS) navigation and tracking devices. This unique technological capability provides the basis for significant advancement in the understanding of field-scale estuarine circulation processes.

During the first half of FY 94, we developed a simple scaling model to highlight areas where specific mixing processes might be important in San Diego Bay. The model uses a mass conservation principle based on the extensive bathymetric data set available for the bay, in conjunction with a simple, standing-wave tide model to estimate mean velocity scales along the central axis of the bay. The model also extracts relevant topographic features from the bathymetry data, including width, mean depth, cross-sectional area, trap volume, etc., again as a function of distance along the bay axis. The velocity scale and these topographic parameters are then used to provide estimates of dispersion coefficients due to shear, trapping, and pumping, as well as an overall dispersion coefficient. The results of this scaling indicate the following: (1) shear dispersion has limited influence in most of the bay due to the long time scale for transverse mixing and short time scale of vertical mixing compared to tidal period; (2) tidal trapping may be a significant mechanism especially in the outer bay near Shelter/Harbor Island where velocities are high, and trap volumes are significant; and (3) tidal pumping is probably the dominant mixing mechanism in much of the bay due to horizontal expansions and contractions. Vertical residual circulation is thought to be small due to limited stratification. The results are in general agreement with recent observations of longitudinal salinity gradients.

Based on these results, a series of field experiments were designed and carried out at three locations in San Diego Bay. During each experiment, cross-sectional and longitudinal flow, tracer, and turbulence characteristics were measured using the instrumentation described above. The field experiments were completed during the fourth quarter of FY 94. Preliminary analysis of the field data suggests that (1) dispersion and transport near the mouth of the bay is dominated by the time-dependent variations associated with the tidal pumping process, with second-order effects due to vertical and lateral residual circulation and (2) sections deeper within the bay are more strongly influenced by lateral residual circulation and tidal trapping effects due to side basins. During FY 95, data analysis will be completed, and a series of numerical simulations will be performed using a high-resolution, two-dimensional model of the bay. Final analysis of the field data should provide a quantitative description of the dispersion mechanisms and tidal transport associated with them. Results from the model will be compared to the field experiments to examine the viability of the model for studying these processes and predicting the important aspects of tidal transport in a coastal environment. The field measurement methodology and results, and the model validation will serve to enhance the Navy's ability to quantify the transport, fate, and ultimate ecological risks associated with maintaining ships and facilities in the coastal zone.

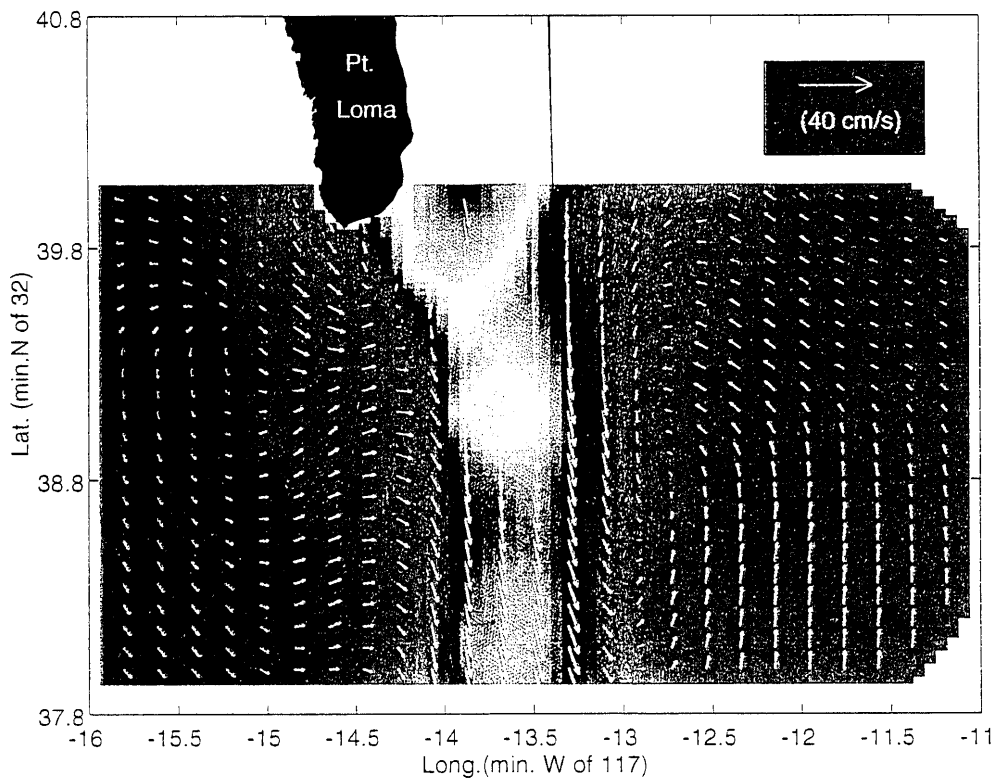


*Figure 1. Flow and tracer fields off the mouth of San Diego Bay showing the structure of the outflow jet and the large-scale eddy structure associated with the tidal pumping mechanism.*

Principal Investigator:  
D. B. Chadwick

0601152N  
NRaD ZW86



## n-type Doping of Diamond Using Li and Na

*Objective(s).* Determine the electron mobility for the interstitial n-type dopants lithium (Li) and sodium (Na) in semiconducting diamond.

*Accomplishment(s).* Used ion implantation to introduce potential n-type dopants lithium, sodium, and phosphorous into insulating diamond; n-type conductivity was observed but could be attributed to a defect mechanism.

Current diamond-based electronic devices are generally unipolar devices relying on p-type conduction with boron as a substitutional acceptor. Nitrogen-doped diamond has been shown to be n-type; however, the donor level is about 2 eV from the conduction band edge. Phosphorous-doped diamond, produced by doping during CVD growth, is also n-type. Due to the size of the P atom relative to that of the carbon atom, it is difficult to incorporate substitutionally. A second class of dopants is the interstitial dopants. The alkali metals, particularly those of smaller size, are an example of interstitial donors. Various reports in the literature have indicated n-type conductivity after introducing lithium (Li) dopants into diamond. In this work, we have investigated the use of ion implantation to introduce the interstitial donors Li and sodium (Na). A potential advantage of Na is that it is a larger atom and should be much less mobile than Li in diamond. In addition, ion implantation of P into diamond was studied to allow comparison of substitutional and interstitial dopants.

Type IIa natural diamond plates were implanted with Li, Na, or P ions. A tri-level implantation process was used for each ion to produce approximately uniform layers of almost the same thickness. Li ions were implanted (42 keV, 21 keV, and 10 keV) at room temperature and at 450°C. For Na ions, the energies were 150 keV, 75 keV, and 37 keV at room temperature and at 450°C. For P ions, the energies used were 200 keV, 100 keV, and 50 keV at 77 K and at room temperature. All samples were post-implant annealed at 500°C for 10 minutes. Van der Pauw resistivity and Hall effect measurements made over a range of temperatures did indicate n-type conductivity. Observed carrier concentrations and mobilities were very low. Annealing at higher temperatures, however, lead to lower n-type effective carrier concentrations, indicating that the primary conductivity mechanism in these cases was via a defect mechanism, rather than via an electrically active donor species.

Principal Investigator:  
C. A. Hewett

0601152N  
NRaD ZW69

## **Implementation of Fuzzy Logic to Choose and Apply Soil Characteristics— Dependent Calibration Curves for Environmental Measurements in the Field**

*Objective(s).* Validate the use of fuzzy logic for the integration of laboratory-determined, soil-characteristic-dependent calibration factors for *in situ* environmental field measurements.

*Accomplishment(s).* Developed and integrated fuzzy logic-based rules or parameters to characterize environmental conditions relevant to the calibration of *in situ* environmental measurements in a software-based fuzzy logic system. Validated these rules on laboratory-generated measurements.

NCCOSC is involved in many aspects of marine and land-based *in situ* sensor development. One concern of the Navy is improved environmental screening for more effective and cost-efficient remediation and compliance. Real-time, *in situ* sensors are an ideal way to effectively map subsurface plumes undersea and underground. Several features differentiate a remote spectroscopic system from a standard optical measurement in solution in the laboratory. While issues such as effective cell size, moisture content, contaminant type, and sample volume are relatively straightforward in the laboratory, these values may not be directly quantifiable when making *in situ* measurements in seawater, sediments, or soils. Often, these controlling features are determined only in a semiquantitative or even qualitative way. As such, they are difficult to formalize in a quantitative approach, but critical to the interpretation of results. Because of this difficulty, qualitative information is often simply ignored in data processing, resulting in data that must be heavily qualified to be interpreted. In this case, the descriptive qualifiers must still be considered with the data, leaving the data user to take them into account. Fuzzy logic is an ideal way to integrate this linguistic, “fuzzy” information (which is inherent in a real, field measurement) into a rigorous approach to data interpretation. This improved quantification would greatly enhance the capability of using *in situ* optical chemical sensors as screening tools for mapping out subsurface contaminant plumes.

Specifically, the Environmental Chemistry/Biotechnology Branch has developed an advanced development model of an optical Cone Penetrometer Test (CPT) system for *in situ* measurements of fuels in soils. The test will be used to enhance evaluation of the location and extent of fuel contamination at Navy sites. One of the first things that is being done with this system is an extensive field validation effort in which established field and laboratory methods for evaluating fuel contamination are intercalibrated with the *in situ* fluorescence measurements obtained by the optical CPT. We have shown that the soil class, reflected in soil behavior, significantly affects the fluorescent response of a given fuel in soil. Further work has shown that soil moisture, fuel type, age of spill, and spill history can all affect the fluorescent response. The effects of several controlling variables on *in situ* fluorescent response of fuels in soils have been determined. Essentially, what we have is a large matrix of calibration curves for the conversion of fluorescent response of several fuels to concentration under various environmental parameters. This project is designed to develop a protocol for the integration of these laboratory-determined factors into the soil environmental factors determined in the field for effective real-time field screening of contaminants. Fuzzy logic, such as “sandy,” “moist,” “oily,” or “fresh,” is used to normalize these qualitative or linguistic parameters that control the calibration parameters of *in situ* contaminant measurements.

In FY 93, the fuzzy logic rules based upon laboratory measurements were developed and integrated in an off-the-shelf fuzzy logic software system. This fuzzy system was then tested and validated on

laboratory data, and final verification will take place during FY 95. What remains is the testing of the fuzzy system with field data. This will be carried out in parallel with the CPT field validation program in FY 94. Results of this project will then be published in peer-reviewed journals and technical reports.

Principal Investigator:  
Dr. S. E. Apitz

0601152N  
NRaD ZW74

## ZnSe Blue Light-Emitting Devices and Lasers

*Objective(s).* Develop suitable ohmic contacts to p-type ZnSe and evaluate the carrier concentration and the efficiency of site-specific arsenic doping of ZnSe.

*Accomplishment(s).* Evaporated metals with high work functions that could overcome the deep valence band of ZnSe, on molecular beam epitaxy (MBE)-grown ZnSe samples in a transmission line pattern. Found that a large barrier still existed between the semiconductor and the metal, possibly due to the low hole concentration of the samples.

The development of improved ohmic contacts to p-type ZnSe was conceived as a joint effort between the Naval Air Warfare Center (NAWC) in China Lake and NRaD. Blue light-emitting diodes and lasers are currently being developed using a variety of materials and structures in the (Zn, Cd) (S, Se) system. Two materials problems relevant to these devices are achieving higher levels of p-type doping and contacts with a lower contact resistivity to the p-type material. This project was to support NAWC's ZnSe materials development program involving MBE growth of ZnSe and site-specific arsenic doping. The contact resistances of various metalization schemes were to be investigated, as well as determinations made of the hole concentration, activation energy, and doping efficiency.

Several chemical etching schemes were investigated to establish a process for patterning the ZnSe samples as necessary for characterization. Many of these etches were undesirable in that they left either a rough surface or a discoloration of the surface due to a selenium residue. The most effective of the etches studied was a potassium dichromate-based etch. Preliminary electrical characterization of both undoped n-type samples and arsenic-doped p-type samples was attempted using mercury probe capacitance voltage (CV) measurements and Hall effect measurements using large-area indium contacts. The n-type samples were found to have carrier concentrations in the  $10^{16} \text{ cm}^{-3}$  range, while the results for the p-type samples were inconclusive, but consistent with a hole concentration of  $10^{16} \text{ cm}^{-3}$  or less.

Contact metalization schemes of gold for the n-type material, and gold, platinum, or palladium for the p-type material, were evaporated in a transmission line pattern. The use of platinum and palladium was based on the high work function of these metals. It was thought that this would offset the large electronegativity of ZnSe and make possible ohmic contacts to p-type material, particularly for the higher hole concentrations. The IV characteristics of these contacts showed a large barrier existed between the metal and the semiconductor, but this was expected for a hole concentration of  $10^{16} \text{ cm}^{-3}$ . This was the highest hole concentration achieved in the NAWC samples during the period of this project. Several ZnSe samples were obtained from the University of Notre Dame. These samples were MBE grown and doped p-type by nitrogen doping with a known hole concentration in the mid  $10^{17} \text{ cm}^{-3}$  range. Platinum and palladium contacts evaporated on these samples showed a reduced barrier height for the higher hole concentration material, but were still nonohmic. It is expected that this technique would require material with a hole concentration in at least the mid  $10^{18} \text{ cm}^{-3}$  range to be successful.

Principal Investigator:  
Dr. D. P. Mullin

0601152N  
NRaD ZW92

## Quantum Well Mirror

*Objective(s).* Determine the feasibility of using a quantum well (QW) as an optical phase shifter (at 6328 angstroms) for biasing the ring laser gyroscope (RLG) out of the lock-in region.

*Accomplishment(s).* Formulated a design from theoretical calculations that provides the required phase shift of 6328 angstroms.

Theoretical investigations were performed to formulate a QW design with a phase shifting ability at 6328 angstroms.

The study included the Franz-Keldysh effect and the Stark shift of the exciton bands to produce a phase shift on the front surface of the corner mirror of an RLG and a phase shifter for transmitted light. The study included, but was not limited to, the following: (a) determination of suitable materials with band-gap energies at 1.9 eV; (b) barrier layers with the required conduction and valence band energies; (c) the position of the energy levels within the valence and conduction bands of the well and the shift in these levels with the application of an applied electric field; and (d) the determination of the index of refraction, the absorption coefficient, and the number of multiple layers to produce a phase shift.

An  $\text{Al}_{0.37}\text{Ga}_{0.63}\text{As}$ -AlAs sample was selected for initial investigation and fabrication. Details of the well and barrier width, number of layers, aluminum concentration, position for electrodes, and design structure will be provided to Bell Laboratory for comment prior to fabrication.

The FY 95 schedule is as follows: Following fabrication, the substrate of the superlattice (multiple quantum wells) will be etched and the electrodes mounted prior to experimentation. The superlattice will be experimentally evaluated for transmission, reflection and absorption, and its ability to optically phase. Mounting/deposition of the superlattice on the corner mirror will be performed prior to evaluation as a corner mirror.

Principal Investigator:  
F. Karwacki

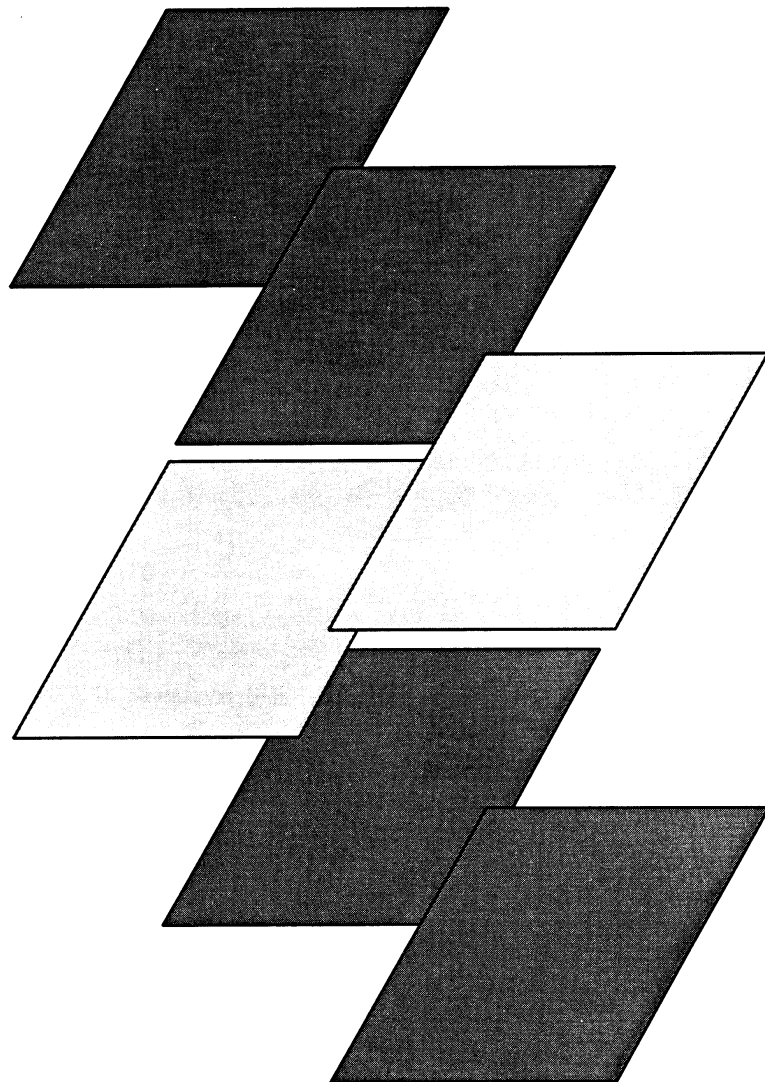
0601152N  
NRaD ZW90



---

## PUBLICATIONS AND PRESENTATIONS

---





## External Publications (Accepted/In Press)

### Independent Research

- Bamber, D. E. December 1994. "Probabilistic Entailment of Conditionals by Conditionals." *IEEE Transactions on Systems, Man, and Cybernetics*, vol. 24, no. 12, pp. 1714–1723.
- Boss, R. D., J. S. Briggs, E. W. Jacobs, T. E. Jones, and P. A. Mosier-Boss. 1995. "Preparation of Superconducting  $K_3C_{60}$  and  $Rb_3C_{60}$  by Precipitation from Liquid Ammonia." *Physica C*, vol. 243, nos. 1 & 2, pp. 29–34.
- Bucker, H. P. May 1994. "A Simple 3-D Gaussian Beam Sound Propagation Model." *Journal of the Acoustical Society of America*, vol. 95, pp. 2437–2440.
- Bucker, H. P. December 1994. "Use of Matched-Field Tracking for Shallow Water Detection." *Journal of the Acoustical Society of America*, vol. 96, pp. 3809–3811.
- Hanson, F. E. and P. Poirier. October 1994. "Efficient Intracavity Frequency Doubling of a High-Repetition-Rate, Diode-Pumped Nd:YAG Laser." *Optics Letters*, vol. 19, p. 1526.
- McDonnell, J. R. and D. E. Waagen. 1994. "Evolving Recurrent Perceptrons for Time-Series Modeling." *IEEE Transactions on Neural Networks*, vol. 5, no. 1, pp. 24–38.
- McDonnell, J. R. and D. E. Waagen. March 1995. "Evolving Cascade-Correlation Networks for Time-Series Forecasting." *International Journal on Artificial Intelligence*, World Scientific.
- McDonnell, J. R. and D. E. Waagen. "Evolving Cascade-Correlation Networks for Time-Series Forecasting." *IEEE Transactions on Systems, Man, and Cybernetics* (in press).
- Russell, S. D., W. B. Dubbelday, P. Georgief, R. L. Shimabukuro, and P. R. de la Houssaye. November 1994. "The Effects of Microcrystalline Structure on the Photoluminescence of Porous Silicon on Sapphire." *Journal of Applied Physics*, vol. 76, no. 10, pp. 6012–6013.
- Scheps, R. 1993. "Visible Conversion of a Dual Wavelength Ti:Sapphire Laser." *Bulletin of the American Physical Society*, vol. 38, pp. 17–21.
- Scheps, R. June 1994. "Simultaneous 3-Wavelength Operation of a Coupled-Cavity Laser Containing Two Gain Elements." *Journal of Optical Materials*, vol. 3, pp. 129–138.
- Scheps, R. and J. F. Myers. April 1994. "Intracavity Sum-Frequency Generation in a Doubly Resonant Ti:Sapphire Laser." *IEEE Journal of Quantum Electronics*, vol. 30, pp. 1050–1057.
- Waagen, D. E., M. D. Parsons, J. R. McDonnell, and J. D. Argast. "Evolving Multivariate Mixture Density Estimates for Classification." Invited for submission into the *Handbook on Evolutionary Computation*, Oxford Press (in press).

**External Publications (Submitted)**  
**Independent Research**

- Axford, R. A., L. B. Milstein, and J. R. Zeidler. "On the Misconvergence of the Constant Modulus Algorithm (CMA) for Blind Equalization in the Reception of PN Sequences." Submitted to *IEEE Transactions on Signal Processing*.
- Hanson, F. E. and P. Poirier. "Multiple Wavelength Operation of a Diode-Pumped Nd:YAlO<sub>3</sub> Laser." Submitted to the *Journal of the Optical Society (B)*.
- Kevorkian, A. K. "An Ordering Algorithm for Exposing Parallelism in Large Sparse Symmetric Matrices." Submitted to *SIAM Journal on Scientific Computing*.
- McDonnell, J. R. and D. E. Waagen. "An Empirical Study of Recombination in Evolutionary Search." Submitted to *Evolutionary Computation*.
- Pugh, J. K. "Constant Amplitude Pulse Signal Detection: A Comparison of Two Approaches." Submitted to *IEEE Transactions on Aerospace and Electronic Systems*.
- Rohr, J. J. "The Characteristic Response of *in situ* Luminescent Organisms to Hydrodynamic Shear." Submitted to *Deep Sea Research*.
- Shensa, M. J. "Discrete Inverses for Nonorthogonal Wavelet Transforms." Submitted to *IEEE Transactions on Signal Processing*.
- Small, J. F. "Visibility Representations from a Bridge-Cycle Recursion." Submitted to *Journal for Visual Languages and Computing*.
- Stein, D. W. J. "Detection of Random Signals in Gaussian Mixture Noise." Submitted to *IEEE Transactions on Information Theory*.
- Stein, D. W. J. "Statistical Characteristics of Moving Acoustic Sources in Ocean Waveguides." Submitted to the *Journal of the Acoustic Society of America*.

**In-House Publications**  
**Independent Research**

- Adams, G. 1994. "Tunable Filter." NRaD TR 1643 (Mar). Naval Command, Control and Ocean Surveillance Center, RDT&E Division, San Diego, CA.
- Kevorkian, A. K. 1994. "A Decomposition Method for the Least Squares Solution of Nonsquare Sparse Systems of Linear Equations." NRaD TR 1653 (June). Naval Command, Control and Ocean Surveillance Center, RDT&E Division, San Diego, CA.
- Kevorkian, A. K. "An Ordering Algorithm for Exposing Parallelism in Large Sparse Symmetric Matrices." NRaD TR 1697 (in preparation). Naval Command, Control and Ocean Surveillance Center, RDT&E Division, San Diego, CA.
- Rohr, J., J. Losee, and G. Anderson. 1994. "The Response of Bioluminescent Organisms to Fully Developed Pipe Flow." NRaD TR 1360 (Aug). Naval Command, Control and Ocean Surveillance Center, RDT&E Division, San Diego, CA.
- Shum, A. 1994. "Quantitative Performance Evaluation of an ATM-based Multiplexer." NRaD TR 1670 (Sept). Naval Command, Control and Ocean Surveillance Center, RDT&E Division, San Diego, CA.

**In-House Publications**  
**Independent Exploratory Development**

Nguyen, H. G. and M. R. Blackburn. 1995. "A Simple Method for Range Finding via Laser Triangulation." NRaD TD 2734 (Jan). Naval Command, Control and Ocean Surveillance Center, RDT&E Division, San Diego, CA.

**Presentations to Professional Meetings**  
**Independent Research**

Invited Papers and Lectures

Axford, R. A., L. B. Milstein, and J. R. Zeidler. "Improved CMA Blind Equalizer Convergence Performance for QAM Signals Using a Lattice Filter Structure." NSF ICAS Annual Review, University of California at San Diego, 20 January 1994.

Axford, R. A., L. B. Milstein, and J. R. Zeidler. "On the Misconvergence of CMA Blind Equalizers in the Reception of PN Sequences." *Proceedings of the IEEE Milcom*, pp. 281–286, October 1994.

Axford, R. A., L. B. Milstein, and J. R. Zeidler. "On the Misconvergence of the Constant Modulus Algorithm (CMA) for Blind Equalization in the Reception of PN Sequences." NSF ICAS Annual Review, University of California at San Diego, 7 November 1994.

Hewett, C. A. "Fabrication of Diamond-Based FETs Using Ion Implantation." Fourth International Conference on the New Diamond Science and Technology, Kobe, Japan, 17–22 July 1994.

Shensa, M. J. "Discrete Inverse for Nonorthogonal Wavelet Transforms." Presented and appeared in the *Proceedings (Wavelet Applications)* of the SPIE International Symposium on Optical Engineering in Aerospace Sensing, in Orlando, FL, April 1994.

Stein, D. W. J. "Detection of Random Signals in Gaussian Mixture Noise." Presented and appeared in the *Proceedings of the 28th Asilomar Conference on Signals, Systems, and Computers*, Pacific Grove, CA, 31 October – 2 November 1994, pp. 791–795.

## Contributed Papers and Lectures

- Bamber, D. E. "A Characterization of Probabilistic Entailment in Adams' Logic of Conditionals." *Proceedings of the 1994 Symposium on Command and Control Research and Decision Aids*, pp. 637–642, Naval Postgraduate School, Monterey, CA, 21–23 June 1994.
- Bucker, H. P. "Matched-Field Tracking of Acoustic Sources in Shallow Water." Meeting of the Acoustic Society of America, Boston, MA, May 1994.
- Bucker, H. P. "Calculation of Source Spectra Using Matched-Field Tracking." Meeting of the Acoustic Society of America, Austin, TX, November 1994.
- Chadwick, D. B., J. Largier, and R. Cheng. "The Role of Thermal Stratification in Tidal Exchange at the Mouth of San Diego Bay." 7th International Conference on Estuaries and Coastal Seas, Woods Hole, MA, 28–30 November 1994.
- Dubbelday, W. B., S. D. Russell, A. S. Katz, M. Winton, M. A. Wendman, P. R. de la Houssaye, R. C. Dynes, K. L. Kavanagh, A. C. Kummel, R. L. Shimabukuro, and R. Gronsky. "Fabrication of Single Crystal Silicon Nanowires on a Sapphire Substrate." 27th Annual Symposium of the Southern California Chapter of the American Vacuum Society, Session B: Advances in Solid-State Materials and Microelectronics, Pasadena, CA, 13 September 1994.
- Dubbelday, W. B., S. D. Russell, and K. L. Kavanagh. "The Effect of Starting Silicon Crystal Structure on Photoluminescence Intensity of Porous Silicon." *Materials Research Society Proceedings*, Boston, MA, (in press).
- Gilbert, G. D. and M. H. North. "Studies of Optical Ringing in Sea Water." *SPIE Ocean Optics XII Proceedings*, vol. V. 2 2 5 8, pp. 472–479, Bergen, Norway, 13–15 June 1994.
- Latz, M. I. and J. Rohr. "Are Plankton Indifferent to the Nature of Shear Stress? Evidence from Bioluminescence Studies." *EOS 75:184*, Ocean Sciences Meeting, San Diego, CA, 1994.
- McDonnell, J. R., W. C. Page, and D. E. Waagen. "Neural Network Construction Using Evolutionary Search." *Proceedings of the Third Annual Conference on Evolutionary Programming*, A. V. Sebald and L. J. Fogel (eds.), World Scientific, pp. 9–16, 1994.
- McDonnell, J. R. and D. E. Waagen. "Evolutionary Optimization of Cascaded Networks." *Neural and Stochastic Methods in Image and Signal Processing III*, SPIE vol. 2304, pp. 234–245, San Diego, CA, 1994.
- McDonnell, J. R. and D. E. Waagen. "Evolving Cascade-Correlation Networks for Time-Series Forecasting." *Intelligent Systems*, E. A. Yfantis (ed.), Kluwer Academic Publishers, pp. 497–506, 1994.
- McDonnell, J. R. and D. E. Waagen. "An Empirical Study of Recombination in Evolutionary Search." *Proceedings of the Fourth Annual Conference on Evolutionary Programming*, J. R. McDonnell, D. B. Fogel, and R. G. Reynolds (eds.), MIT Press (in press).
- Paul, A. K. and R. A. Sprague. "Diurnal, Seasonal, and Solar Activity Variations of F-region Parameters." Paper presented at the 1994 National Radio Science Meeting, Boulder, CO, 5–8 January 1994.
- Pugh, J. K. "Monitoring Medical Signs in the Field." WG24 62nd Military Operations Research Society Symposium (MORSS), U.S. Air Force Academy, Colorado Springs, CO, June 1994.
- Russell, S. D., W. B. Dubbelday, P. Georgief, R. L. Shimabukuro, and P. R. de la Houssaye. "Porous SOS, BESOS, and SOQ for Flat Panel Emissive Displays." *1994 IEEE SOI International Conference Proceedings*, pp. 105–106, Nantucket, MA, 3–6 October 1994.

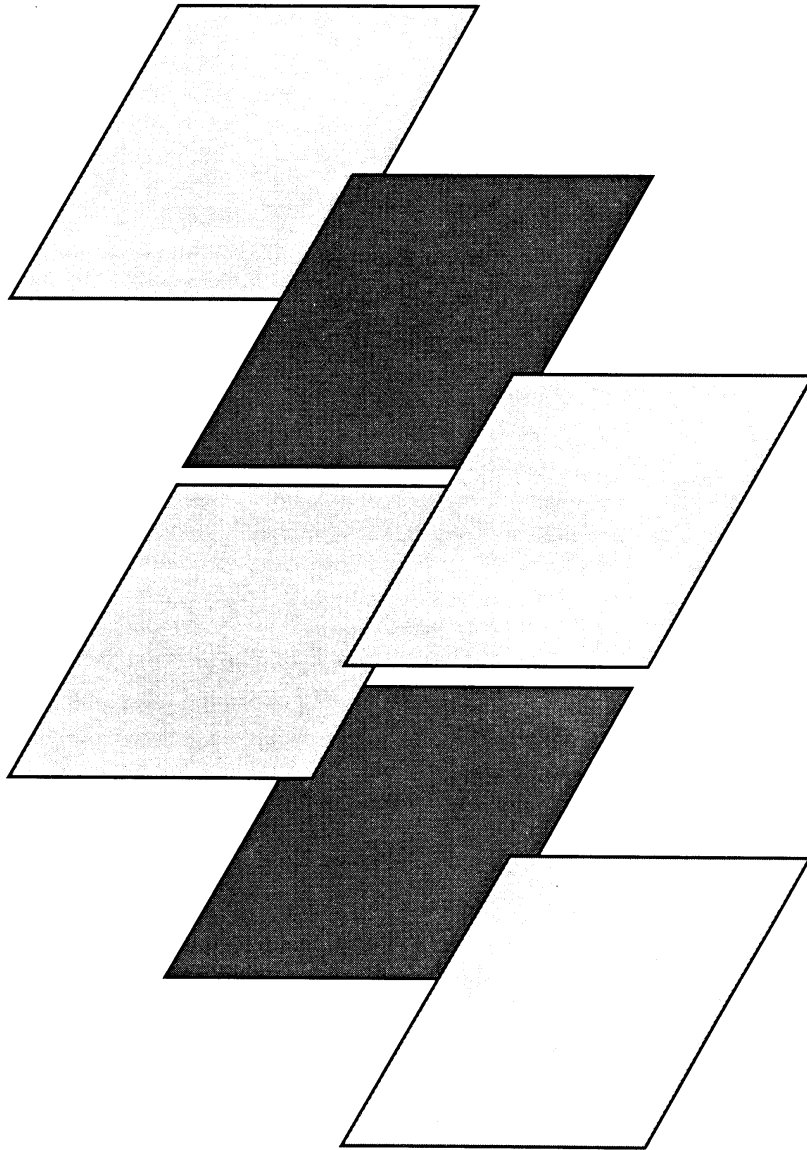
- Ryan, F. J. "Comparison of Various Parabolic Equation Methods in a Shallow Water Environment." *Journal of the Acoustic Society of America*, vol. 95, no. 5, p. 2907, 1994.
- Ryan, F. J. "A Variable Terrain Electromagnetic Parabolic Equation Model for Anomalous Propagation in Complex Environments." Presented at the Beyond Line-of-Sight (BLOS) Conference, Austin, TX, 1994.
- Stein, D. W. J. "Detection of Acoustic Signals in Shipping Noise." Presented and published in the *Proceedings of the 39th Navy Symposium on Underwater Acoustics*, Gaithersberg, MD, 1–3 June 1994.
- Waagen, D. E., M. D. Parsons, J. R. McDonnell, and J. D. Argast. "Evolving Multivariate Mixture Density Estimates for Classification." *Neural and Stochastic Methods in Image and Signal Processing III*, SPIE vol. 2304, pp. 175–186, San Diego, CA, July 1994.



---

# HONORS AND AWARDS

---



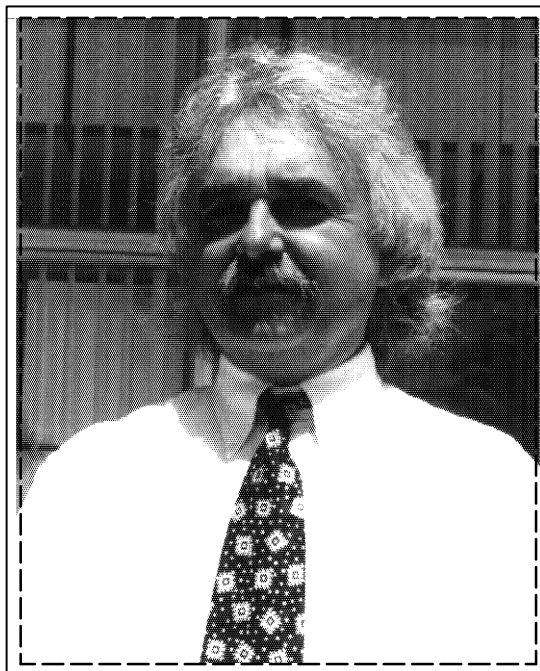


## Honors and Awards

The 1994 Lauritsen-Bennett Award for Science was presented to **Dr. Stephen Lieberman**. The Lauritsen-Bennett Award annually recognizes employees who have made significant contributions in science, engineering, and staff support. The contributions may be for developing imaginative applications of new technology or scientific principles, doctrine, or concepts that open the way for further scientific study or applications.

Dr. Lieberman is the principal investigator and senior scientist for the Site Characterization and Analysis Penetrometer Systems (SCAPS) Program. Dr. Lieberman's contributions to this field-screening system are revolutionizing the way hazardous waste sites will be accessed in the future, and will save hundreds of millions of dollars by significantly reducing assessment and remediation costs. The system provides capability for real-time, *in situ* measurement of petroleum hydrocarbon contamination and soil type to depths of 50 meters. The method consists of using a hydraulic ram in a truck with a 20-ton reaction mass to push an instrumented probe into the ground. The basis for the system is a fiber-optic-based, laser-induced-fluorescence chemical sensor that was developed as a result of research performed by Dr. Lieberman in FY 86 and FY 87 under the IR Program. A fluorogenic-indicator system that can be immobilized on the end of an optical fiber for remote sensing was developed for remote sensing of chemical species in seawater. The system was later modified and adapted to a truck-mounted cone penetrometer. Fluorescence from aromatic hydrocarbons in the soil is excited through a sapphire window in the probe by light generated with a pulsed nitrogen laser and transmitted over a silica-clad optical filter. The resulting laser-induced fluorescence stimulated in the soil is returned to the surface over a second fiber where it is dispersed with a spectrograph and quantified with an intensified linear photodiode array.

Dr. Lieberman has a bachelor's degree in chemistry from the University of California, San Diego, a master's degree from San Diego State University, and a Ph.D. degree in oceanography from the University of Washington. He has published extensively and has applied for and holds numerous patents in the area of chemical sensor technology. His awards and honors include the Naval Ocean System Center Exemplary Achievement Award, appointment as National Research Council Advisor, and the Naval Ocean System Center Certificate of Recognition.



**Dr. Sabine Apitz** was chosen to serve as Navy Liaison for the National Research Council, Marine Board, Committee on Contaminated Marine Sediments.

**Dr. Roy Axford** was invited by Dr. James Bond, NCCOSC, RDT&E Division, to present papers on Adaptive Equalization for High Data Rate Communications at Milcom '93 and Milcom '94. Dr. Axford and associate investigators represented NRaD as experts in signal processing for digital communications on two delegations that visited French naval, commercial, and academic communications R&D facilities under the auspices of the Mutual Weapons Development Data Exchange Agreements 5650 and 5655 for communications and C<sup>2</sup>, respectively.

In 1994, **Dr. Adi Bulsara** received the NRaD Publication of the Year Award: Article in Conference Proceedings for an article cowritten with Everett Jacobs and Jill Bekkedahl entitled "Stochastic Resonance in a Bistable Squid Loop," *Noise in Physical Systems and IF Fluctuations*, AIP 285, 1993. Dr. Bulsara also received an NRaD Publication Award of Excellence for his open literature article cowritten with Gabor Schmera on "Single Effective Neuron: Dendritic Coupling Effects and Stochastic Resonance," *Publications Biological Cybernetics*, 1993.

**Dr. Charles A. Hewett** was Session Chairman at the Fourth International Conference on the New Diamond Science and Technology, held 17–22 July 1994, in Kobe, Japan.

In 1994, **Dr. I. R. Goodman** received the NRaD Publication of the Year Award: Open Literature for an article cowritten with H. T. Nguyen entitled "A Theory of Conditional Information for Probabilistic Inference in Intelligent Systems: I, Interval of Events Approach," *Advances in Fuzzy Theory and Technology*, Vol. 1, 1993. Dr. Goodman also received an NRaD Publication Award of Excellence for his open literature article "Formal Theory of C<sup>3</sup> and Data Fusion," *Progress in Astronautics and Aeronautics*, Vol. 156, 1993.

**John McDonnell** is serving as Chairman of the Fourth Annual Conference on Evolutionary Programming, 1995, and is also President Elect of the Evolutionary Programming Society, 1995.

**Tom Phillips** is serving as Session Chairman of the May 1995 ARPA conference on "High Definition Systems–Information Exchange." Session title: "Applications–Command and Control Displays."

**Frank Ryan** is serving as a member of the Underwater Acoustics technical committee of the Acoustic Society of America.

**Dr. Stephen D. Russell** is serving as a journal referee for *Physical Review Letters* and *Physical Review B*.

**Dr. Richard Scheps** was the Chairperson of the SPIE Visible and UV Lasers Conference in Los Angeles in 1994 and in San Jose in 1995.

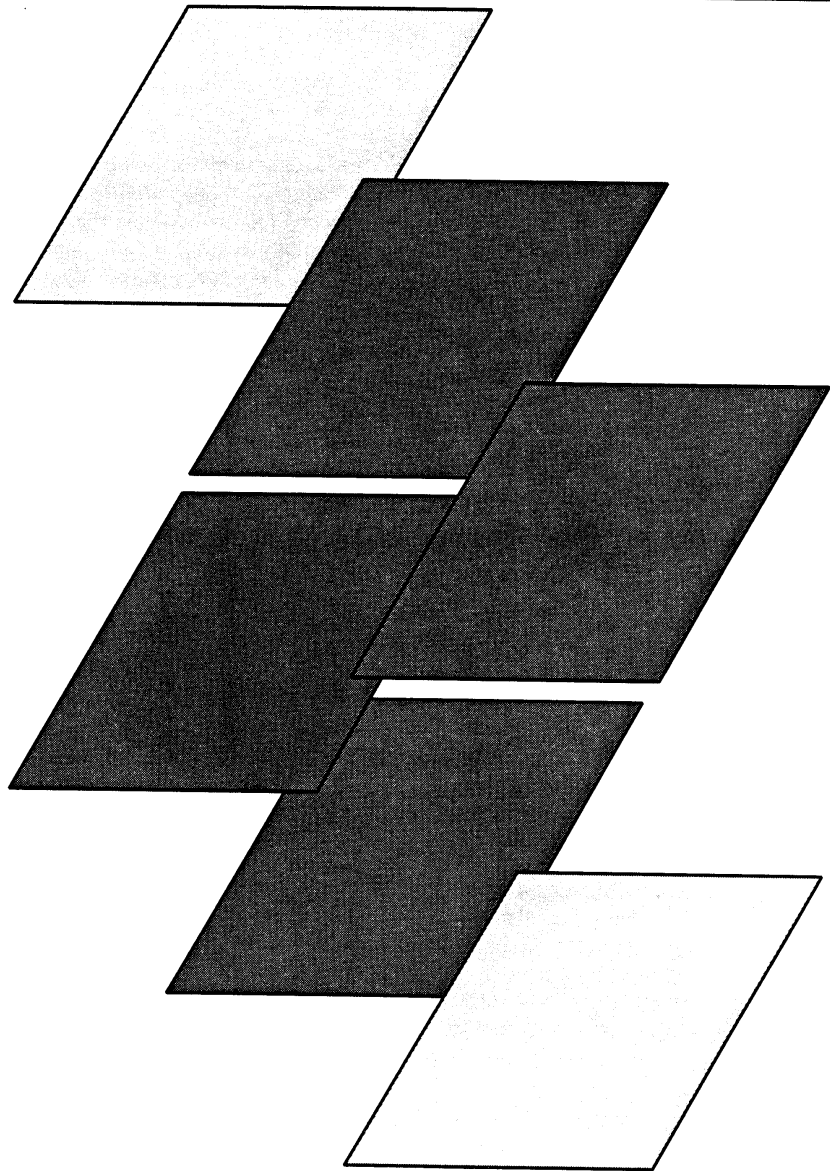
**Dr. Mark Shensa** received an NRaD Publication Award of Excellence for his NRaD Technical Report 1621 entitled "An Inverse DWT for Nonorthogonal Wavelets."

**Dr. David W. Stein** was appointed Chairman of the KTP-3 study group on non-Gaussian signal processing. The KTP study group is the Radar Technical Panel for Signal Processing of The Technical Cooperation Program (TTCP) (US, UK, Canada, and Australia).

---

# PATENT ACTIVITY

---





## Independent Research

### Patents Issued

**Richard Scheps**

**“Wavelength Dispersive Gain Element  
for a Tunable Laser”**

A gain element (for example, Ti:sapphire) is formed in the shape of a prism to allow tuning of the output wavelength without the need for any additional tuning elements. In multifrequency operation, each wavelength is selected by rotating the HR mirrors.

Patent 5,307,358 Navy case 73,765 (Serial 08/607,504) filed 20 May 1993; issued 26 April 1994.

**Stephen D. Russell**

**Douglas A. Sexton**

**Richard J. Orazi**

**“Method for Laser-Assisted Etching of III-V and  
II-VI Semiconductor Compounds Using  
Chlorofluorocarbon Ambients”**

An etching process allows a selective single-step patterning of III-V or II-VI semiconductor compound devices such as GaAs and InP or CdS and ZnSe in a noncorrosive environment. The etching relies on a maskless laser-assisted technique in a gaseous chlorofluorocarbon ambient, such as gaseous dichlorodifluoromethane and chloropentafluoroethane. Laser-assisted photochemical etching reactions on the III-V or II-VI semiconductor compounds occur in these ambients when the incident fluence from an excimer laser at 248 nm exceeds the melt threshold. This provides a means for thin membrane formation in III-V or II-VI semiconductor compounds, rapid etches and processing of packaged devices or partially fabricated dies. The reduction in processing steps as compared to conventional wet chemical etches provides improvements in yield, reliability, and cost.

Patent 5,310,989 Navy case 74,182 (Serial 07/831,830) filed 21 January 1992; issued 10 May 1994.

Patent 5,354,420 Navy case 72,726 (Serial 07/508,317) filed 10 April 1990; issued 11 October 1994.

**Thomas E. Jones**

**Wayne C. McGinnis**

**J. Scott Briggs**

**“Compact Substrate Heater for Use in  
an Oxidizing Atmosphere”**

A heater is described that directly heats a substrate in an atmosphere rich in oxygen during a thin film deposition process. The heater uses a unique combination of advanced technology materials that can operate (without degradation) at high temperature in an oxidizing atmosphere.

Patent 5,329,097 Navy case 74,148 (Serial 08/063,970) filed 19 May 1993; issued 12 July 1994.

**W. Brook Dubbelday**

**Larry D. Flesner**

**“Method of Forming a Very High-Voltage Silicon-on-  
Sapphire Photocell Array”**

The invention discloses a method for fabricating an integrated circuit from epitaxial silicon-on-sapphire. The circuit converts light energy directly into high-voltage electrical energy. The circuit is an array comprised of several thousand silicon photocells electrically connected in a series circuit in order to produce thousands of volts of electrical potential when illuminated. The individual photocells are silicon mesas that are isolated and supported by a sapphire substrate. The epitaxial silicon layers, the fabrication steps, and the circuit design are optimized for producing a high-voltage circuit capable of efficient conversion of optical to electrical energy.

Patent 5,330,918 Navy case 73,776 (Serial 07/938,920) filed 31 August 1992; issued 19 July 1994.

**Richard Scheps**

**“A Technique for Intracavity  
Semi-Frequency Generation  
of Blue-Green Wavelength”**

A Ti:sapphire laser is operated simultaneously at two frequencies, 809 nm and 1.064 microns. A KTP, or other suitable nonlinear crystal, is placed inside the cavity to generate CW 459-nm output. A related

technique uses a double Nd:YAG laser to pump the Ti:sapphire laser. The Ti:sapphire laser cavity is made doubly resonant for 1.06 micron and 809 nm. The unconverted 1.064-micron radiation from the YAG pump propagates into the cavity along the 532-nm pump light. This 1.064-micron radiation from the pump mixes with the 809 nm Ti:sapphire laser radiation to produce 450 nm.

Patent 5,333,142 Navy case 74,211 (Serial 08/108,131) filed 12 August 1993; issued 26 July 1994.

**Thomas E. Jones**  
**Wayne C. McGinnis**

**“Method for Determining the  
Granular Nature of Superconductors  
Using Pulsed Current”**

The method nondestructively determines the granular nature of superconducting materials (thin film, wire, or bulk samples). A granular superconductor exhibits two superconducting transitions—one for the granular regions and one for the intergranular regions. By using pulsed current, this method allows both transitions to be observed over a wide range of current levels, thus revealing the granular character of the sample.

Patent 5,339,025 Navy case 74,274 (Serial 08/010,685) filed 28 January 1993; issued 16 August 1994.

**Monti Aklufi**

**“Method of Forming Thin Films”**

Invention provides a method for constructing thin films using low-temperature chemical vapor deposition with pulsed, vaporized liquid precursors and pulsed microwave plasmas.

Patent 5,399,388 Navy case 74,030 (Serial 08/207,312) filed 28 February 1994; issued 21 March 1995.

## **Independent Research**

### **Claims Allowed; Pending Notice of Allowability**

**Thomas E. Jones**  
**Wayne C. McGinnis**  
**J. Scott Briggs**

**“Superconducting  
Ceramic Magnet”**

This invention describes a method of building a superconducting magnet by using high-temperature superconducting materials without using wire forms of these materials. This design, which uses thin films of a melt-processable, high-temperature superconductor, should enable the generation of magnetic fields, at least in the range of several Tesla.

Navy case 75,143 (Serial 08/060,762) filed 7 May 1993; pending. Notice of Allowance 18 April 1994.

**Stephen D. Russell**  
**Wadad B. Dubbelday**  
**Randy L. Shimabukuro**  
**Diane M. Szarflarski**

**“Method of Controlling Photoemission from  
Porous Silicon Using Ion Implementation”**

This invention describes a method of controlling light emission from porous silicon and porous silicon devices using ion implantation. The emitted light intensity can be either selectively increased or decreased by suitable processing of the silicon prior to the fabrication of the porous layer. Amorphizing the silicon prior to the fabrication of the porous layer quenches the light emission. Ion implantation with doses below the amorphization level enhances the intensity of the emitted light of the subsequently fabricated porous layer.

Navy case 75,726 (Serial 08/118,901) filed 9 September 1993; pending. Notice of Allowance 7 February 1995.

**Independent Research**  
**Patent Applications Filed**

**Monti E. Aklufi**

**“Chemical Sputter Deposition of Dielectric  
Films with Microwave Induced Plasmas”**

Chemical vapor deposition is caused through “chemical” sputtering of an inner chamber. The inner chamber serves as a source material that reacts with a process plasma to form volatile compounds, which, in turn, form desired film composition. The inner chamber may be made of a variety of materials depending upon what “source” material one desires the chamber to provide.

Navy case 72,776 (Serial 07/897,173) filed 11 June 1992; pending.

**Stanislaw J. Szpak**  
**Pamela A. Boss**

**“Electrode and Method for Preparation of  
Electrode for Electrochemical Compression  
of Deuterium into a Metal Lattice”**

This invention provides an electrode and method for preparing the electrode that may be employed to electrochemically compress deuterium into a metal lattice of the electrode. An electrochemical cell is constructed that includes an electrolyte solution comprising a metallic salt and a supporting electrolyte. The metallic salt, when in a reduced state, absorbs deuterium. Both the electrolytic solution and supporting electrolyte are dissolved in heavy water. An anode and cathode are immersed and stable within the electrolytic solution. The anode is stable when polarized. A voltage is applied across the anode and cathode while a constant potential is maintained at the cathode. The constant potential is measured with respect to a reference electrode immersed within the electrolytic solution so that deposition of metallic ions occur in the presence of evolving deuterium during electrolysis of the electrolytic solution. By this method, the cathode is transformed into the electrode.

Navy case 73,311 (Serial 07/632,896) filed 24 December 1990; pending.

**Douglas A. Sexton**  
**Stephen D. Russell**  
**Donald J. Albares**

**“Laser Textured Surface  
Absorber and Emitter”**

A method for fabricating a laser textured surface absorber and/or emitter is devised, thereby increasing the surface area for applications, inhibiting reflected light, or increasing the emissive power of a body.

Navy case 74,124 (Serial 07/970,558) filed 23 October 1992; abandoned 13 July 1994.

**Carl R. Zeisse**  
**James R. Zeidler**  
**Charles A. Hewett**  
**Richard Nguyen**

**“An Ion Implanted Diamond  
Metal-Insulator-Semiconductor  
Transistor”**

A field effect transistor comprises a diamond substrate which has a p-type ion implanted region coterminous with a surface of the diamond substrate, wherein the ion implanted region has a hole concentration in the range of  $1 \times 10^{15}$  to  $1 \times 10^{17}$  holes/cm<sup>2</sup>, and a hole mobility equal to or greater than 1 cm<sup>2</sup>/V-sec; spaced apart source and drain electrodes formed over the p-type ion implanted region on the surface of the diamond substrate; an electrically insulating material formed over the p-type ion implanted region on the surface of the diamond substrate between the source and drain electrodes; and a gate electrode formed on the surface of the insulating material.

Navy case 74,157 (Serial 07/901,615) filed 16 June 1992; SIR #1287 published 1 February 1994.

**Richard Scheps**  
**Joseph F. Myers**

**“Laser with Multiple Gain  
Elements of Different Materials”**

Two or more separate “arms” of a laser resonator contain gain elements that are end-pumped. Each arm operates at a different wavelength. Each gain element can be made of a different material. The two

or more wavelengths are combined in another part of the cavity into a single multiwavelength beam by using a prism. A second waist is established in the cavity for nonlinear processes.

Navy case 75,129 (Serial 08/155,034) filed 19 November 1993; pending.

**Richard Scheps**  
**Joseph F. Myers**

**“Laser With Multiple Gain Elements  
Pumped by a Single Excitation Source”**

A laser produces laser emission at two or more wavelengths simultaneously. The laser includes at least two gain elements, and each gain element generates a different wavelength. A single optical pumping source is used for optically exciting all laser gain elements contained within the laser resonator cavity. A wavelength dispersing element such as a prism is disposed in the laser resonator cavity for dispersing the wavelengths operating simultaneously within the laser resonator cavity and to create separate regions for each laser gain element. Laser gain elements may be tunable laser gain elements or discretely emitting laser gain elements. Arbitrarily large wavelength separations between the wavelengths operating simultaneously may be achieved in this manner to produce stable cw or pulsed output, which may be Q-switched or line narrowed. Intracavity sum frequency generation can be produced efficiently by using a non-linear sum frequency generating crystal disposed at a laser resonator cavity waist. The multiple gain elements may be of different materials or the same material.

Navy case 76,226 (Serial 08/339,993) filed 31 October 1994.

**Independent Research**  
**Invention Disclosures Submitted**

**Richard Scheps**

**“Er:YALO Upconversion Laser”**

A novel technique for upconversion pumping is described which uses intracavity absorption to get 100% conversion efficiency.

Navy case 76,005; disclosure submitted 30 November 1993.

**Willard M. Cronyn**

**“Compact, Phasable, Multioctave,  
Planar, High Efficiency Spiral Mode  
Antenna”**

The antenna consists of eight planar windings, each one of which is an exponential spiral. The windings are connected in groups of 3 to a balanced transmission line, with a “floating” winding between each of the two groups. For the purpose of phasing elements together for directional beam control, the particular grouping of windings can be changed. A sinuous variation is imposed on the spiral windings to increase the path length for each winding rotation so that the circumference through which the phase increases by 360 degrees is correspondingly decreased. This element integrates a planar structure, wideband compact design, and phasability into a single physical structure.

Navy case 76,188; disclosure submitted 15 February 1994.

**Stephen D. Russell**  
**Shannon Kasa**  
**Howard W. Walker**

**“Chemical Sensor Using Ring  
Oscillator Thermometry”**

This invention describes a novel structure using ring oscillator thermometry for use as a chemical or biological sensor. Combustible gas sensors based on thermal sensors have been demonstrated in the prior art. These sensors, called pellistors, depend on a rise in temperature at a catalytic surface due to catalytic oxidation of the combustible gas. The pellistor measures this rise in temperature with a thermistor. The herein disclosed novel gas sensor incorporates a catalytic platinum layer deposited on top of a ring oscillator. Combustible gases will be catalytically oxidized at the platinum surface. The heat released by the reaction will cause local heating of the RO, and thus affect its frequency.

Navy case 76,462; disclosure submitted 23 May 1994.

**Stephen M. Hart**

**“Optoelectronically Controlled  
Frequency Selective Surface”**

A PVFET is used to control the impedance, scattering frequency, and scattering cross-section of the scattering elements on a Frequency Selective Surface. The PVFETs are implanted in the arms of either wire or slot scatterers in order to make their scattering properties adjustable. The resulting OCFSS becomes a programmable electromagnetic shield or pattern control device.

Navy case 76,915; disclosure submitted 15 September 1994.

**Stephen M. Hart**

**“Optoelectronically Controlled Waveguide”**

An OCW is composed of a metallic waveguide, a finline, and a PVFET. The finline is inserted into the waveguide making electrical contact and the PVFET is affixed to the finline in a shunt configuration. The resulting device is capable of attenuating the energy propagating in the waveguide to any desired degree. In this fashion the OCW can function as an attenuator or a switch. A PVFET is a Field Effect Transistor whose gate is controlled by a PhotoVoltaic Cell.

Navy case 76,916; disclosure submitted 15 September 1994.

**Stephen D. Russell**

**“Energy Converting Porous Silicon  
Optical Element”**

This invention describes an optical element made of porous silicon on a transparent substrate for converting light of an incident energy to that of a lower emitted energy. This invention may be used for the efficient detection of normally invisible and undetectable wavelengths.

Navy case 76,947; disclosure submitted 19 October 1994.

**Stephen D. Russell**  
**Robert C. Dynes**  
**Paul R. de la Houssaye**  
**Wadad B. Dubbelday**  
**Andrew Katz**  
**Randy L. Shimabukuro**

**“Silicon Nanostructures in  
Silicon on Insulator”**

This invention discloses a variety of electrical, optical, mechanical, and quantum-effect devices on an insulating substrate and their method of fabrication for advanced electronic, optoelectronic, optical computing and flat panel display applications.

Navy case 76,969; disclosure submitted 22 November 1994.

## Independent Exploratory Development

### Patents Issued

**Randy L. Shimabukuro**  
**Stephen D. Russell**

**“Microelectronic Photomultiplier  
Device with Integrated Circuitry”**

The invention is a microelectronic form of a photomultiplier tube. It is designed to combine the desirable features of conventional photomultiplier tubes with the light-weight, low-power, low-cost advantages of an integrated circuit device.

Patent 5,264,693 Navy case 74,784 (Serial 08/019,414) filed 16 February 1993; issued 23 November 1993.

**Hobart R. Everett, Jr.**  
**J. M. Nieusma**

**“Velocity Feedback System  
for Remotely Operated Vehicles”**

This invention provides means for the remote operator of an unmanned vehicle to sense the velocity of the vehicle without having to read a visual indicator. Information from a velocity sensor located on the vehicle is transmitted to a servocontrolled DC motor having an eccentric weight attached to the output shaft of the motor. The motor assembly is mounted to the frame of the operator’s seat, causing it to vibrate in proportion to the speed of the vehicle. Thus, the operator can “sense” the speed of the vehicle without having to look at a video display of the vehicle speed. The novel feature of the invention is that the operator is provided the means to “sense” the speed of a remote vehicle under the operator’s control without needing to read a digital or analog display of vehicle speed on a video screen.

Patent 5,309,140 Navy case 73,322 (Serial 07/800,341) filed 26 November 1992; issued 3 May 1994.

**Albert Zirino**

**“Light-Powered Synthetic Muscle”**

A transparent fiber (such as cross-linked polyacrylic acid), which contracts and expands upon addition of acid or base to an aqueous medium, is placed in the same solution with a colored (photo-chromatic) indicator dye. The dye is so chosen as to have a kPa value as the pH of the null contraction point of the fiber. By irradiating the solution with light of a wavelength of the absorption band of either the acid or base form of the dye, the solution pH is made to change, and the fiber is made to expand to contract, depending on the wavelength. Thus, light energy can be readily converted to work energy.

Patent 5,334,629 Navy case 73,763 (Serial 07/904,109) filed 25 June 1992; issued 2 August 1994.

## Independent Exploratory Development

### Patent Applications Filed

**Everett W. Jacobs**  
**Roger D. Boss**  
**Yuval Fisher**

**“Iterated Transform Algorithm  
for the Compression of Images”**

This invention provides a method for compressing a digital image comprising the following steps: partitioning the image into squares of a predetermined size (the ranges); searching for a set of “suitable” transformation-domain pairs that map onto the ranges (a domain being the area upon which a transformation acts); and minimizing the error between the transformed domains and their corresponding ranges.

Navy case 73,320 (Serial 07/860,648) filed 30 March 1992; pending.

**Everett W. Jacobs**  
**Roger D. Boss**  
**Yuval Fisher**

**“Method of Encoding a  
Digital Image by Using Adaptive  
Partitioning in an Iterated  
Transformation System”**

This invention is a new adaptive method for partitioning an image resulting in efficient encoding by using the iterated transformation image compression technique.

Navy case 74,198 (Serial 07/859,782) filed 30 March 1992; pending.

**Carol A. Dooley**  
**Elek Lindner**

**“Organotin Biocides Containing  
Mixed Saturated/Unsaturated  
Carbon Chains”**

Biocides consisting of a tin atom covalently bonded to three carbon chains of two atoms each. One or two of these carbon chains contain a double bond at either C-1 or C-3. The anion is labile and irrelevant to the purpose, but is bromide in the isolated product.

Navy case 74,762 (Serial 08/175,890) filed 30 December 1993; pending.

**Terence R. Albert**  
**Adi R. Bulsara**  
**Gabor Schmera**

**“Nonlinear Dynamic Signal Processor,  
Based on Enhancement of Stochastic  
Resonance Effect in Coupled  
Oscillator Arrays”**

Globally coupled nonlinear oscillators are subject to the weak deterministic signal of interest. The background noise enhances the signal-to-noise ratio at the output via the stochastic resonance effect. The enhancement is far greater than would be realized by a single oscillator.

Navy case 75,209 (Serial 08/249,111) filed 25 May 1994; pending.

**Stephen D. Russell**  
**Wadad B. Dubbelday**  
**Randy L. Shimabukuro**  
**Paul de la Houssaye**  
**Diane M. Szarflarski**

**“Photonic Silicon on a  
Transparent Substrate”**

This invention describes light emitting (photonic) silicon on a transparent substrate and its method of fabrication.

Navy case 75,292 (Serial 08/118,900) filed 9 September 1993; pending.

## **Independent Exploratory Development**

### **Invention Disclosures Authorized**

**David M. Bullat  
Po-Yun Tang**

**“Force Transfer Column (Longitudinal  
to Radial) with High-Frequency Filter Isolator  
for Use in Fiber Optic Sonar Transducers”**

The purpose of this proposed concept is to facilitate the use of fiber optic cables to measure in-water acoustic perturbations.

Navy case 75,649; authorized for preparation of patent application 21 July 1994.

### **Invention Disclosures Submitted**

**Wadad B. Dubbelday  
Randy L. Shimabukuro  
Stephen D. Russell**

**“Electroluminescent Devices in  
Porous Silicon on Sapphire”**

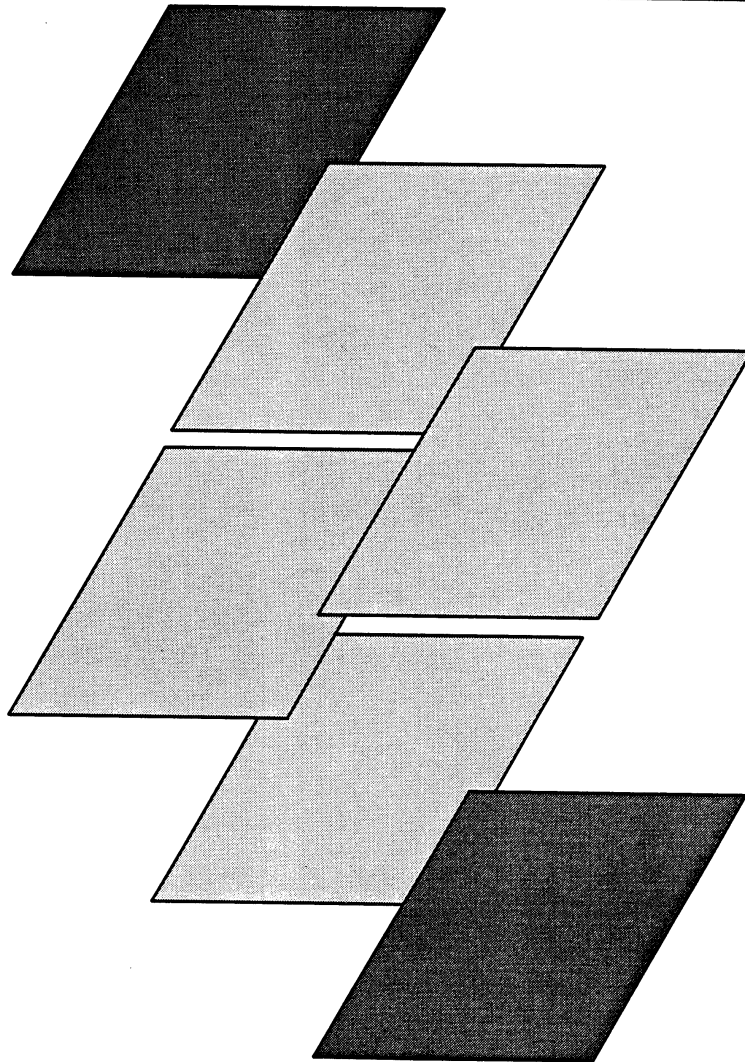
An electroluminescent device is integrated on a sapphire substrate that is transparent to light generated by electroluminescence. Crystalline silicon is formed on the sapphire substrate and patterned into an island. A titanium silicide electrode is formed in the silicon around the island by a titanium silicide reaction and covered by an electrically insulating layer. The island is etched to expose the silicon, and a porous silicon layer is formed on the crystalline silicon. An aluminum electrode is formed on the porous silicon layer. An outer insulating layer may be formed on the aluminum electrode and the titanium silicide electrode. Additional electrodes may be formed on and through the outer insulating layer to make electrical contact with the titanium silicide and aluminum electrodes, respectively. A voltage source may be connected to the electrodes to cause light to be emitted from the porous silicon through the sapphire substrate.

Navy case 75,291; disclosure submitted 26 January 1993.

---

# IR PROJECT TABLES

---





**Independent Research Projects for FY 94  
0601152N**

Work Unit Identification		Project Title	Principal Investigator			FY 94 Funds \$K
Local	DTIC DN#					
ZW71	302 246	Measurement of Refractive Index and Dispersion in LiSAF and LiCAF Crystalline Materials for Use in Iso-Index Birefringent Filters	Greg L. Adams			52
ZW74	303 010	Implementation of Fuzzy Logic to Choose and Apply Soil Characteristics—Dependent Calibration Curves for the Environmental Measurements in the Field	Dr. Sabine Apitz			15
ZW80	302 248	Lattice Blind Equalizers for High Data Rate Communications	Roy Axford			105
ZW84	304 020	Deductive Inferences in a Non-Monotonic Logic	Dr. Donald Bamber			67
ZW68	303 011	Synthesis and Studies of Alkali-Doped C <sub>60</sub>	Dr. Roger Boss			131
ZW85	304 017	Matched-Field Tracking	Dr. Homer Bucker			67
ZW86	304 005	Tidal Dispersion Mechanisms in a Coastal Embayment	Bart Chadwick			82
ZU01	304 134	Ultra-Wideband Impulse Radio Propagation	Jeffrey Coleman			45.9
ZW87	304 015	Combining Combinatorial Search with Learning for Command Control	Michael Gherrity			67
ZW88	304 016	Studies of Optical Ringing in Seawater	Dr. Gary Gilbert			63
ZW89	304 004	Multiwavelength UV Source Development	Dr. Frank Hanson			107
ZW69	303 006	n-type Doping of Diamond Using Li and Na	Dr. Charles Hewett			95
ZW90	304 037	Elimination of the Mechanical Dither of a Ring-Laser Gyroscope by the Implementation of a Quantum-Well Window	Fran Karwacki			66
ZW62	302 038	Parallel Solution of Large Sparse Systems of Equations	Dr. Aram Kevorkian			108
ZW67	303 002	Evolving Neural Network Pattern Classifiers	John R. McDonnell			104
ZW91	304 010	Three-Dimensional Electric Field Measurements in Shallow Water	Michael Morey			17.1

**Continued**

Work Unit Identification		Project Title	Principal Investigator			FY 94 Funds \$K
Local	DTIC DN#					
ZW92	304 018	ZnSe Blue Light-Emitting Devices and Lasers	Dr. Don Mullin			101
ZW73	304 134	Further Investigations into the Effects of Using Lasers in Display Devices: Colorimetry and Laser Speckle	Tom Phillips			101
ZW93	304 009	Signal Detection Based on Limited Clues	Jamie Pugh			70
ZW94	304 013	Acoustic Bottom Interaction Using the Parabolic Equation	Dr. David Rees			80
ZW77	303 010	Hydrodynamic Characterization of Bioluminescent Stimulus: Part II—Prediction	Dr. Jim Rohr			110
ZW70	303 005	Photonic Silicon Device Physics	Dr. Stephen Russell			177
ZW79	302 344	Shallow-Water Three-Dimensional Parabolic Equation Model	Frank Ryan			68
ZW95	304 014	Wavelets for Ultrabroadband Radar	Dr. Mark Shensa			97
ZW96	304 006	Quantitative Performance Evaluation of an ATM-Based Statistical Multiplexer	Allen Shum			69
ZW97	304 026	Real Solutions to Maximum Clique and Graph Coloring Patterns	Dr. Joel Small			72
ZW82	302 243	Observation of Ionospheric Dynamics	Richard Sprague			86
ZW98	304 008	Coupling Adaptive Beamforming and Adaptive Locally Optimal Detection Algorithms in Non-Stationary Noise	Dr. David Stein			83

**Multisponsored IR Projects for FY 94**

IR Project					Other Funding				
NRaD	DTIC	Title	Funding	\$K	NRaD	DTIC	Title	Funding	\$K
ZW68	303 011	Synthesis and Studies of Alkali-Doped C <sub>60</sub>	0601152N	131	MJ43	301 122	A Fullerene-Based Neutron Detector	OFGVT	200
ZW95	304 014	Wavelets for Ultrabroadband Radar	0601152N	97	CD30	302 036	Wavelets	0601153N	66
					XD80	—	Wavelet Transforms	0601153N	10
ZW97	304 026	Real Solutions to Maximum Clique and Graph Coloring Problems	0601152N	72	SA35	301 080	Program Management Support	0603013N	50
ZW82	302 243	Observation of Ionospheric Dynamics	0601152N	86	MPB1	302 214	Electromagnetic Propagation	0602435N	60
ZW80	302 248	Lattice Blind Equalizers for High-Data-Rate Communication	0601152N	105	CG17	303 156	Multichannel Adaptive Equalization for High-Data-Rate Mobile Communication	0601153N	74.3
ZW71	302 246	Measurements of Refractive Index	0601152N	52	CH41	307 481	Applied Physics Support	0601153N	15
					EE51	301 025	Solid-State Laser Technology	0602334N	10

**Independent Research Projects  
Terminated in FY 94  
0601152N**

Principal Investigator		Work Unit Identification		Project Title	Reason for Termination and/or Cancellation
		Local	DTIC DN#		
Adams		ZW71	302 246	Investigation of New LiSAF and LiCAF Crystal-line Materials for Use in Iso-Index Birefringent Filters	Completed
Apitz		ZW74	303 001	Investigation into the Use of Fuzzy Logic to Choose and Apply Soil Characteristic Dependent Calibration Curves for the Environmental Measurements in the Field	Completed
Boss		ZW68	303 011	Synthesis and Studies of Alkali-Doped C <sub>60</sub>	Completed
Gilbert		ZW88	304 016	Studies of Optical Ringing in Marine Water	Completed. Transitioned to ONR Environmental Optics Project.
Hewett		ZW69	303 006	n-type Doping of Diamond Using Li and Na	Terminated. Negative results indicate work should not be pursued.
Kevorkian		ZW62	302 038	Parallel Solutions of Large Sparse Systems of Equations	Completed
McDonnell		ZW67	303 002	Evolving Neural Network Pattern Classifiers	Completed
Morey		ZW91	304 010	Three-Dimensional Electric Field Measurements in Shallow Water	Terminated. Cost increases and loss of capabilities by contractor precluded pursuing the project.
Mullin		ZW92	304 018	ZnSe Blue Light-Emitting Devices and Lasers	Terminated. Arsenic doping levels not high enough to make technique feasible.

**Continued**

Principal Investigator		Work Unit Identification		Project Title	Reason for Termination and/or Cancellation
		Local	DTIC DN#		
Phillips		ZW73	303 022	Further Investigations into the Effects of Using Lasers in Display Devices: Colorimetry and Laser Speckle	Color work was successfully completed.
Pugh		ZW93	304 009	Signal Detection Based on Limited Clues	Completed. Transitioned to USPH and DBOF.
Russell		ZW70	303 005	Photonic Silicon Device Physics	Completed
Ryan		ZW79	302 344	Shallow Water 3-D Parabolic Equation Model	Completed. Transitioned to 6.2A Deployable Sensors Project.
Shensa		ZW95	304 014	Wavelets for Ultrabroadband Radar	Completed
Small		ZW97	304 026	Real Solutions to Maximum Clique and Graph Coloring Problems	Completed
Sprague		ZW93	304 008	Observation of Ionospheric Dynamics	Research aspect completed. Transitioned to 6.2 Atmospheric Effects Assessment Program (0602435N, NRaD MPB1).

**Independent Research Projects for FY 95  
As Approved December 1994  
0601152N**

Work Unit Identification		Project Title	Principal Investigator			FY 95 Funds \$K
Local	DTIC DN#					
ZW80	302 248	Blind Equalizers for High-Data-Rate Digital Communications	Roy Axford			85.0
ZW84	304 020	Deductive Calculus, Decision Procedure, and Confidence Algorithm for a Nonmonotonic Logic	Dr. Donald Bamber			68.5
ZU02	305 319	Over-Ocean Two Wavelength Correlation in the 3 to 5 and 8 to 12 Micron Spectral Bands	Dr. Charles Bendall			84.0
ZW85	304 017	Matched-Field Tracking	Dr. Homer Buckner			56.7
ZU03	305 312	Cooperative Dynamics in an Array of Globally Coupled rf SQUIDS	Dr. Adi Bulsara			71.5
ZW86	304 005	Tidal Dispersion Mechanisms in a Coastal Embayment	Bart Chadwick			86.5
ZU04	305 313	An Integrated Hybrid Neural Network and Hidden Markov Model Algorithm for Classification Applications	Dr. George Chen			79.5
ZU01	304 134	Ultra-Wideband Impulse Radio Propagation	Jeffrey Coleman			77.5
ZU05	305 303	Near Vertical Incidence Skywave Antenna	Dr. Will Cronyn			94.2
ZU06	305 322	Task Profiling for Heterogeneous Computing	Dr. Richard Freund			51.7
ZW87	304 015	Strategy Development in Environments with Incomplete Information for Command Control	Michael Gherrity			66.5
ZU07	305 301	Development and Applications of Relational Event Algebra	Dr. I. R. Goodman			91.0
ZU08	305 333	Measurement and Prediction of Sediment Assimilation Capacity	Robert K. Johnston			64.1
ZW90	304 037	Elimination of the Mechanical Dither of a Ring Laser Gyroscope by the Implementation of a Quantum Well Mirror	Francis Karwacki			84.5
ZU09	305 334	Micro Power Pack (MPP)	Dr. Eric Lind			94.5

**Continued**

Work Unit Identification		Project Title	Principal Investigator			FY 95 Funds \$K
Local	DTIC DN#					
ZU10	305 315	Photonic Frequency Converting Feed Network for Broadband Transmit/Receive Antennas	Dr. Stephen Pappert			123.2
ZW89	304 004	Multi-Wavelength UV Source Development Continuation and Filter Material Characterization	Pete Poirier			129.5
ZW94	304 013	Acoustic Bottom Interaction Using the Parabolic Equation	Dr. David Rees			73.0
ZU12	305 318	Analysis of Adaptive Equalization Performance as Applied to Interference Suppression in a Dynamic LOS Digital Communication Environment	Michael Reuter			100.0
ZW77	303 010	Bioluminescent Signatures of Underwater Bodies	Dr. Jim Rohr			75.0
ZU13	305 326	Broadband Radar Pulse Focusing in an Atmospheric Surface Duct	Frank Ryan			82.5
ZU14	305 320	High Modulation Rate Tunable Laser	Dr. Richard Scheps			94.0
ZU15	304 204	The Effect of Sediment Bed Characteristics on Reflectivity	Jon Schoonmaker			68.1
ZU16	305 316	Generating Software Objects from Functional Requirements Model	Lydia Shen			80.0
ZW96	304 006	Quantitative Performance Evaluation of an ATM-Based Statistical Multiplexer	Allen Shum			69.5
ZW98	304 008	Robust Adaptive Locally Optimal Detection	Dr. David Stein			72.0
ZU17	305 321	Modeling for Super Composite Projectors of Simple Shapes	Dr. Po-Yun Tang			115.0
ZU18	305 314	Integrated UHF Transceiver on Fully Depleted SOS/SOI	Dr. Michael Wood			185.0



## EXTERNAL DISTRIBUTION

Office of Naval Research  
Arlington, VA 22217-5000 (24)

Naval Air Warfare Center  
Washington, DC 20361-6000

Naval Surface Warfare Center  
Washington, DC 20362-5101

Naval Undersea Warfare Center  
Washington, DC 20362-5101

Naval Command, Control and Ocean  
Surveillance Center  
San Diego, CA 92147-5042

Naval Research Laboratory  
Washington, DC 20375-5000

Naval Air Warfare Center  
Aircraft Division  
Warminster, PA 18974-5000

Naval Air Warfare Center  
Weapons Division  
China Lake, CA 93555-6001

Naval Surface Warfare Center  
Carderock Division  
Bethesda, MD 20084-5000

Naval Surface Warfare Center  
Dahlgren Division  
Dahlgren, VA 22448-5000

Coastal Systems Station  
Panama City, FL 32407-5000

Naval Undersea Warfare Center Division  
Newport, RI 02841-5047

Naval Civil Engineering Laboratory  
Port Hueneme, CA 93043

Naval Training Systems Center  
Orlando, FL 32826-3224

Navy Personnel Research and  
Development Center  
San Diego, CA 92152-6800

Naval Medical Research and  
Development Command  
Bethesda, MD 20014

Naval Postgraduate School  
Monterey, CA 93940 (6)

U.S. Naval Academy  
Annapolis, MD 21402